The integral role of phytoplankton stoichiometry in ocean biogeochemical dynamics

A Dissertation
SUBMITTED TO THE FACULTY OF THE
UNIVERSITY OF MINNESOTA
BY

Tatsuro Tanioka

IN PARTIAL FULFILLMENT OF THE REQUIREMENTS
FOR THE DEGREE OF
DOCTOR OF PHILOSOPHY

Katsumi Matsumoto

November, 2019

© Tatsuro Tanioka 2019
ALL RIGHTS RESERVED

Acknowledgements

I would like to thank my advisor Katsumi Matsumoto who has given me the best advice and encouragement whenever I needed. I am also grateful to the members of my committee- Jake Bailey, Jim Cotner, and Bill Seyfried for their time and energy. I would also like to thank Kathy Tokos for helping me with MESMO. This work was supported by student fellowships from the Earth Sciences Department, Doctoral Dissertation Fellowship from the University of Minnesota Graduate School, and by NSF grant awarded to Dr. Katsumi Matsumoto. Thank you to all my friends and colleagues from the department and outside the department; and to my teammates from the Australian Rules Football Team, Minnesota Freeze. Finally, thank you to my family for their support over the years.

Tatsuro Tanioka
November, 2019

Dedication

To my life-coach, my late grandfather Mitsugu.

Abstract

Photosynthesis by ocean algae (phytoplankton) contributes roughly half of the earth's net carbon production. Organic matter produced using carbon dioxide in the atmosphere not only supports marine food webs, but also acts as a climate stabilizer, because carbon is subsequently transported to the deep ocean and stored there for thousands of years.

Attempts to model global marine biological production and its impacts on global biogeochemical cycles often assume a constant elemental stoichiometry of carbon, nitrogen, and phosphorus in phytoplankton biomass. This ratio, known as the Redfield ratio, was determined on the basis of an analysis of many samples of marine plankton collected over 70 years ago. This notion is well established in the oceanographic community but there is no clear physiological justification for why the C:N:P ratios in phytoplankton should strictly follow the Redfield ratio. Many recent studies revealed that C:N:P ratio of particulate organic matter can deviate significantly from the Redfield Ratio with some noticeable spatial and temporal variability. Studies suggest that factors such as nutrient availability, light, and temperature play a crucial role in modifying C:N:P ratio of phytoplankton.

In this dissertation, I investigate the roles of marine phytoplankton stoichiometry in the global marine biogeochemical dynamics by combining meta-analysis, numerical modeling, and remote sensing. I propose a mechanistic framework for predicting C:N:P in phytoplankton under different environmental conditions and I incorporate this framework into an Earth System Model to show their effects on global carbon cycle. I also present results on how the change in elemental composition of phytoplankton could affect the feeding behavior of zooplankton as well the ecosystem stoichiometry. Finally, I show that C:N:P is closely tied to the rate at which oxygen is consumed during organic matter remineralization and I propose that the change in phytoplankton stoichiometry could ameliorate the rate of marine deoxygenation. In summary, C:N:P of phytoplankton is flexible and will play key roles in future global ocean biogeochemical dynamics.

Contents

Acknowledgements **i**

Dedication **ii**

Abstract **iii**

List of Tables **viii**

List of Figures **ix**

1 Introduction **1**

1.1 Overview of Chapters 2

2 Phytoplankton stoichiometry and global export production **4**

2.1 Synopsis 4

2.2 Introduction 5

2.3 New Stoichiometry Sensitivity Factor 7

2.3.1 Derivation 7

2.3.2 Estimation of Parameters 10

2.3.2.1 Nonlinear Least Squares Regression 11

2.3.2.2 Estimation of Parameters from First Principles 12

2.4 First-Order Estimation of Global Stoichiometric Buffer Effect 13

2.5 Flexible Stoichiometry in a Global Ocean Model 16

2.5.1 Model Description 17

2.5.2 Model Results 22

2.6 Conclusions . . . 25
2.7 Acknowledgments . . . 26

3 Environmental drivers of phytoplankton stoichiometry: a meta-analysis 27
3.1 Synopsis . . . 27
3.2 Introduction . . . 28
3.3 Materials and Methods . . . 30
3.3.1 Bibliographic search and screening . . . 30
3.3.2 Stoichiometry sensitivity factor as effect size . . . 32
3.3.3 Meta-analysis . . . 33
3.4 Results . . . 34
3.4.1 Effects of Phosphate . . . 34
3.4.2 Effects of Nitrate . . . 35
3.4.3 Effects of Nitrate:Phosphate supply ratio . . . 35
3.4.4 Effects of Irradiance . . . 35
3.4.5 Effects of Temperature . . . 37
3.4.6 Effects of Iron . . . 37
3.5 Discussion . . . 37
3.5.1 Basic framework . . . 37
3.5.2 Macronutrients (Phosphate and Nitrate) . . . 43
3.5.3 Irradiance . . . 45
3.5.4 Temperature . . . 47
3.5.5 Iron . . . 49
3.6 Implications for global biogeochemical cycles . . . 50
3.6.1 Conclusions . . . 53
3.6.2 Acknowledgements . . . 54

4 Phytoplankton stoichiometry and feeding behavior of zooplankton 55
4.1 Synopsis . . . 55
4.2 Introduction . . . 56
4.3 Method . . . 57
4.3.1 C:N:P as a function of age . . . 59
4.3.2 Maximum assimilation rate as a function of age . . . 60

4.3.3 Flexible grazing preference as a function of age 62
4.3.4 Experimental setup 65
4.4 Results 66
4.5 Discussion 70
4.6 Acknowledgments 71

5 Phytoplankton stoichiometry and organic matter respiration 72
5.1 Synopsis 72
5.2 Introduction 73
5.3 Methods 75
5.3.1 Estimating O_2:C from satellite-dericed phytoplankton macromolecular composition 75
5.3.2 Estimating O_2:C from the vertical gradient method of dissolved nutrients and oxygen 76
5.3.3 Estimating O_2:C from laboratory and *in situ* measurements of phytoplankton macromolecules 77
5.3.4 Monte Carlo simulation 78
5.4 Results and Discussion 79
5.5 Implications for the Future Marine Oxygen Cycle 84
5.6 Acknowledgments 86

6 Concluding Remarks 88

References 91

Appendix A. Supporting Information For Chapter 2 126

Appendix B. Supporting Information For Chapter 3 128

Appendix C. Supporting Information For Chapter 4 130

Appendix D. Supporting Information For Chapter 5 131
D.1 Uncertainties associated with O_2:C remineralization ratio calculated from the satellite-derived estimate of macromolecules 132
D.2 Derivation of equation(5.4) in the main text 132

D.3 Assumptions and limitations of the vertical gradient method 134
D.4 Validating the vertical gradient method 134

List of Tables

2.1 Comparison of Flexible P:C Formulations 9
2.2 Model Parameters for the Preindustrial and Transient Simulation . . . 18
2.3 Model Results for the Preindustrial and Transient Simulations 23
3.1 Breakdown of the number of experimental units 32
3.2 Summary of s-factors for P:C and N:C 41
3.3 Projected change in C:P and C:N between 1981-2000 and 2081-2100 . . 51
B.1 List of 64 studies used in the meta-analysis 128
C.1 Default food preference of mesozooplankton in the original ERSEM model 130
D.1 Assumed elemental composition of main phytoplankton macromolecules obtained from literatures 145
D.2 Uncertainties in satellite-derived estimate of macromolecules 145
D.3 Effects of changing percent fraction of nucleic acid in estimating $O_2 : C_{rem}$ from the satellite-derived estimate of phytoplankton macromolecules . . 146
D.4 Summary of macromolecular data from Roy (2018) 147
D.5 $O_2 : C_{rem}$ from 9 sensitivity analyses accounting for seasonal variability and depth choice 148

List of Figures

2.1 Observed particulate P:C versus surface PO_4 concentrations 11
2.2 Stoichiometry sensitivity factor against PO_4 14
2.3 Change in export production from 1990s as a function of the fractional change in PO_4 from 1990s 16
2.4 Modeled community stoichiometry sensitivity factor under preindustrial condition 19
2.5 Modeled nutrient limitation under preindustrial condition in the surface layer 20
2.6 Modeled C:P and N:P of phytoplankton in the surface layer 21
2.7 Simulated changes in surface PO_4 and total export production in 2090s relative to 1990s 22
2.8 Results from a global ocean model under IPCC RCP8.5 scenario 25
3.1 low chart showing the preliminary selection criteria and the refined selection criteria used for determining s-factors 31
3.2 S-factors for P:C and N:C with respect to changes in macronutrients . . 36
3.3 S-factors for P:C and N:C with respect to changes in irradiance 38
3.4 S-factors for P:C and N:C with respect to changes in temperature . . . 39
3.5 S-factors for P:C and N:C with respect to changes in iron 40
3.6 Illustration of how the five environmental drivers under a typical future climate scenario affect the cellular allocation 43
4.1 Biogeochemical model ERSEM used in simulations 58
4.2 C:N:P ratios and maximum assimilation rate during copepod ontogeny . 61
4.3 Schematic diagram showing the effect of food quality on food preference of copepod (mesozooplankton) 64

4.4 Equilibrium biomass of plankton functional types as a function of mesozooplankton N:P ratio 67
4.5 Equilibrium food preference of mesozooplankton as a function of mesozooplankton N:P ratio 68
4.6 N:P ratio of released nutrient and large POM as a function of mesozooplankton N:P ratio 69
5.1 Satellite-derived annually averaged phytoplankton macromolecular content and O_2:C remineralization ratio binned into 11 oceanographic regions 80
5.2 Export and remineralization ratios determined from the vertical gradient method 81
5.3 $O_2 : C_{rem}$ estimated from laboratory-based measurements of phytoplankton macromolecule content 83
5.4 $O_2 : C_{rem}$ in various marine ecosystems estimated from biochemical composition of phytoplankton 85
A.1 Observed and modeled global annual mean surface nutrient distributions 126
A.2 Zonally averaged POC export 127
D.1 Comparison of N:P, $O_2 : P_{rem}$, and C:P obtained from the vertical gradient method with previous estimates 138
D.2 Comparison of true vs. vertical gradient based estimate of $N : P_{exp}$ across six model configurations and 3 depth choices 139
D.3 Comparison of true vs. vertical gradient based estimate of $N : P_{exp}$ (% error) 140
D.4 Comparison of true vs. vertical gradient based estimate of $O_2 : P_{rem}$ . . 141
D.5 Comparison of true vs. vertical gradient based estimate of $O_2 : P_{rem}$ (% error) 142
D.6 Comparison of true vs. vertical gradient based estimate of $O_2 : C_{rem}$ . . 143
D.7 Comparison of true vs. vertical gradient based estimate of $O_2 : C_{rem}$ (% error) 144

Chapter 1

Introduction

Marine phytoplankton plays fundamental roles in shaping earth's surface environments and society. Not only has it been providing the breathable oxygen since 2.4 billion years ago (Lyons, Reinhard, & Planavsky 2014), phytoplankton also converts atmospheric CO_2 into organic matter through photosynthesis. Marine organisms at higher levels of the food chain then consume this organic matter. Since photosynthesis and the subsequent transport of carbon (C) from the surface to the deep ocean constitute one of the key removal mechanisms of atmospheric CO_2, the slowing down of this removal could speed up the accumulation of CO_2 in the atmosphere. Therefore, understanding how phytoplankton will respond to environmental changes in the future is critical from the standpoint of food security, conservation, and carbon sequestration.

Under current rates of CO_2 emission by humans, the amount of organic carbon transported to the deep ocean is expected to decrease by 7-15% by the 2090s compared to the 1990s (Bopp et al. 2013). This decline is largely due to surface warming, which stratifies the ocean and reduces the vertical supply of nutrients from the deep ocean to the sun-lit surface ocean. However, such model-based projections are subject to large uncertainties, which arise from our imperfect understanding of plankton physiology and ecology (Cabré, Marinov, & Leung 2015; Laufkötter et al. 2015). The overall goal of my research is to incorporate more realistic biology into ocean models and to give better projections of carbon stored in the ocean.

Although current global ocean models are highly sophisticated, they contain biological assumptions, which were reasonable when they were first introduced but are

questionable today. One such assumption is that the elemental composition of phytoplankton in terms of C:X, where X is the element of interest (e.g., nitrogen, phosphorus) is constant globally (Redfield 1958; Redfield, Ketchum, & Richards 1963). The ratio discovered by Alfred Redfield in the early 20th century has been the "standard global average" in the field of ocean chemistry. However, numerous recent observations have revealed that the elemental composition of phytoplankton varies systematically due to changes in nutrients, temperature, and light (Galbraith & Martiny 2015; Martiny, Pham, et al. 2013; Yvon-Durocher, Dossena, Trimmer, Woodward, & Allen 2015). The variability in the C:X ratio of phytoplankton under different environmental conditions means organic matter is not exported from the surface to the deep ocean in the same manner everywhere. My research is hence focused on improving how ocean models incorporate temporal and spatial variability in the elemental composition of phytoplankton and organic matter. By doing this, models will be able to give more accurate projections of future carbon cycle and thus climatic conditions.

1.1 Overview of Chapters

Each chapter of this dissertation addresses the separate topic related to the overarching theme of this dissertation: "the roles of phytoplankton elemental stoichiometry in global ocean biogeochemical dynamics."

- **Chapter 2** explores how flexible elemental stoichiometry of phytoplankton could mitigate the reduction in carbon export production under future global warming scenario using numerical model. We also newly define "stoichiometry sensitivity factor" that relates fractional change in phytoplankton elemental stoichiometry with respect to fractional change in nutrient concentration and other environmental factors from observations.

- In the following **Chapter 3**, I conduct meta-analysis of published laboratory experiment studies to quantify "stoichiometry sensitivity factor" (described in **Chapter 2**) for 5 different environmental drivers (phosphate, nitrate, irradiance, temperature, and iron). Values obtained here can be incorporated into the biogeochemical models to accurately determine C:N:P of marine phytoplankton.

- A relationship between phytoplankton stoichiometry and ecosystem stoichiometry is presented in **Chapter 4**. I investigate using state-of-the-art marine ecosystem model how change in N:P ratio of phytoplankton affects the feeding behavior of zooplankton, which in turn affects N:P of the whole ecosystem.

- In **Chapter 5**, I calculate global distribution of organic matter remineralization and export ratios based on the macromolecular composition of phytoplankton. I posit a new hypothesis that a shift in phytoplankton cellular composition could ameliorate future open ocean deoxygenation.

- In the final Chapter 6, I summarize the results from the preceding chapters and discuss future potential work that would deepen our understanding of the roles of phytoplankton stoichiometry in global ocean biogeochemical dynamics.

Chapter 2

Phytoplankton stoichiometry and global export production

The contents of this section were originally published in the journal *Global Biogeochemical Cycles* (Volume 31, Issue 10, 1528-1542) under the title 'Buffering of ocean export production by flexible elemental stoichiometry of particulate organic matter'. This work included below is its published form with permission of all authors. See Tanioka and Matsumoto (2017) for details. To view the published open abstract, go to `http://dx.doi.org` and enter the DOI (10.1002/2017GB005670). Copyright (2017) American Geophysical Union.

2.1 Synopsis

Sinking of particulate organic carbon (C) from the surface to the deep ocean acts to draw down atmospheric CO_2. Essential nutrients such as nitrogen (N) and phosphorus (P) both limit C export production and control its efficiency. The efficiency of C export for a given amount of N or P is expressed by their relative abundances in terms of their elemental ratios in organic matter. This P:N:C ratio is assumed to be fixed ("Redfield ratio") in the most global biogeochemical models. Here we present a new method for allowing P:C to vary. Using this newly developed model, we quantify how flexible P:C can buffer changes in export production under a future warming scenario.

2.2 Introduction

Export production (EP) of carbon from the surface to deep ocean as sinking particulate organic matter (POM) is one of the key processes that act as major sinks of atmospheric CO_2 (Falkowski et al. 2000). In the modern ocean, approximately 10 PgC are exported annually from the surface to the ocean interior (Dunne, Sarmiento, & Gnanadesikan 2007). This is comparable to the amount of carbon emitted by fossil fuels combustion each year (Le Quéré et al. 2016).

EP over the 21st century is generally expected to decline due to decrease in upward nutrient flux in response to surface ocean warming and freshening (Bopp et al. 2013; W. Fu, Randerson, & Moore 2016; J. K. Moore, Doney, & Lindsay 2004). In the framework of the fifth phase of the Coupled Model Intercomparison Project (CMIP5), EP is expected to decline by 7-18% by the 2090s relative to the 1990s under the most aggressive CO_2 concentration scenario, the RCP8.5 (Bopp et al. 2013). However, this and other projections of future changes in global EP are subject to uncertainties, which arise from our imperfect understanding about phytoplankton community structure (Marinov, Doney, & Lima 2010), the efficiency of the biological pump (Henson, Yool, & Sanders 2015), and top-down control such as grazing and particle formation (Laufkötter et al. 2016).

In order to improve our understanding of EP and its future variability, we focus on the elemental stoichiometry of POM. One of the key assumptions made today in most biogeochemical components of global ocean models is the fixed Redfield ratio (P:N:C) for organic matter production (Redfield 1958). By assuming the Redfield ratio, particulate organic carbon (POC) is exported from the surface to the deep ocean, along with nitrogen and phosphorus, in a very predictable manner (e.g., the canonical Redfield ratio of 1:16:106 or by the modified ratio of 1:16:117; L. A. Anderson & Sarmiento 1994). This ratio is generally observed in POM captured in sediment traps and is believed to reflect temporal and spatial averaging of the elemental composition of life forms in the oceans that emerge from interactions between biotic and abiotic components (Flynn 2010). The ratio remains one of the foundations of chemical oceanography and is used in the most ocean biogeochemical models including those in CMIP5 (Bopp et al. 2013).

However, numerous recent observations have revealed that elemental stoichiometry

of POM varies both spatially (Martiny, Pham, et al. 2013; Martiny, Vrugt, Primeau, & Lomas 2013) and temporally (Karl et al. 2001; Singh, Baer, Riebesell, Martiny, & Lomas 2015; Talarmin et al. 2016) due to various environmental factors such as nutrient supply, temperature, and light. There is a clear global pattern especially in P:C, which is elevated in phosphorus rich regions and low in the phosphorus limited oligotrophic regions (Galbraith & Martiny 2015; Martiny, Pham, et al. 2013). The variability likely reflects both the plasticity of phytoplankton nutrient content (Geider & La Roche 2002; Klausmeier, Litchman, Daufresne, & Levin 2004; Klausmeier, Litchman, & Levin 2004) and the phytoplankton community structure (Bonachela, Klausmeier, Edwards, Litchman, & Levin 2016; Weber & Deutsch 2010). Smaller plankton with lower P:C are more dominant in the nutrient poor regions, while large plankton with higher P:C but with faster growth rate are more dominant in the nutrient rich regions (Martiny, Pham, et al. 2013). The large variability in P:N:C suggests that climate change may alter regional differences in the stoichiometry and therefore the global ocean carbon cycle (Broecker 1982; DeVries & Deutsch 2014; Omta, Bruggeman, Kooijman, & Dijkstra 2006). In particular, future expansion of nutrient-depleted waters could result in lower P:C ratio as a result of phytoplankton plasticity and shift in community composition toward smaller plankton with lower optimal P:C (Teng, Primeau, Moore, Lomas, & Martiny 2014).

In this paper, we quantify the effect of flexible P:C on future EP by using a new, simple power law model that predicts P:C as a function of ambient phosphate concentration. The model is motivated by Galbraith and Martiny (2015) (hereafter GM15), who predict P:C as a linear function of PO4, and by Sterner et al. (2008), who propose a use of power functions to model seston P:N:C. Using this new model, we first provide a first-order estimation of the effects of flexible P:C on global EP under a future warming scenario. Second, we use a global ocean model, enabled with our new power law model of stoichiometry, to demonstrate the spatial and temporal effects of flexible P:C on future EP.

2.3 New Stoichiometry Sensitivity Factor

2.3.1 Derivation

We developed a new stoichiometry sensitivity factor, $s^{P:C}_{PO_4}$, which relates a fractional change in P:C ratio of POM to a fractional change in the surface PO_4 concentration. In the discrete form, $s^{P:C}_{PO_4}$ can be written as

$$s^{P:C}_{PO_4} = \frac{([P:C](t) - [P:C](t-\Delta t))/[P:C](t-\Delta t)}{([PO_4](t) - [PO_4](t-\Delta t))/[PO_4](t-\Delta t)} \tag{2.1}$$

By definition, this is a power law where a relative change in one quantity results in a proportional relative change in the other quantity. In the continuous form ($\Delta t \to 0$), $s^{P:C}_{PO_4}$ can be written as

$$s^{P:C}_{PO_4} = \frac{\partial [P:C]/[P:C]}{\partial [PO_4]/[PO_4]} = \frac{\partial \ln[P:C]}{\partial \ln[PO_4]} \tag{2.2}$$

where the partial differentials indicate that other variables such as light and temperature are kept constant. This form of expressing the sensitivity of a chemical property of seawater to another property is analogous to the formulation of the Revelle factor, R ($R = \partial \ln[CO_2]/\partial \ln[DIC]$). In chemical oceanography, this factor is widely used to quantify the sensitivity of ocean's carbon chemistry to changes in atmospheric pCO_2.

In essence, $s^{P:C}_{PO_4}$ is a measure of how sensitive the P:C ratio of POM is to a change in ambient PO_4. In the traditional Redfield view, $s^{P:C}_{PO_4}$ would equal zero by definition, because P:C ratio of particulate organic matter is constant and therefore not at all sensitive to any change in PO_4 concentration. On the other hand, $s^{P:C}_{PO_4}$ takes a positive value if P:C changes in the same direction as the change in PO_4. Our understanding of phytoplankton stoichiometry would indeed predict a positive relationship, such that as PO_4 becomes increasingly more available in the environment, phytoplankton will uptake more PO_4 (Lomas, Bonachela, Levin, & Martiny 2014), driving cellular P:C ratio to rise. A larger value of $s^{P:C}_{PO_4}$ means that P:C is more sensitive to a change in PO_4. As elaborated below, the magnitude of $s^{P:C}_{PO_4}$ is also a measure of how well the plasticity in P:C buffers EP of carbon when PO_4 changes.

For illustration, we assume that stoichiometry sensitivity factor $s^{P:C}_{PO_4}$ is at a steady

state. Equation (2.2) can be solved by separation of variables to give a simple power function that relates P:C and PO_4:

$$[\mathrm{P:C}] = [\mathrm{P:C}]_0 \left(\frac{[\mathrm{PO_4}]}{[\mathrm{PO_4}]_0} \right)^{\mathrm{s}_{\mathrm{PO_4}}^{\mathrm{P:C}}} \tag{2.3}$$

where $[\mathrm{P:C}]_0$ is the P:C ratio when PO_4 is equal to some arbitrary reference value $[PO_4]_0$. This formulation can simulate different kinds of response of P:C according to $\mathrm{s}_{\mathrm{PO_4}}^{\mathrm{P:C}}$ a linear response of P:C with respect to PO_4 ($\mathrm{s}_{\mathrm{PO_4}}^{\mathrm{P:C}} = 1$), a near hyperbolic response that saturates at high PO_4 ($0 < \mathrm{s}_{\mathrm{PO_4}}^{\mathrm{P:C}} < 1$), and a null response ($\mathrm{s}_{\mathrm{PO_4}}^{\mathrm{P:C}} = 0$). An advantage of our new formulation is that it can incorporate important biological and geochemical information about ocean ecosystem in a single parameter $\mathrm{s}_{\mathrm{PO_4}}^{\mathrm{P:C}}$. We believe that the ability of this model to describe nonlinearity often seen in biological and chemical systems represents a viable, alternative to an earlier linear formulation by GM15 (Table 2.1). A linear formula would predict unrealistically that P:C changes continuously without bound as PO_4 becomes very large, while the new power law formulation show saturation at high PO_4, which is typical of biological systems.

Table 2.1: Comparison of Flexible P:C Formulations

Model	**Unbinned (n = 610)**		**Binned (n = 9)**		**Reference**
	$\mathbf{r^2}$	**Equation**	$\mathbf{r^2}$	**Equation**	
Linear (GM15)	0.36	$\mathrm{P:C} = 6.9‰\ \mu\mathrm{M}^{-1} \times \mathrm{PO_4} + 6.0‰$	0.95	$\mathrm{P:C} = 7.3‰\ \mu\mathrm{M}^{-1} \times \mathrm{PO_4} + 4.8‰$	Galbraith and Martiny (2015)
Morel's formula	0.35	$\mathrm{P:C} = 37.8‰ \times \frac{0.49+\mathrm{PO_4}}{3.2+\mathrm{PO_4}}$	0.92	$\mathrm{P:C} = 37.8‰ \times \frac{0.37+\mathrm{PO_4}}{3.2+\mathrm{PO_4}}$	This study
Power law	0.30	$\mathrm{P:C} = 13.3 \times \mathrm{PO_4}^{0.3}$	0.86	$\mathrm{P:C} = 12.4 \times \mathrm{PO_4}^{0.4}$	This study

Another advantage of our power law formulation of P:C ratio is that it can be expanded to account for the sensitivity of P:C with respect to other environmental factors such as light and temperature. For example, the sensitivity with respect to temperature T would be $\mathrm{s}_{\mathrm{T}}^{\mathrm{P:C}} = \partial \ln[\mathrm{P:C}]/\partial \ln \mathrm{T}$. Similarly, the sensitivity factor of P:C with respect to light level λ would be $\mathrm{s}_{\lambda}^{\mathrm{P:C}} = \partial \ln[\mathrm{P:C}]/\partial \ln \lambda$. In the Southern Ocean, for example, where macronutrients are replete but temperature is low and light can be seasonally limiting (Arteaga, Pahlow, & Oschlies 2014; Weber & Deutsch 2010; Yvon-Durocher et al. 2015), these latter dependencies are expected to be important. If we were to incorporate dependencies of multiple environmental factors such as temperature (T) and light (λ), those factors can be superimposed to give a single equation:

$$[\mathrm{P:C}] = [\mathrm{P:C}]_0 \left(\frac{[\mathrm{PO_4}]}{[\mathrm{PO_4}]_0}\right)^{\mathrm{s}_{\mathrm{PO_4}}^{\mathrm{P:C}}} \left(\frac{\mathrm{T}}{\mathrm{T}_0}\right)^{\mathrm{s}_{\mathrm{T}}^{\mathrm{P:C}}} \left(\frac{\lambda}{\lambda_0}\right)^{\mathrm{s}_{\lambda}^{\mathrm{P:C}}} \tag{2.4}$$

where T_0 and λ_0 are reference temperature and light level, respectively. While this study is focused on P:C, the power law formulation can be similarly extended to other elemental ratios such as N:C and Fe:C. Thus, the two strengths of our new power law formulation are its ability to represent nonlinear biological characteristics and account for multiple environmental factors. In addition, parameters in a power law formulation can easily be estimated from observations using linear fitting in the log space, an advantage not shared by other formulations such as Q_{10} formulation (Raven & Geider 1988).

2.3.2 Estimation of Parameters

We estimated the mean value of $\mathrm{s}_{\mathrm{PO_4}}^{\mathrm{P:C}}$ for the modern ocean using global P:C and $\mathrm{PO_4}$ data from GM15. We have constrained the mean value in two different methods: fitting equation (2.3) to the data by a least squares regression in log space and recasting a first principle equation of Morel (1987) to the power law form. We note that it is possible, in yet a different method, to estimate $\mathrm{s}_{\mathrm{PO_4}}^{\mathrm{P:C}}$ from a time series using equation (2.1). However, we have not identified a suitable time series of $\mathrm{PO_4}$ and POM stoichiometry measurements to constrain $\mathrm{s}_{\mathrm{PO_4}}^{\mathrm{P:C}}$ with sufficient precision and accuracy.

2.3.2.1 Nonlinear Least Squares Regression

In the first method of estimation of $s_{PO_4}^{P:C}$ in equation (2.3), a log linear regression is applied to the GM15 globally compiled data. The particulate P:C data are a global compilation of 610 surface P:C observations (upper 30 m) and PO_4 in the same location. We chose reference $[PO_4]_0$ in (2.3) to be 1.0 μM, as this is the simplest way to remove dimensionality from (2.3). Mathematically, the estimated value of $s_{PO_4}^{P:C}$ is not affected by the choice of $[PO_4]_0$. Log linear regression yields $[P:C]_0$ of 13.3‰ and $s_{PO_4}^{P:C}$ of 0.3. The regression coefficient (r^2, Pearson) is 0.30, which is slightly lower than the regression by a simple linear model of GM15 ($r^2 = 0.36$). Figure 2.1 shows the observed data, the power law curve, linear model of GM15, and Morel's formula (see section 2.3.2.2), where all the parameters are estimated from the same data set.

Owing to the nonlinearity in equation (2.3), P:C dependence on PO_4 is strong where PO_4 is less than 0.1 μM (Figure 2.1). That is, under low nutrient condition (i.e., as PO_4 decreases), there is a tendency toward strong frugality, which is indicated by large

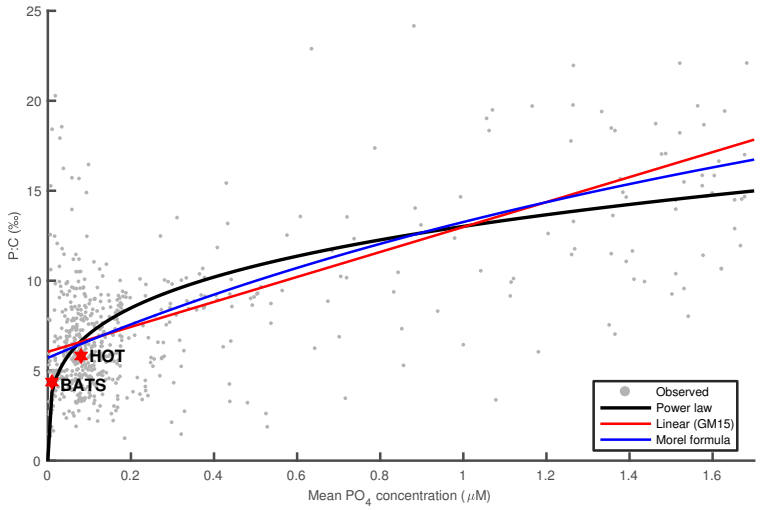

Figure 2.1: Observed particulate P:C versus surface PO_4 concentrations (n = 610). The black line is the power law model (equation (2.3)), the red line is the linear equation ("the line of frugality") from Galbraith and Martiny (2015), and the blue line is Morel's formula (equation (2.5)). Parameters used in each model are summarized in Table 2.1. Also shown are average P:C and PO_4 at Bermuda Atlantic time series (BATS, P:C = 4.4‰, PO_4 = 0.01 μM) and Hawaiian Ocean Time Series (HOT, P:C = 5.8‰, PO_4 = 0.08 μM) from Martiny, Pham, et al. (2013).

deviation in P:C toward smaller values compared to both the Redfield ratio (P:C of 9.4‰) and GM15. In a typical oligotrophic ocean region such as the Bermuda Atlantic Time-series Study (BATS), where surface PO_4 concentration is on the order of 0.1 to 0.01 μM (Sarmiento & Gruber 2006), P:C calculated by the power law model would be 6.7‰ - 3.3‰ (C:P of 149 to 303). This is consistent with the average observed C:P of 229:1 at BATS (Martiny, Pham, et al. 2013). In comparison, GM15 would predict much higher P:C ratio of 6.7‰ - 6.1‰ (C:P of 149 to 165) for the same PO_4 concentration range.

It makes biological sense that P:C changes most rapidly at the lowest PO_4 concentrations and the rate of change of P:C gradually falls at the highest concentrations. When PO_4 is low and limiting, nutrient availability controls the uptake, which controls the cellular P:C ratio and subsequently growth (Flynn 2008). Since the rate of change of PO_4 uptake is greatest when PO_4 is at its lowest and decreases rapidly as PO_4 increases (Lomas et al. 2014), rate of change of P:C should also decrease as PO_4 increases. Furthermore, power law formulation can predict a saturating behavior at high nutrient concentrations ($PO_4 > 1.0$ μM), which is typical in biological systems. Such behavior is expected in high latitudes where light, temperature, and iron in the case of the Southern Ocean can be stronger limiting factors than PO_4 (C. M. Moore et al. 2013).

2.3.2.2 Estimation of Parameters from First Principles

Morel (1987) has shown, using Michaelis-Menten-Monod uptake and Droop's growth model, that phytoplankton's cellular quota (Q) can be expressed as a function of external nutrient (S) under steady state condition. From equation (C1.11) in Table 1 of Morel (1987), cellular quota can be expressed as

$$Q = Q_{max} \frac{K_\mu + S}{K_{\mu Q} + S} \tag{2.5}$$

where Q_{max} is the maximal cellular quota, K_μ is the saturation constants for growth, and $K_{\mu Q}$ is the saturation constant for uptake. For the case of phosphorus quota, $Q = [\mathrm{P} : \mathrm{C}]$, $S = [PO_4]$, and $Q_{max} = [\mathrm{P} : \mathrm{C}]_{max}$. It is possible to recast equation (2.5) to the power law form by taking a Taylor expansion in the logarithmic space around an operation

point to obtain a first-order power law relationship:

$$[\mathrm{P:C}] = [\mathrm{P:C}]_{max}\frac{K_\mu + [\mathrm{PO_4}]}{K_{\mu Q} + [\mathrm{PO_4}]} \approx [\mathrm{P:C}]_0[\mathrm{PO_4}]^{\mathrm{s}^{\mathrm{P:C}}_{\mathrm{PO_4}}} \tag{2.6}$$

where

$$\mathrm{s}^{\mathrm{P:C}}_{\mathrm{PO_4}} = \frac{\partial \ln[\mathrm{P:C}]}{\partial \ln[\mathrm{PO_4}]} = \frac{\partial[\mathrm{P:C}]}{\partial[\mathrm{PO_4}]} \cdot \frac{[\mathrm{PO_4}]}{[\mathrm{P:C}]} = \frac{(K_{\mu Q} - K_\mu)[\mathrm{PO_4}]}{(K_\mu + [\mathrm{PO_4}])(K_{\mu Q} + [\mathrm{PO_4}])} \tag{2.7}$$

and

$$[\mathrm{P:C}]_0 = [\mathrm{P:C}] \cdot [\mathrm{PO_4}]^{-\mathrm{s}^{\mathrm{P:C}}_{\mathrm{PO_4}}}. \tag{2.8}$$

Recasting equations into power law formalism is a widely used technique in the field of biochemical system analysis (Savageau 1976; Voit 2013).

In developing equation (2.6), we first determined its parameters from the same GM15 global data set. We used maximal P:C ($[\mathrm{P:C}]_{max}$) of 37.8‰ from the data and estimated parameters K_μ and $K_{\mu Q}$ using nonlinear least squares regression to obtain values of 0.49 μM and 3.2 μM, respectively. We then obtained $\mathrm{s}^{\mathrm{P:C}}_{\mathrm{PO_4}}$ as a function of $\mathrm{PO_4}$ using equation (2.7) (Figure 2.2). Global average value of $\mathrm{s}^{\mathrm{P:C}}_{\mathrm{PO_4}}$ is 0.4 for the operational $\mathrm{PO_4}$ concentration of 0.6 μM, which is a global surface average phosphate concentration from World Ocean Atlas (H. E. Garcia et al. 2013). This $\mathrm{s}^{\mathrm{P:C}}_{\mathrm{PO_4}}$ value compares reasonably well with that estimated with the first method, leading us to conclude that our best estimate for the global $\mathrm{s}^{\mathrm{P:C}}_{\mathrm{PO_4}}$ is between 0.3 and 0.4. At face value, this means that a 1% change in $\mathrm{PO_4}$ translates to a 0.3 to 0.4% change in P:C. We have also carried out the same analyses using binned data (not shown) according to $\mathrm{PO_4}$ concentration and obtained similar value of $\mathrm{s}^{\mathrm{P:C}}_{\mathrm{PO_4}}$ (Table 2.1).

2.4 First-Order Estimation of Global Stoichiometric Buffer Effect

A simple thought experiment illustrates the potentially strong impact that flexible P:C ratio of particulate organic matter has on EP of carbon. According to the traditional Redfield ratio (i.e., P:C ratio of 1/106), EP of 1 mole of $\mathrm{PO_4}$ (limiting nutrient) would lead to EP of 106 moles of POC. If the ambient $\mathrm{PO_4}$ concentration is reduced to 0.5 moles

while the P:C ratio is fixed, then the EP of carbon would also halve. However, if the P:C ratio mirrors the change in PO_4 by becoming half of the initial value, then the EP of carbon remains unchanged at 106 moles. In this particular case, the stoichiometry sensitivity factor, $s^{P:C}_{PO_4}$, would be 1 ($s^{P:C}_{PO_4}$ = -0.5/-0.5 = 1). This example illustrates a perfect stoichiometric buffer, where a change in P:C completely buffers against or compensates for the change in EP of carbon that would otherwise have been caused by a change in PO_4. Fixed P:C stoichiometry represents the opposite case of no buffering or compensation (i.e., $s^{P:C}_{PO_4} = 0$), whereby a fractional change in EP equals the same fractional change in PO_4.

In the simple limiting case where EP of carbon is a function of PO_4 and P:C, EP can be estimated by

$$\mathrm{EP} = \mathrm{Constant} \cdot [PO_4]/[\mathrm{P} : \mathrm{C}]. \tag{2.9}$$

This is a first-order estimation of EP as a function of the ambient nutrient concentration used in previous studies (Chavez & Barber 1987; Eppley & Peterson 1979; Eppley, Renger, & Betzer 1983). We can express the future change in EP as a function of changes in PO_4 and P:C, referenced to some recent time (e.g., decade of the 1990s), in

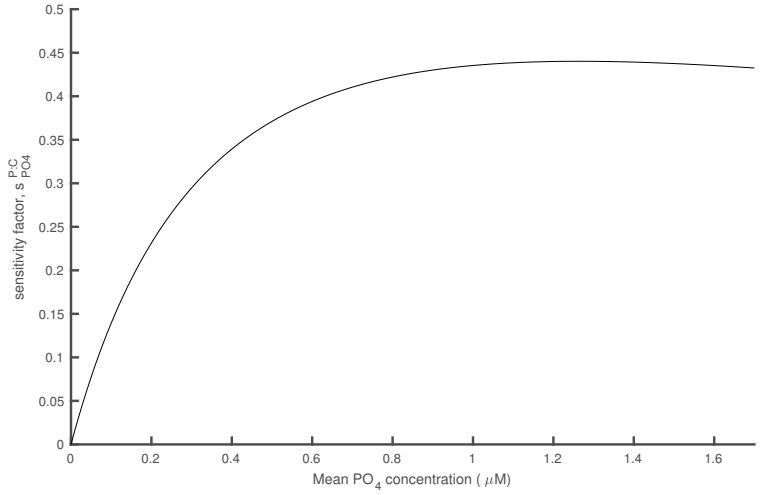

Figure 2.2: Stoichiometry sensitivity factor against PO_4 calculated by equation (2.7) with parameters obtained from fitting Morel's formula to observed data in Figure 2.1.

a simple equation,

$$\frac{\Delta \mathrm{EP}}{\mathrm{EP}_{1990}} = \frac{\Delta\left(\frac{[\mathrm{PO_4}]}{[\mathrm{P{:}C}]}\right)}{\left(\frac{[\mathrm{PO_4}]_{1990}}{[\mathrm{P{:}C}]_{1990}}\right)} = \frac{\frac{[\mathrm{PO_4}]}{[\mathrm{P{:}C}]} - \frac{[\mathrm{PO_4}]_{1990}}{[\mathrm{P{:}C}]_{1990}}}{\frac{[\mathrm{PO_4}]_{1990}}{[\mathrm{P{:}C}]_{1990}}} \tag{2.10}$$

This equation, combined with equation (2.3) and assuming $[\mathrm{PO_4}]_0 = 1.0$ μM, can be rearranged as

$$\frac{\Delta \mathrm{EP}}{\mathrm{EP}_{1990}} = \left(\frac{\Delta[\mathrm{PO_4}]}{[\mathrm{PO_4}]_{1990}} + 1\right)^{1-\mathrm{s}_{\mathrm{PO_4}}^{\mathrm{P:C}}} \tag{2.11}$$

Figure 2.3 illustrates $\Delta \mathrm{EP}/\mathrm{EP}_{1990}$ for values of $\mathrm{s}_{\mathrm{PO_4}}^{\mathrm{P:C}}$ ranging from 0 to 1. We can appreciate a sense of the buffer effect on EP by comparing the red lines (variable P:C, $0 < \mathrm{s}_{\mathrm{PO_4}}^{\mathrm{P:C}} < 1$) to the x axis (perfect buffer case, $\mathrm{s}_{\mathrm{PO_4}}^{\mathrm{P:C}} = 1$) and the 1:1 line (fixed P:C, $\mathrm{s}_{\mathrm{PO_4}}^{\mathrm{P:C}} = 0$). For a change in $\mathrm{PO_4}$, the buffer effect for a variable P:C ($0 < \mathrm{s}_{\mathrm{PO_4}}^{\mathrm{P:C}} < 1$) is given by the difference in the fractional change of EP from that predicted for a fixed P:C ($\mathrm{s}_{\mathrm{PO_4}}^{\mathrm{P:C}} = 0$). The magnitude of the stoichiometric buffer effect increases as $\mathrm{s}_{\mathrm{PO_4}}^{\mathrm{P:C}}$ increases and takes the maximum value when $\mathrm{s}_{\mathrm{PO_4}}^{\mathrm{P:C}}$ equals 1 (perfect buffer).

In a close-up view (Figure 2.3b), the projected changes in surface $\mathrm{PO_4}$ and EP between 1990s and 2090s under RCP8.5 scenario from six different CMIP5 models are overlaid. These models assume constant Redfield P:N:C ratios (see Table 2 of Fu et al., 2016): MPI-ESM-LR, MPI-ESM-MR, IPSL-CM5A-LR, IPSL-CM5A-MR, CESM1(BGC), and NorESM1-ME. The fractional change in surface $\mathrm{PO_4}$ (0 - 100 m) between 1990s and 2090s has a range from -11.3% to -23.9% with geometric mean of -15%. The fractional change in EP from 1990s to 2090s ranges from -9.2% to -18.3% with geometric mean of -14% (Figure 2.3b). The fractional changes in PO4 and EP in the CMIP5 models (i.e., -15%, -14%) are thus nearly the same and consistent with our expectation that fixed ratio models should lie close to the 1:1 line ($\mathrm{s}_{\mathrm{PO_4}}^{\mathrm{P:C}} = 0$).

For the same 15% decrease in $\mathrm{PO_4}$, equation (2.11) would predict the percent change in EP to be -11% to -9% with our estimated $\mathrm{s}_{\mathrm{PO_4}}^{\mathrm{P:C}}$ of 0.3 to 0.4. Taking this prediction at face value, the CMIP5 models with fixed P:N:C are overestimating the reduction in EP from 1990s to 2090s by $\sim$5%. Essentially, this is the stoichiometric buffer (or compensation) effect on carbon EP. We have also shown with the green lines in Figure 2.3 $\Delta \mathrm{EP}/\mathrm{EP}_{1990}$ that GM15 would predict using 1990s global mean surface phosphate concentration of 0.6 μM. In Figure 2.3b, GM15-based prediction closely follows the

contour line of $s^{P:C}_{PO_4} = 0.4$, indicating similar magnitudes of stoichiometric buffer on EP for the future. This first attempt at estimating the buffer effect should be considered preliminary because we assumed that PO_4 is the sole limiting nutrient that drives EP. More realistically, the reduction in EP would also be affected by other limiting nutrients and environmental factors.

2.5 Flexible Stoichiometry in a Global Ocean Model

In our effort to more realistically assess the buffer effect on EP where PO_4 is not the sole driver of EP, we have implemented the new power law model in Minnesota Earth System Model for Ocean Biogeochemistry (Matsumoto, Tokos, Huston, & Joy-Warren 2013; Matsumoto, Tokos, Price, & Cox 2008), a 3-D global ocean model with two functional

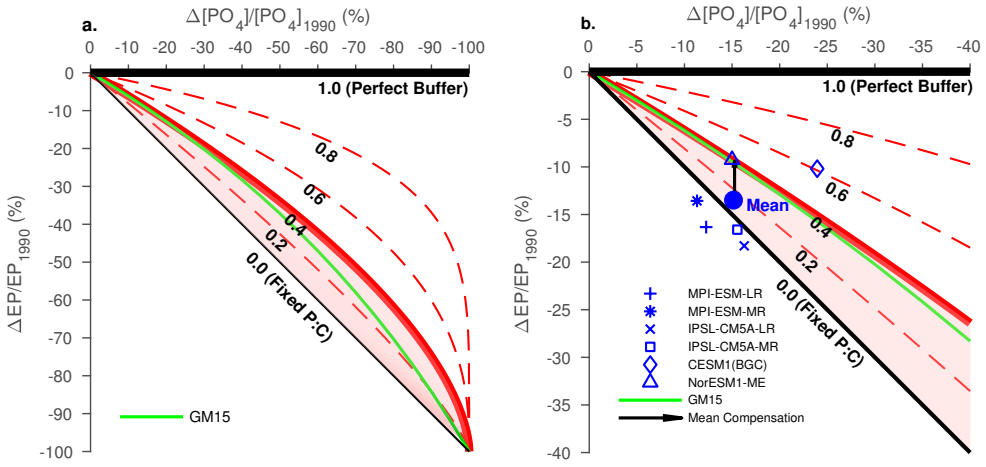

Figure 2.3: Fractional change in EP (%) from 1990s as a function of the fractional change in PO_4 from 1990s (%). (a) Fractional change in EP over different $s^{P:C}_{PO_4}$ values of 0.0, 0.2, 0.4, 0.6, 0.8, and 1.0 according to equation (2.11). Our data-based estimate of $s^{P:C}_{PO_4}$ lies between 0.3 and 0.4 (red shade). The green line is the fractional change in EP predicted from GM15, with 1990s PO_4 concentration of 0.6 μM. (b) Close up of Figure 2.3a with results from each of the six CMIP5 models with fixed P:N:C (W. Fu et al. 2016). The blue dot is the mean fractional change of EP in 2090s relative to 1990s for six CMIP5 models. The mean PO4 change is -15%, and the mean EP change is -14% in 2090s relatives to 1990s. The black arrow shows the mean compensation (buffer effect) on carbon EP of 5%, which is the difference in fractional change of EP predicted by the CMIP5 models and by equation (2.11) with $s^{P:C}_{PO_4}$ of 0.4 for a 15% PO_4 reduction.

phytoplankton types. In the remaining portion of this paper, we will discuss elemental ratio of carbon to nitrogen to phosphorus of POM in terms of C:N:P as well as P:N:C because the former is more commonly used in the context of global biogeochemical cycles.

2.5.1 Model Description

The global ocean model used here is the second version of MESMO (MESMO2, Matsumoto et al. 2013). It is composed of a 3-D dynamical ocean model, an energy-moisture balanced model of the atmosphere, and a 2-D thermodynamic and dynamic model of sea ice. The ocean model has 10°horizontal resolution and 16 vertical levels. Ocean biogeochemistry is driven by two phytoplankton classes (small and large), whose growth is a function of Michaelis-Menten uptake kinetics of colimiting nutrients (P, N, Si, and Fe), light, mixed layer depth, and temperature. EP is calculated at the base of the second vertical layer corresponding to 100 m in water depth. The biogeochemical component of the ocean model is updated 20 times per year or 18.25 days/step.

For this study, two modifications were made to biogeochemical component of the model. First, the small and large phytoplankton have a variable uptake ratio of P:C (hence C:P) as a function of PO4 according to equation (2.3). In order to account for the wide variability in the global P:C data (Figure 2.1) with two phytoplankton classes, their $[P:C]_0$ and $s_{PO_4}^{P:C}$ values have to encompass the global values estimated in section 2. On the basis of confidence intervals calculated for $[P:C]_0$ and $s_{PO_4}^{P:C}$, we assigned a low value of $[P:C]_0$ (= 8.8‰) and a high value of $s_{PO_4}^{P:C}$ (= 0.6) for the small phytoplankton and a high value of $[P:C]_0$ (= 13.0‰) and a low value of $s_{PO_4}^{P:C}$ (= 0.2) for the large phytoplankton (Table 2.2). Although there is no rigorous justification to the choice of these values, both theory (Klausmeier, Litchman, & Levin 2004) and observations (Goldman, McCarthy, & Peavey 1979; Hillebrand et al. 2013) indicate that fast growing, large phytoplankton have less flexibility in their cellular elemental ratio. In addition, large phytoplankton generally have a lower allocation of cellular space to resource acquisition and more on storage (Sterner & Elser 2002), which means that they are likely to be less sensitive to changes in nutrient supply. Further, the choice of reference P:C is based on the observation that small phytoplankton such as Prochlorococcus have lower P:C values than larger phytoplankton such as diatoms in

Table 2.2: Model Parameters for the Preindustrial and Transient Simulation

Biogeochemical model parameters		MESMO2	MESMO2-*Fix*	MESMO2-*Var*
Large Phytoplankton (LP): K_{PO_4}	μmol kg^{-1}	0.39	0.39	0.39
Small Phytoplankton (SP): K_{PO_4}	μmol kg^{-1}	0.03	0.17	0.17
LP: K_{NO_3}	μmol kg^{-1}	5.00	3.00	3.00
SP: K_{NO_3}	μmol kg^{-1}	0.50	0.50	0.50
LP: K_{CO_2}	μmol kg^{-1}	0.925	0.925	0.925
SP: K_{CO_2}	μmol kg^{-1}	0.075	0.075	0.075
LP: K_{Fe}	nmol kg^{-1}	0.1	0.1	0.1
SP: K_{Fe}	nmol kg^{-1}	0.01	0.01	0.01
$K_{Si(OH)_4}$	μmol kg^{-1}	1.00	1.00	1.00
Cond. Stability, ligand-bound Fe		1.25	1.25	1.25
Fe scavenging rate by POC		0.7	0.7	0.7
Particle sinking speed	m d^{-1}	30	20	20
Maximum C:Fe		200000	200000	200000
Minimum C:P		-	-	26.6
Maximum C:P		-	-	546.7
C:P		117	117	Variable
C:N		117/16	117/16	7.06
N:P		16	16	Variable
O_2:P		-170	-170	-170
Power law model parameters				
LP: $s_{PO_4}^{P:C}$		-	-	0.2
SP: $s_{PO_4}^{P:C}$		-	-	0.6
LP: $[P:C]_0$	‰	-	-	13.0
SP: $[P:C]_0$	‰	-	-	8.8
LP: $[PO_4]_0$	μmol kg^{-1}	-	-	1.0
SP: $[PO_4]_0$	μmol kg^{-1}	-	-	1.0

low phosphate environments (Martiny, Pham, et al. 2013). We also impose a minimum P:C of 1.83‰ (C:P of 546.7) and a maximum P:C of 37.7‰ (C:P of 26.6), which are the lower and upper confidence intervals of observed P:C, respectively (Martiny, Pham, et al. 2013). This assumption is necessary to keep calculated P:C within a reasonable range at both very low and very high PO_4. We refer to this version of MESMO2, enabled with the power law model of flexible stoichiometry, as MESMO2-*Var*. With these choices for the small and large phytoplankton classes, MESMO2-*Var*'s EP-weighted global average $s_{PO_4}^{P:C}$ is 0.38 (Figure 2.4), which is close to our global estimate value of $0.3 \sim 0.4$. C:N is fixed to a global mean 7.06 (Martiny, Vrugt, et al. 2013), and N:P is therefore calculated by dividing C:P by C:N. For comparison, we also have MESMO2 with fixed C:N:P stoichiometry, MESMO2-*Fix*.

The second modification to MESMO2 is a simple model of nitrogen fixation and denitrification. In order to simulate the effect of N-fixation, we have added nitrate directly proportional to the amount of dust input, which is derived from the projected atmospheric depositional flux field by Mahowald et al. (1999). The total global annual N-fixation is 140 TgN yr^{-1} and is consistent with the global estimation by Gruber and Galloway (2008). Simple denitrification is simulated in MESMO2-*Var* and MESMO2-*Fix* by removing nitrate at depths where the oxygen concentration is lowest. The addition and removal of nitrate is balanced globally so as to conserve the oceanic nitrogen inventory. To account for these two changes in biogeochemistry, half-saturation constants of Michaelis-Menten kinetics were slightly modified from MESMO2 (Table 2.2). Nutrient limitation under preindustrial condition for MESMO2-*Var* is shown in Figure 2.5. It reveals a more widespread iron limitation for small phytoplankton in North Atlantic and South Pacific subtropical gyres than other biogeochemical models such as BEC (J. K. Moore et al. 2004). This is largely due to the effect of simplified N cycling schemes and a more robust representation of the ecosystem, and the marine nitrogen cycle will likely improve preindustrial runs for MESMO2-*Var*. In particular, a more robust method for prescribing biological nitrogen fixation (e.g., Luo, Lima, Karl, Deutsch, & Doney 2014) is needed to be explored in the future simulation studies.

The preindustrial equilibrium state of MESMO2 serves as the starting point of the

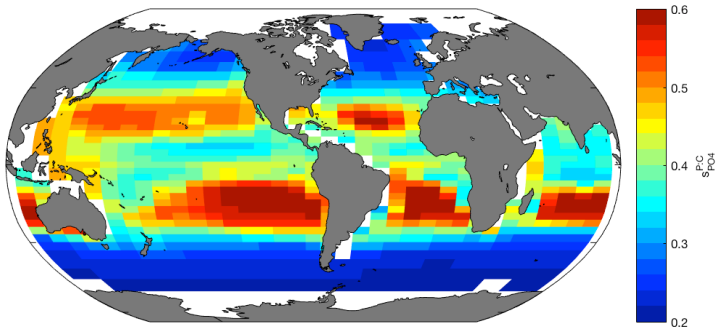

Figure 2.4: Community $s^{P:C}_{PO_4}$ under preindustrial condition with MESMO2-*Var* calculated by taking EP-weighted mean of small phytoplankton $s^{P:C}_{PO_4}$ (= 0.6) and large phytoplankton $s^{P:C}_{PO_4}$ (= 0.2).

experiments. After 3,000 years of spin-up run under preindustrial pCO_2, the average C:N:P ratio in the upper 50 m is 169:24:1 and the EP-weighted average is 103:15:1 in MESMO2-*Var* (Table 2.3). Community C:P and N:P ratios are elevated in the subtropical gyres and are low in the nutrient-rich regions (with the maximum C:P and N:P of 323 and 46, respectively, in the phosphorus-depleted North Atlantic subtropical gyres; Figures 2.6a and 2.6e). These high values are consistent with observations (Martiny, Pham, et al. 2013). The model also gives higher C:P and N:P values in the Atlantic Ocean than in the Pacific Ocean. This interbasin asymmetry is a result of lower phosphorus concentrations in the Atlantic (Figure A.1 in the Appendix A) and consistent with results from a recent inverse modeling study (Teng et al. 2014). Small phytoplankton have more elevated C:N:P (average of 221:31:1) than large phytoplankton (average of 95:13:1). The disparity is largest in the subtropical gyres and smallest in the nutrient rich regions such as the Southern Ocean.

Steady state global annual EP of MESMO2-*Fix* is 11.95 PgC yr^{-1}, while that of MESMO2-*Var* is 11.99 PgC yr^{-1}. These two values are consistent with estimated values of $9 \sim 13$ PgC yr^{-1} (Laws, Ducklow, & McCarthy 2000; Schlitzer 2004). The maximum difference in the zonally average total EP of carbon between MESMO2-*Var* and MESMO2-*Fix* occurs at 20°N (i.e., 1.20 PgC yr^{-1} with MESMO2-*Fix* and 1.38 PgC yr^{-1} with MESMO2-*Var*) (Figure A.2a). For small phytoplankton, EP of carbon at 35°N in MESMO2-*Var* is 45% greater than MESMO2-*Fix* (Figure A.2b), a consequence of significantly elevated C:P ratio in the former model over the latter.

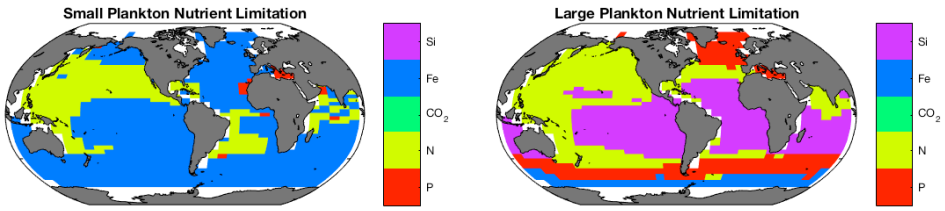

Figure 2.5: Nutrient limitation under preindustrial condition with MESMO2-*Var* in the surface layer (0-50 m). Nutrient limitation for (a) small phytoplankton and (b) large phytoplankton during the time step with highest productivity within an annual seasonal cycle.

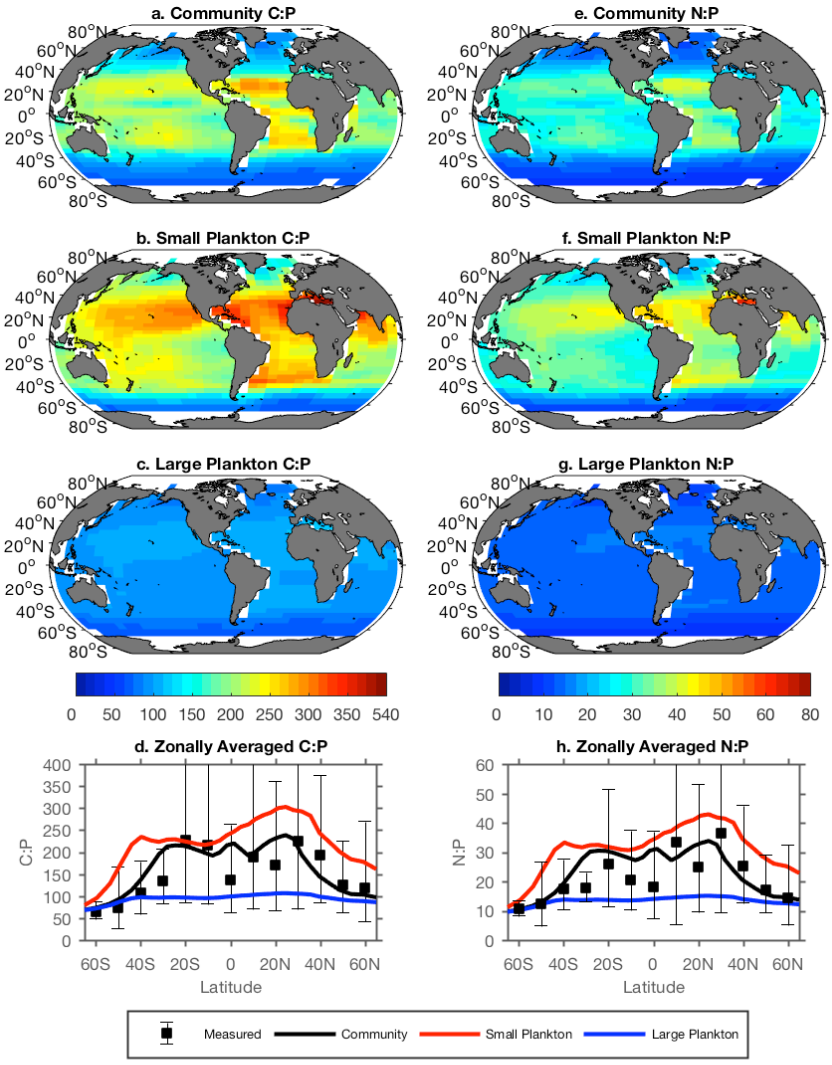

Figure 2.6: Modeled C:P and N:P of phytoplankton in the surface (0-50 m) layer. (a) Modeled C:P of community, (b) small phytoplankton, and (c) large phytoplankton. (d) Zonally averaged C:P ratio. (e) Modeled N:P of community, (f) small phytoplankton, and (g) large phytoplankton calculated by diving C:P by a fixed C:N value of 7.06. (h) Zonally averaged N: P ratio. Community C:P and N:P are export production-weighted average of small phytoplankton and large phytoplankton C:P and N:P, respectively. The black squares in Figures 2.6d and 2.6h are measured C:P and N:P of particulate organic matter in the top 50 m binned by the latitudes (Martiny, Pham, et al. 2013). The error bars indicate 95% confidence intervals for the measured C:P and N:P ratios.

2.5.2 Model Results

Postindustrial transient experiments with both models were carried out from 1765 to 2100 with the pCO_2 value obtained from observations between 1765 to 2005 and IPCC RCP8.5 scenario for 2006 to 2100 (Meinshausen et al. 2011). In these models, CO_2 radiative feedback drives global warming, which stratifies the water column so that global mean surface PO_4 decreases by 9% in both models by the 2090s relative to the 1990s. As previously seen in MESMO under global warming (Matsumoto, Tokos, Chikamoto, & Ridgwell 2010), stratification is strongest in the Southern Ocean and subpolar North Atlantic, where surface PO_4 is reduced by as much as 50% (Figures 2.7a and 2.7c). In MESMO2-*Var*, the global average surface C:P of POM concurrently increased by 4% from 171:1 in 1990s to 178:1 in 2090s reflecting both the increase in the cellular stoichiometry of phytoplankton and a community shift toward smaller phytoplankton with higher C:P (Figures 2.8b and 2.8c).

In both MESMO2-*Var* and MESMO2-*Fix*, the global EP decreases under global

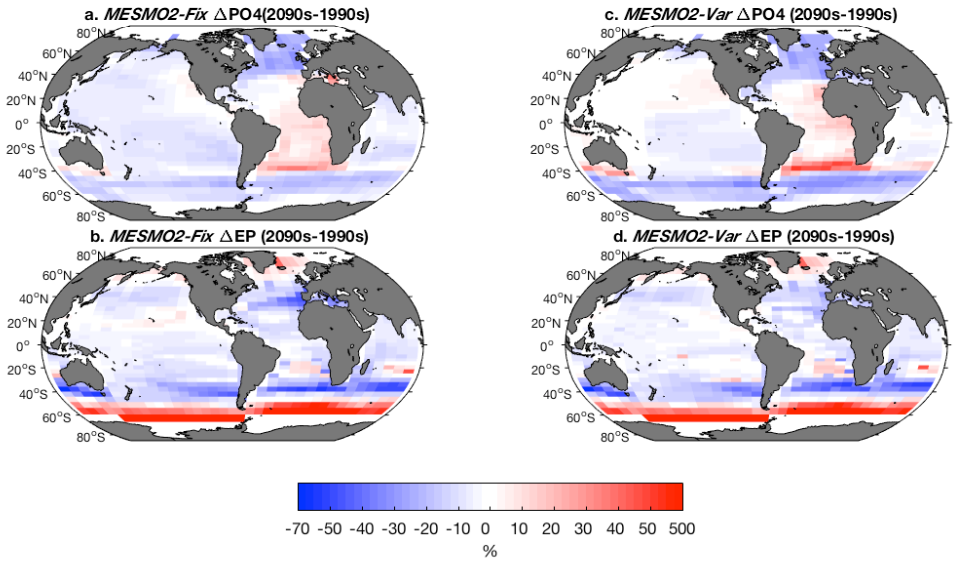

Figure 2.7: Simulated fractional changes in surface PO_4 (0-100 m) and total EP in 2090s relative to 1990s with (a and b) MESMO2-*Fix* and (c and d) MESMO2-*Var* under RCP8.5 scenario. Fractional change in EP was calculated for the regions where annual mean EP was greater than or equal to 0.2 mol C m^{-2} in 1990s (i.e., not completely covered by sea ice) to avoid having exceedingly large fractional change.

Table 2.3: Model Results for the Preindustrial and Transient Simulations

	MESMO2-*Fix*	MESMO2-*Var*
Simulation ID#		
Preindustrial (Annual)	161220d	170108a
Preindustrial (Seasonal)	170109b	170109a
Transient	170207a	170207b
PO_4 (0-100 m) (μmol kg^{-1})		
Preindustrial	0.65	0.54
1990s	0.64	0.52
2090s	0.58	0.47
Total EP (PgC yr^{-1})		
Preindustrial	11.95	11.99
1990s	11.80	11.87
2090s	11.44	11.59
Small Plankton EP (PgC yr^{-1})		
Preindustrial	4.08	4.47
1990s	4.09	4.48
2090s	4.11	4.55
Large Plankton EP (PgC yr^{-1})		
Preindustrial	7.87	7.52
1990s	7.71	7.39
2090s	7.33	7.04
Community C:N:P (0-50 m)		
Preindustrial		169:24:1
1990s	117:16:1	171:24:1
2090s		178:25:1
Community C:N:P (EP-weighted)		
Preindustrial		103:15:1
1990s	117:16:1	104:15:1
2090s		105:15:1
Small Plankton C:N:P (0-50 m)		
Preindustrial		221:31:1
1990s	117:16:1	223:32:1
2090s		229:32:1
Small Plankton C:N:P (EP-weighted)		
Preindustrial		192:27:1
1990s	117:16:1	192:27:1
2090s		193:27:1
Large Plankton C:N:P (0-50 m)		
Preindustrial		95:13:1
1990s	117:16:1	95:13:1
2090s		96:14:1
Large Plankton C:N:P (EP-weighted)		
Preindustrial		85:12:1
1990s	117:16:1	85:12:1
2090s		85:12:1

warming as upper ocean stratification reduces nutrient supply (Figures 2.7b and 2.7d). However, the global EP reduction by 2090s ($\sim 3\%$ decrease) for both MESMO2-*Var* and MESMO2-*Fix* is less than that predicted by equation (2.11) for the simulated drop in surface ocean PO_4 concentration by 9% globally. As noted above, this underestimation of EP for a given change in PO_4 is expected because PO_4 is not the sole driver of EP. Indeed, in our simulations, PO_4 is not limiting nor decreasing everywhere (Figures 2.5, 2.7a, and 2.7c). Further, biological production in the polar regions is affected greatly by sea ice; EP increases by up to 500% from 1990s by year 2100 as sea ice retreats (Figures 2.7b and 2.7d). In MESMO2, two other processes that can offset EP reduction due to stratification include shoaling of the mixed layer depth and warming-induced enhancement of biological production rates (Matsumoto et al., 2010). All these factors likely contributed to the smaller than expected global EP reduction in both MESMO2-*Var* and MESMO2-*Fix*.

The simulated total stoichiometric buffer effect due to flexible C:P in 2090s (i.e., carbon EP difference between MESMO2-*Var* and MESMO2-*Fix*) is 0.7% globally (Figure 2.8a and Table 2.3), which is smaller than the buffer effect of 3% that would be expected for a 9% reduction in PO_4 with a global mean $s_{PO_4}^{P:C}$ of 0.4. This underestimation can be explained by two reasons. First, the simulated reduction in global EP (-3%) is significantly smaller than expected from our simple theory (-9%), because as already noted, PO_4 is not the sole driver of EP. For example, PO_4 becomes less important as a limiting nutrient in the North Pacific and South Atlantic gyres. As a result, surface PO_4 accumulates in these waters and leads to lower C:P (i.e., negative buffer effect). Second, as sea ice retreats, large phytoplankton in high-latitude waters make a greater contribution to the global EP in MESMO2-*Var* (Figure 2.4). The C:P ratio of large phytoplankton with low $s_{PO_4}^{P:C}$ increases minimally during the future transient simulation (Figure 2.8d).

In other regions such as the North Atlantic and South Pacific gyres, the stoichiometry buffer effect on carbon EP reaches up to 40% (Figure 2.8a). These areas experience both an increase in C:P ratios in each phytoplankton type as well as an increase in relative abundance of small phytoplankton. Globally, the stoichiometry buffer effect in these high C:P, high $s_{PO_4}^{P:C}$, low productivity regions (e.g., subtropical North Atlantic) is being offset by more highly productive, lower C:P and lower $s_{PO_4}^{P:C}$ regions (e.g., Southern

Ocean) and by the negatively compensated regions where surface PO_4 increases (e.g., North Pacific gyre). The results presented here qualitatively illustrate the importance of stoichiometric buffer effect on carbon EP in certain regions for the future global warming scenario. However, the result presented here is preliminary, and further exploration is possibly needed with a more sophisticated nitrogen cycling scheme and ecosystem model in order to give a robust quantitative prediction.

2.6 Conclusions

Quantifying the effects of flexible elemental stoichiometry of POM on global carbon cycles is essential for understanding past, present, and future marine ecosystems. In this effort, we developed a simple power law model with $s_{PO_4}^{P:C}$, a sensitivity factor, for

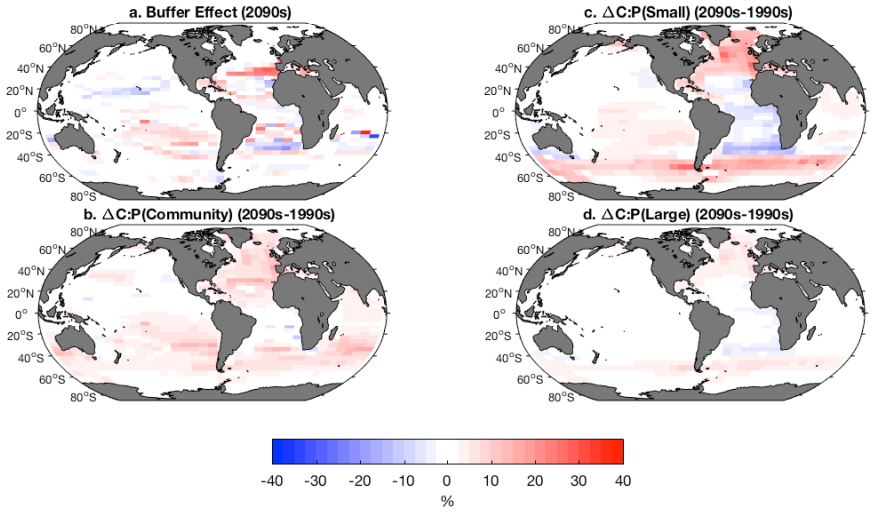

Figure 2.8: Results from a global ocean model under IPCC RCP8.5 scenario. (a) Stoichiometric buffer effect on carbon EP in 2090s, which is the difference between the fractional change of EP with MESMO2-*Var* (Figure 2.7d) and the fractional change of EP with MESMO2-*Fix* (Figure 2.7b). Positive value indicates positive buffer effect (i.e., smaller reduction in EP for MESMO2-*Var* with respect to MESMO2-*Fix*), while the negative value indicates negative buffer effect (smaller increase in EP for MESMO2-*Var* with respect to MESMO2-*Fix*). (b-d) Percent change of community C:P, small phytoplankton C:P, and large phytoplankton C:P at the export layer (50-100 m) in 2090s relative to 1990s with MESMO2-*Var*.

how much the P:C ratio of POM changes in response to PO_4. This power law formulation is similar to the linear fit of GM15 but predicts saturating P:C at high PO_4 and rapidly rising P:C at low PO_4. The nonlinear, saturating behavior of our formulation has a biological underpinning, but the small number of available observations today cannot distinguish it from the linear model. Future field work that better constrains community P:C would be very useful.

We used the new sensitivity factor to derive first-order estimations of how changes in stoichiometry can buffer against or compensate for the reduction in carbon EP expected under ongoing global change. We also implemented the new factor in a 3-D global ocean model and showed that the effects of incorporating flexible stoichiometry are globally modest but regionally significant. We pose a testable hypothesis that both the plasticity of cellular stoichiometry and phytoplankton community composition contribute to the strong buffer effect in areas such North Atlantic. Conversely, buffer effect is expected to be minimal in areas dominated by large phytoplankton with low $s_{PO_4}^{P:C}$ (e.g., Southern Ocean) or areas where surface PO_4 becomes less limiting. Our study focused on only the importance of PO_4 in driving future EP changes. A more complete understanding would require further investigations into the role of other limiting nutrients and environmental factors. Our power law model of flexible stoichiometry may be very useful in this effort because it can be extended to include dependence on other environmental factors such as light and temperature. Furthermore, our approach represents a simple, promising strategy to incorporate flexible elemental stoichiometry in global ocean models. Our new model of stoichiometry thus holds promise in linking laboratory based analysis, macroecological understanding of elemental stoichiometry, and the global carbon cycle.

2.7 Acknowledgments

I thank K. Tokos for technical assistance with MESMO. A.C. Martiny provided us useful comments and ideas during a visit to the University of Minnesota in September 2016. E. Galbraith and an anonymous reviewer provided useful suggestions and comments. Numerical simulations were carried out at the Minnesota Supercomputing Institute (MSI) at the University of Minnesota.

Chapter 3

Environmental drivers of phytoplankton stoichiometry: a meta-analysis

The contents of this section is under preparation for submission to the journal *Biogeosciences* under the title 'A meta-analysis on environmental drivers of marine phytoplankton C:N:P'.

3.1 Synopsis

The elemental stoichiometry of marine phytoplankton plays a critical role in global carbon cycle through carbon export. Although extensive laboratory experiments have been carried out over the years to assess the influence of different environmental drivers on elemental composition of phytoplankton, a comprehensive quantitative assessment of the processes is still lacking. Here, we synthesized the responses of P:C and N:C ratios of marine phytoplankton to five major drivers (phosphate and nitrate, irradiance, temperature, and iron) by meta-analysis of laboratory experimental data available in the literature. Overall, our findings highlight the high stoichiometric plasticity of diatoms and importance of macronutrients in determining P:C and N:C ratios, which both provide us insights on how to understand and model plankton diversity and productivity.

3.2 Introduction

Elemental stoichiometry of biological production in the surface ocean plays a crucial role in cycling of elements in the global ocean. The elemental ratio between carbon and the key limiting macronutrients, nitrogen (N) and phosphorus (P), in exported organic matter expressed in terms of C:N:P ratio helps determine how much atmospheric carbon is sequestered in the deep ocean with respect to the availability of limiting nutrients. On geologic timescale, N:P ratio reflects the relative availability of nitrate with respect to phosphate, both of which are externally supplied from atmosphere via nitrogen-fixation and/or continents via river supply (Broecker 1982; Lenton & Watson 2000; Redfield 1958; Tyrrell 1999). On shorter timescales the average stoichiometry of exported bulk organic matter reflects elemental stoichiometry of phytoplankton (Bonachela et al. 2016; C. A. Garcia et al. 2018; Martiny, Pham, et al. 2013) with additional influences of biological diversity and secondary processing of organic matter by zooplankton and heterotrophic bacteria. In the face of global change, understanding and quantifying the mechanisms that leads to variability in C:N:P ratio are crucial in order to have an accurate projection of future climate change.

A key unresolved question is what determines C:N:P of individual phytoplankton? Phytoplankton grow in the upper light-lit layer of the ocean where the amount of inorganic nutrients, light, and temperature vary spatially and temporally. Laboratory studies show that these fluctuations trigger responses at the cellular level, whereby cells modify resource allocation in order to adapt optimally to their ambient environment (Geider & La Roche 2002; Moreno & Martiny 2018). For example, phytoplankton may alter resource allocation between P-rich biosynthetic apparatus, N-rich light-harvesting apparatus, and C-rich energy storage reserves. Under a typical future warming scenario, the global ocean is expected to undergo changes in nutrient availability, temperature, and irradiance (Boyd, Strzepek, Fu, & Hutchins 2010). These changes are likely to have profound effects on physiology of phytoplankton (Finkel et al. 2010; van de Waal, Verschoor, Verspagen, van Donk, & Huisman 2010) and observations show that competitive phytoplankton species are able to acclimate and adapt to changes in temperature, irradiance, and nutrients on decadal timescales (Irwin, Finkel, Müller-Karger, & Troccoli Ghinaglia 2015). Over 100 laboratory and field experiments have been conducted thus

far to study the relationship between C:N:P ratio of phytoplankton and environmental drivers. It is however challenging to synthesize those studies and generalize the response of phytoplankton C:N:P to changes in environmental drivers. One reason for the challenge is that the acclimation and adaptation strategies as well as genetic composition differ amongst different species, and so the response of phytoplankton differs by species even if the experiment is conducted at otherwise identical conditions. In addition, individual studies employ different sets of statistical analyses to characterize effects of environmental driver(s) on elemental ratios, ranging from a simple t-test to more complex mixed models, which makes interstudy comparisons challenging.

Meta-analysis/systematic-review is a powerful statistical framework for synthesizing and integrating research results obtained from independent studies and for uncovering general trends (Gurevitch, Koricheva, Nakagawa, & Stewart 2018). It has a number of advantages over narrative review and "vote counting" because it compares the common measure of outcome (effect size) that includes information on both the sign and magnitude of an effect of interest from each study. Effect size from individual studies can be combined across studies to estimate the grand mean effect size and its confidence interval, which are then used to test whether overall effect is statistically significant. In addition, with its comprehensive and rigorous procedure for study inclusion criteria, meta-analysis avoids the pitfall of "cherry-picking" data aimed toward supporting particular hypothesis.

We present results from a systematic literature review and subsequent meta-analysis to quantify how five key environmental drivers affect P:C and N:C ratios of marine phytoplankton. Unlike previous meta-analyses on elemental stoichiometry of phytoplankton that strictly synthesized the effect of a single environmental driver, our study assessed the effects of five drivers, specifically for marine phytoplankton species. Importantly, we use a unique newly defined measure of effect size, a *stoichiometry sensitivity factor* (Tanioka & Matsumoto 2017), which is a dimensionless parameter that relates fractional change in P:C or N:C with a fractional change in a particular environmental driver, while the other drivers are kept constant. The five environmental drivers are: (1) phosphate, (2) nitrate, (3) irradiance, (4) temperature, and (5) iron. These are the top drivers of open-ocean phytoplankton group (Boyd et al., 2010). Although CO_2 is

another potentially important driver, we did not consider the effects of CO_2 on elemental ratios as a previous meta-analysis study showed that no generalization can be made with respect to the direction of trends in P:C or N:C ratios as a function of CO_2 concentration (Liu, Weinbauer, Maier, Dai, & Gattuso 2010). We systematically screened peer-reviewed publications on monoculture laboratory experiment studies, which isolate the effect of a specific driver from other confounding drivers. We compute effect size for each driver-stoichiometry pair from independent studies and subsequently determine the grand mean across all studies to quantify the effectiveness of each driver on P:C and N:C ratios. Further, we compare grand mean effect size for different major phytoplankton groups for detecting any systematic variability between phytoplankton groups.

3.3 Materials and Methods

3.3.1 Bibliographic search and screening

We selected experimental studies that assessed the effects of nutrients (dissolved inorganic phosphorus, dissolved inorganic nitrogen, iron), irradiance, and temperature on P:C and N:C ratios of marine phytoplankton. In order to compute stoichiometric sensitivity factors (section 3.3.2), we selected experiments conducted over at least three different levels of the driver of interest while other driver values are kept constant. Firstly, we conducted a literature search using Web of Science (last accessed in February 2019) with the following sequence of key terms: (TS=(phytoplankton OR algae OR microalgae OR diatom OR coccolithophore* OR cyanobacteri* OR diazotroph*) AND TS=(stoichiometr* OR "chemical composition" OR "element* composition" OR "nutritional quality" OR "nutrient composition" OR "nutrient content" OR "nutrient ratio*" OR C:N OR C:P OR N:P OR P:C OR N:C OR "cellular stoichiometr*" OR C:N:P OR "element* ratio*" OR "food qualit*" OR "nutrient concentration" OR "carbon budget") AND TS = (phosph* OR "phosph* limit*" OR nitr* OR "nitr* limit*" OR iron OR "iron limit*" OR nutrient OR "nutrient limit*" OR "nutrient supply" OR "nutrient availabilit*" OR "supply ratio*" OR eutrophication OR fertili* OR enrichment OR temperature OR warming OR light OR irradiance OR "light limit*") AND TS = (marine or sea or ocean OR seawater OR aquatic)). This search yielded 4899

hits. We also closely inspected all the primary studies mentioned in the 8 recent review papers including meta-analyses studies on elemental stoichiometry of phytoplankton in aquatic environment (Flynn et al. 2010; Geider & La Roche 2002; Hillebrand et al. 2013; Moreno & Martiny 2018; Persson et al. 2010; Thrane, Hessen, & Andersen 2016; Villar-Argaiz, Medina-Sánchez, Biddanda, & Carrillo 2018; Yvon-Durocher et al. 2015). The list is also augmented with data from additional four studies that did not appear in the literature search or in the review papers but were cited in the original studies. Subsequent selection processes based on abstracts, graphs, tables, and full text, and removal of duplicates led to a total of 64 papers (Figure 3.1; Appendix B: Table B.1). The N:C and P:C ratios were extracted with use of GraphClick (Arizona Software, 2010) to read off values from graphs when necessary. In cases where N:P and only one of either P:C or N:C is provided, the remaining ratio is determined by either multiplying or dividing by N:P. Similarly, elemental ratios are computed from the measurements of

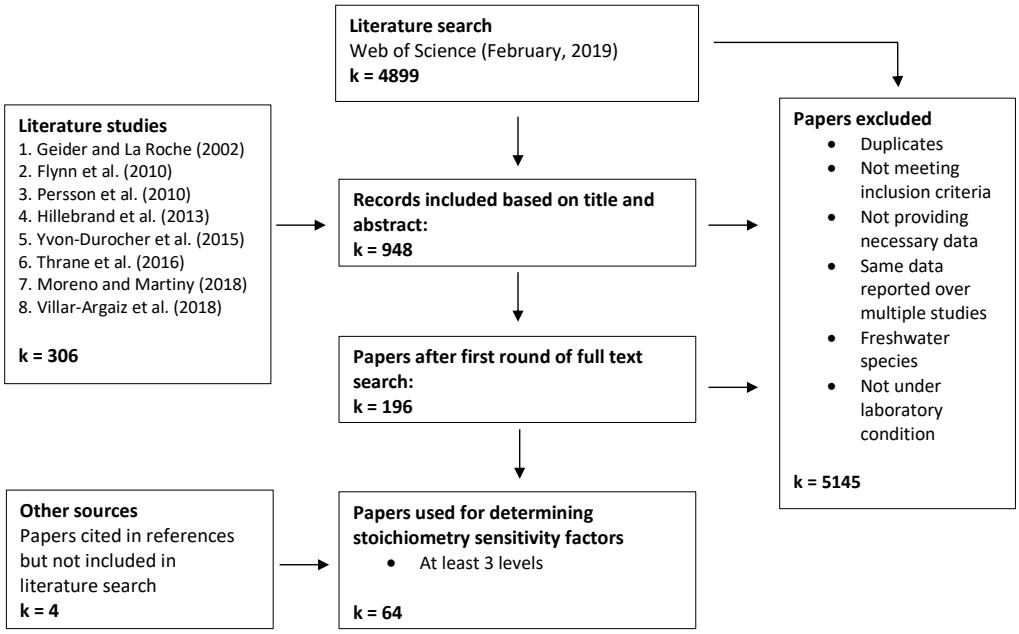

Figure 3.1: Flow chart showing (1) the preliminary selection criteria and (2) the refined selection criteria used for determining s-factors. Numbers (k values) correspond to the number of studies selected or rejected. See Appendix B (Table B.1) for a list of studies included in the meta-analysis.

Table 3.1: Breakdown of the number of experimental units for environmental driver-stoichiometry pairs for P:C and N:C.

Driver	P:C				N:C			
	Diatoms	Eukaryotes	Cyanobacteria	Total	Diatoms	Eukaryotes	Cyanobacteria	Total
P	2	3	3	8	2	3	3	8
N	2	1	0	3	8	4	1	13
NO_3/PO_4	4	12	1	17	5	15	1	21
I	10	5	2	17	45	9	5	59
T	13	9	12	32	24	15	15	54
Fe	1	0	1	2	7	0	3	10
Total	32	30	19	81	91	46	28	165

phytoplankton POC, PON, and POP when the ratios are not explicitly given in the original studies. When more than two factors were manipulated in the same studies, multiple experimental units are extracted. Here, experimental unit refers to a controlled experiment of stoichiometry of a phytoplankton species under some growth conditions (e.g., nutrients, temperature, irradiance) with a minimum of three levels of independent variable. The only exception was when the additional driver was CO_2, and in this case we utilized responses to each driver at the ambient or control CO_2 level. We only considered experimental monoculture studies of marine phytoplankton species to isolate the effects of specific environmental driver from other confounding drivers that cannot be controlled in the field. When the species habitat was not noted in the original study, AlgaeBase (`www.algaebase.org`) was used to determine whether the species is marine or freshwater species. Our final dataset consists of 81 experimental units of P:C and 165 experimental units of N:C from 64 studies encompassing 7 taxonomic phyla (Bacillariophyta, Chlorophyta, Cryptophyta, Cyanobacteria, Haptophyta, Miozoa, and Ochrophyta) (Table 3.1).

3.3.2 Stoichiometry sensitivity factor as effect size

The effect size in this study is the stoichiometry sensitivity factor s_Y^X (Tanioka & Matsumoto 2017), which relates a fractional change in a stoichiometry (response variable

X) to a fractional change in environmental driver (variable Y):

$$s_Y^X = \frac{\partial X/X}{\partial Y/Y} = \frac{\partial \ln X}{\partial \ln Y} \tag{3.1}$$

where the partial differentials indicate that other factors are kept constant. For convenience, we use the term "s-factor" in the rest of this paper when describing s_Y^X in a generic sense. In essence, the magnitude of s-factor is a measure of how sensitive X (P:C or N:C) is to a change in stressor level Y, and the sign indicates whether X changes in the same direction as Y (positive sign) or in the opposite direction to Y (negative sign). The s-factor allows for different kinds of response: a linear response of X with respect to Y ($s_Y^X = 1$), a near hyperbolic response that saturates at high X ($0 < s_Y^X < 1$), an exponential response ($1 < |s_Y^X|$), and the null response ($s_Y^X = 0$). Importantly, an advantage of using s_Y^X as effect size is that its magnitude is a direct measure of the strength of interaction over range of stressor values as opposed to measures such as Hedge's d and log response ratio which only compares the effect of stressor on two end point values (control and treatment). Further, ability of s_Y^X to describe nonlinear, saturating behavior often displayed in biological and chemical systems is more realistic than a simple linear regression.

3.3.3 Meta-analysis

Stoichiometry s-factor and its standard error for each individual experiment unit are obtained by carrying out linear regression on the log-transformed X and Y. When using temperature as the environmental driver, we converted degrees Celsius into absolute temperature scale Kelvin. In analyzing iron manipulation experiments, we computed stoichiometry s-factor with respect to change in biologically available free dissolved inorganic iron concentration (Fe'). We estimated Fe' from total dissolved iron concentration, temperature, irradiance, and pH (Sunda & Huntsman 2003) when iron availability in the original research is provided in terms of total dissolved iron concentration instead of Fe'. For calculating s-factors for PO_4 ($s_{PO_4}^{P:C}$and $s_{PO_4}^{N:C}$), we only selected experiments where NO_3 concentrations are kept constant. The same was true for calculating dependency on NO_3 ($s_{NO_3}^{P:C}$and $s_{NO_3}^{N:C}$). We defined s-factors separately ($s_{NP}^{P:C}$and $s_{NP}^{N:C}$) for studies where both PO_4 and NO_3 are manipulated simultaneously to adjust the N:P supply ratio.

We summarized s-factors by a random-effects model meta-analysis to determine the weighted mean s-factor using the *metafor* R package (Viechtbauer 2010). For each environmental driver-stoichiometry pair, we conducted an overall meta-analysis across all the studies (where $n \geq 5$) as well as meta-analysis within 3 plankton functional types (PFT) as a categorical moderator. To calculate the PFT averaged s-factors, we fitted separate random-effects model within each level of PFT. A Wald-type test (Viechtbauer 2010) was used to test whether mean s-factors are statistically different from each other. PFTs classified in our study are diatoms (Bacillariophyta), eukaryotes excluding diatoms, and cyanobacteria. This classification is chosen in order to give a relatively balanced distribution of studies and power across moderator categories. Similar classification of PFTs are commonly employed in the global ocean biochemical models (e.g., Dunne et al. 2013; Ilyina et al. 2013; J. K. Moore et al. 2004). All the statistical analyses were performed with R v3.5.2 (R Core Team 2018) and the codes of the functions used to run all the analyses are available in the Zenodo data repository (`https://doi.org/10.5281/zenodo.3515471`).

3.4 Results

We present s-factors for each of the five environmental factors and discuss whether the s-factors obtained are: (1) consistent or mixed signs across studies and across PFTs; (2) positive or negative sign; and (3) significantly different from 0. The summary of s-factors for each driver-stoichiometry pair is provided in Table 3.2.

3.4.1 Effects of Phosphate

The response of P:C ratio to changes in phosphate was consistent, positive, and significant across studies (Figure 3.2a) where increase in PO_4 lead to higher P:C ratios. Diatoms have the largest stoichiometric flexibility ($s^{P:C}_{PO_4} = 0.75 \pm 0.08, n = 2,\ p < 0.0001$) followed by eukaryotes ($s^{P:C}_{PO_4} = 0.39 \pm 0.06,\ n = 3,\ p < 0.0001$) and cyanobacteria ($s^{P:C}_{PO_4} = 0.29 \pm 0.04,\ n = 3,\ p < 0.0001$). The overall mean $s^{P:C}_{PO_4}$ across all the studies is 0.43 ± 0.09 ($n = 8,\ p < 0.0001$), which means that on average P:C ratio of phytoplankton changes by 0.43% for every 1% change in PO_4 concentration. On the other hand, the effect of phosphate on N:C was weak and not significant overall ($s^{N:C}_{PO_4} =$

$0.02 \pm 0.02, \mathrm{n} = 8,\ \mathrm{p} = 0.4$) where the magnitudes of s-factors are less than 0.10 in all but one experimental unit.

3.4.2 Effects of Nitrate

The response of N:C to changes in NO_3 was similar to the response of P:C to PO_4 changes and was consistent, positive, and significant. An increase in NO_3 lead to higher N:C ratios with the statistically significant overall mean s-factor of 0.20 ± 0.03 ($\mathrm{n} = 13,\ \mathrm{p} < 0.0001$) (Figure 3.2b). This result indicates that NO_3 is one of the primary drivers of N:C. Again, diatoms are the most sensitive PFT with the highest s-factor ($s^{N:C}_{NO_3} = 0.22 \pm 0.04, \mathrm{n} = 8,\ \mathrm{p} < 0.0001$), followed by eukaryotes ($s^{N:C}_{NO_3} = 0.17 \pm 0.04, \mathrm{n} = 4,\ \mathrm{p} < 0.0001$). The s-factor for cyanobacteria is negative ($s^{N:C}_{NO_3} = -0.12 \pm 0.18$) but the sample size is minimal ($\mathrm{n} = 1$). There were not enough observations ($\mathrm{n} < 5$) to conduct meta-analysis on the effects of nitrate on P:C but our analysis shows that s-factors are positive for both diatoms and eukaryotes.

3.4.3 Effects of Nitrate:Phosphate supply ratio

An increase in NO_3:PO_4 supply ratio increases P limitation and decreases N limitation. As anticipated from the two previous subsections, increase in NO_3:PO_4 resulted in lower P:C and increased N:C with negative mean $s^{P:C}_{NP}$ of -0.30 ± 0.04 ($\mathrm{n} = 17,\ \mathrm{p} < 0.0001$) and positive mean $s^{N:C}_{NP}$ of 0.09 ± 0.03 ($\mathrm{n} = 21,\ \mathrm{p} = 0.0002$) (Figure 3.2c). Diatoms have the largest mean s-factor out of the 3 PFTs with $s^{P:C}_{NP}$ and $s^{N:C}_{NP}$ of -0.41 ± 0.08 ($\mathrm{n} = 4,\ \mathrm{p} < 0.0001$) and 0.12 ± 0.02 ($\mathrm{n} = 5,\ \mathrm{p} < 0.0001$) respectively. Overall, the magnitudes of $s^{P:C}_{NP}$ consistently exceed those of $s^{N:C}_{NP}$ which suggests that P:C is more plastic than N:C with respect to changes in N:P supply ratio.

3.4.4 Effects of Irradiance

The response of P:C to changes in irradiance was not consistent or statistically significant overall (Figure 3.3). The mean $s^{P:C}_{I}$ across all studies and across each PFT are not statistically different from 0, reflecting the weak and mixed responses. N:C ratio meanwhile showed weak but consistent responses where increase in irradiance lead to lower N:C, giving negative $s^{N:C}_{I}$ overall ($s^{N:C}_{I} = -0.05 \pm 0.01, \mathrm{n} = 59,\ \mathrm{p} < 0.0001$). Mean

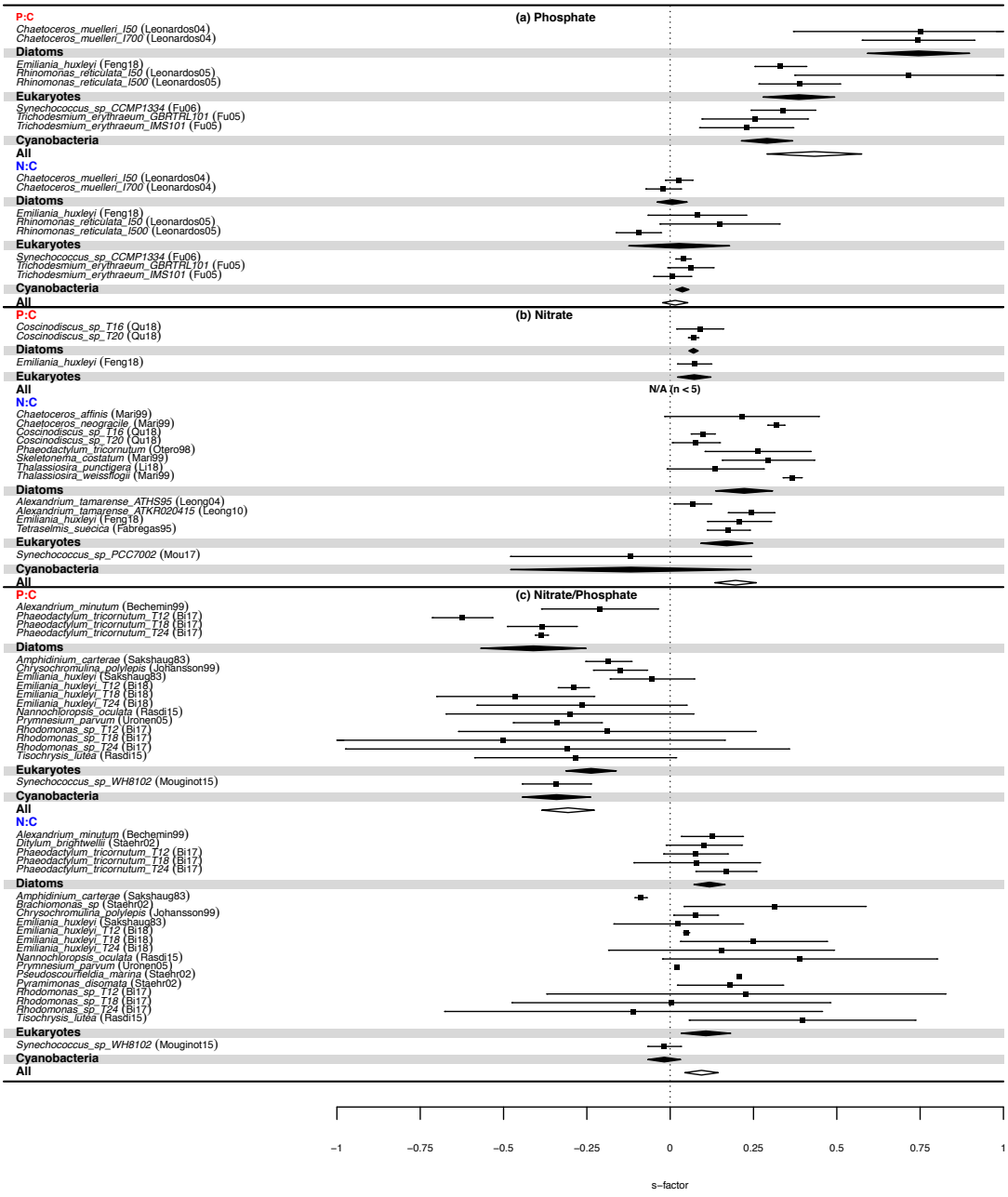

Figure 3.2: S-factors for P:C and N:C with respect to changes in (a) Phosphate, (b) Nitrate, and (c) Nitrate/Phosphate for individual experimental units and different phytoplankton functional types. Mean for the types are indicated by filled diamond. Mean across all types are indicated by open diamonds. Error bars represent the 95% confidence intervals. "N/A" signifies that the total experimental units were less than five for a given driver-stoichiometry pair in order to carry out a meta-analysis. Name in bracket corresponds to an individual study (see Appendix B: Table B.1).

$s_I^{N:C}$ for all the PFTs are similar in magnitude and are not statistically different from each other ($p > 0.05$).

3.4.5 Effects of Temperature

The response of P:C to temperature changes was variable across different species and PFTs (Figure 3.4). Diatoms display mixed responses, and the mean s-factor is negative overall but not significant. Eukaryotes also show mixed responses but the overall mean is positive because of the large s-factor associated with *Rhodomonas sp* (Bi, Ismar, Sommer, & Zhao 2017). In contrast to diatoms and eukaryotes, cyanobacteria have consistently negative s-factors for all 12 experimental units but one. As a result, mean s-factor for cyanobacteria is statistically significant with a negative sign ($s_T^{P:C} = -7.8 \pm 3.3, n = 12,\ p = 0.02$).

The effect of temperature on N:C was also variable across different species and PFTs (Figure 3.4). Although mean s-factors across all studies and for all PFTs are positive, none are statistically significant. Compared to $s_T^{P:C}$, the magnitude as well as the standard error of $s_T^{N:C}$are smaller which suggest that change in N:C with respect to temperature is less pronounced compared to P:C.

3.4.6 Effects of Iron

Iron availability increased P:C and s-factors for diatoms and cyanobacteria are positive ($s_{Fe}^{P:C} = 0.09 \pm 0.05$ and $s_{Fe}^{P:C} = 0.19 \pm 0.07$, respectively) (Figure 3.5). Yet, the insufficient of sample size precluded us from carrying meta-analysis on overall effects of iron on P:C. The effect of iron on N:C was generally weak and s-factors the magnitude of $s_{Fe}^{N:C}$ does not exceed 0.05. For cyanobacteria however, $s_{Fe}^{N:C}$ is consistently negative and the overall s-factor is significant ($s_{Fe}^{N:C} = -0.03 \pm 0.01, n = 3,\ p < 0.0001$).

3.5 Discussion

3.5.1 Basic framework

One of the fundamental tenets of the chemical oceanography is the Redfield Ratio, which implies that phytoplankton cells at balanced growth achieve a constant cellular P:N:C

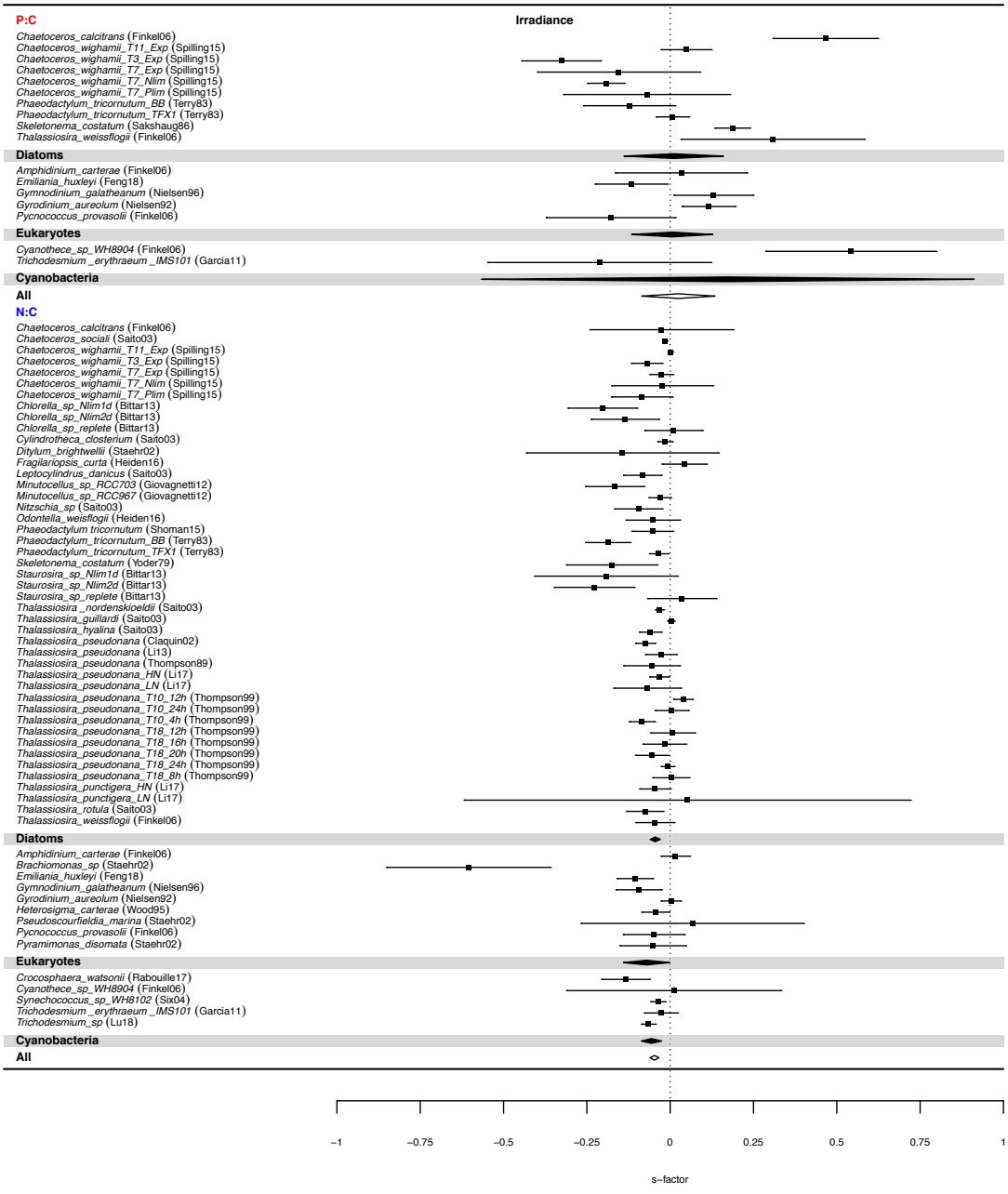

Figure 3.3: S-factors for P:C and N:C with respect to changes in irradiance for individual experimental units and different phytoplankton functional types. Legend and error bars are as Figure 3.2.

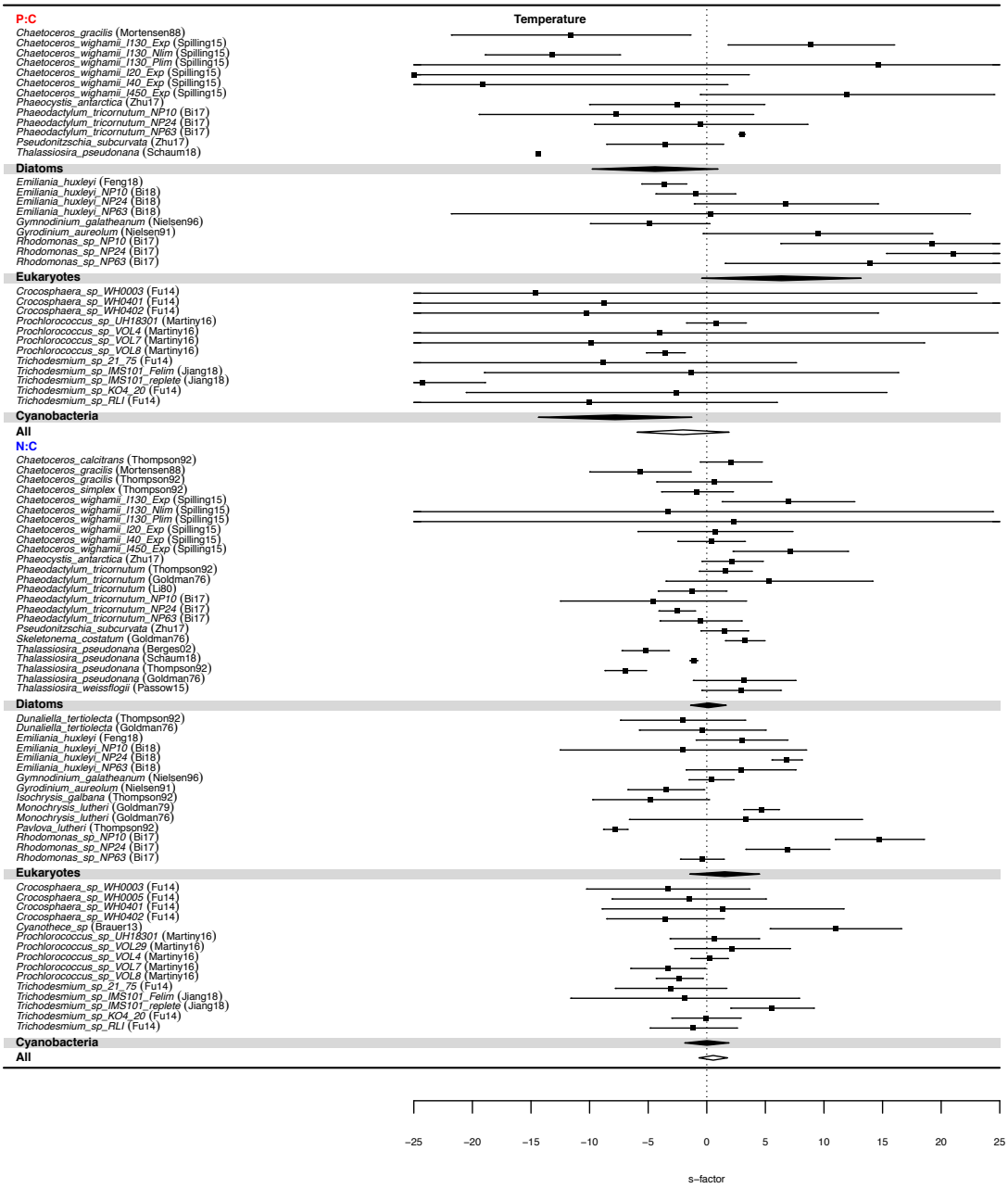

Figure 3.4: S-factors for P:C and N:C with respect to changes in temperature for individual experimental units and different phytoplankton functional types. Legend and error bars are as Figure 3.2.

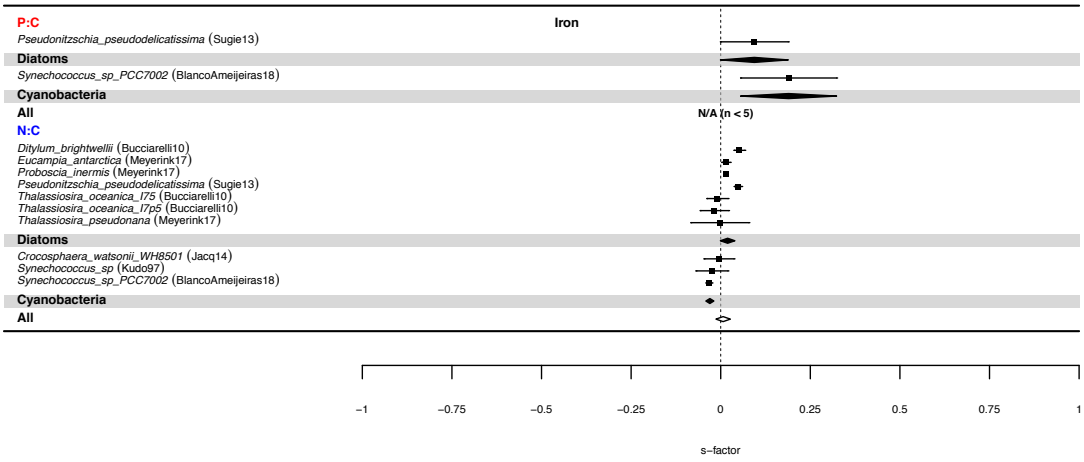

Figure 3.5: S-factors for P:C and N:C with respect to changes in iron for individual experimental units and different phytoplankton functional types. Legend and error bars are as Figure 3.2.

ratio at the well-known molar ratio of 1:16:106 (Redfield et al. 1963). Balanced growth is in theory achieved for nutrient-replete algal cells growing under steady state conditions where the balance between uptake of elements and assimilation into cellular functional pool is achieved (Berman-Frank & Dubinsky 1999; Klausmeier, Litchman, Daufresne, & Levin 2004). Under such conditions, the growth rate of all cellular constituents averaged over one generation is the same, whether it is the carbon-specific, nitrogen (protein)-specific, or phosphorus (DNA)-specific growth rates (Falkowski & Raven 2007). In the real ocean however, the ideal condition required for balanced growth is rarely achieved as the phytoplankton growth is usually limited by one or more factors (C. M. Moore et al. 2013; J. K. Moore & Doney 2007). For example, the deficiency of essential nutrients limits the formation of building blocks of new cells (e.g., N for proteins, P for nucleic acids and ATP), light limitation slows carbon assimilation (i.e. making of carbohydrates and reductase), and low temperature slows down the essential cellular transport and enzymatic reactions for growth (Madigan, Martinko, Parker, & Others 2017). Similarly, excess supply above cellular requirement can lead to reduction in growth rate via nutrient toxicity; photoinhibition from excess irradiance; protein denaturation, collapse of cytoplasmic membrane, and thermal lysis from excess warming although such cases in the marine environment are rarer compared to those in freshwater environment. The

Table 3.2: Summary of s-factors for (a) P:C and (b) N:C. Values represent the means ±SE. Numbers in bold are statistically significant ($p < 0.05$). Different letters indicate significant differences between PFTs ($p < 0.05$) for a given driver. Overall s-factor across all studies are not calculated if the total experimental units were less than 5.

Driver	(a) $s^{P:C}$			
	Diatoms	Eukaryotes	Cyanobacteria	Overall
P	$\mathbf{0.75 \pm 0.08^{b}}$	$\mathbf{0.39 \pm 0.06^{a}}$	$\mathbf{0.29 \pm 0.04^{b}}$	$\mathbf{0.43 \pm 0.09}$
N	$\mathbf{0.07 \pm 0.01^{a}}$	$\mathbf{0.07 \pm 0.03^{a}}$	N/A	N/A ($n < 5$)
NO_3/PO_4	$\mathbf{-0.41 \pm 0.08^{a}}$	$\mathbf{-0.24 \pm 0.04^{a}}$	$\mathbf{-0.34 \pm 0.08^{a}}$	$\mathbf{-0.30 \pm 0.04}$
I	0.01 ± 0.08^{a}	0.01 ± 0.06^{a}	0.17 ± 0.38^{a}	0.03 ± 0.06
T	-4.4 ± 2.7^{a}	6.4 ± 3.5^{b}	$\mathbf{-7.8 \pm 3.3^{a}}$	-2.0 ± 2.0
Fe	0.09 ± 0.05^{a}	N/A	$\mathbf{0.19 \pm 0.07^{a}}$	N/A($n < 5$)

Driver	(b) $s^{N:C}$			
	Diatoms	Eukaryotes	Cyanobacteria	Overall
P	0.01 ± 0.02^{a}	0.03 ± 0.08^{a}	$\mathbf{0.04 \pm 0.01^{a}}$	0.02 ± 0.02
N	$\mathbf{0.22 \pm 0.04^{a}}$	$\mathbf{0.17 \pm 0.04^{a}}$	-0.12 ± 0.18^{a}	$\mathbf{0.20 \pm 0.03}$
NO_3/PO_4	$\mathbf{0.12 \pm 0.02^{b}}$	$\mathbf{0.11 \pm 0.04^{ab}}$	-0.02 ± 0.03^{a}	$\mathbf{0.09 \pm 0.03}$
I	$\mathbf{-0.05 \pm 0.01^{a}}$	$\mathbf{-0.07 \pm 0.04^{a}}$	$\mathbf{-0.06 \pm 0.02^{a}}$	$\mathbf{-0.05 \pm 0.01}$
T	0.14 ± 0.78^{a}	1.5 ± 1.5^{a}	0.01 ± 0.97^{a}	0.55 ± 0.62
Fe	0.02 ± 0.01^{b}	N/A	$\mathbf{-0.03 \pm 0.01^{a}}$	0.01 ± 0.01

steady state assumption is also not always justified due to short-term and long-term changes in physical conditions of ocean. A good example of such change is phytoplankton bloom in the spring where the transient changes in surface temperature, irradiance and nutrient supply rate alter the growth rate and elemental stoichiometry of phytoplankton (Polimene et al. 2015; Talarmin et al. 2016). Growth limitations and transient changes in the environmental conditions are likely to be the two fundamental drivers for the divergence of measured P:N:C of phytoplankton from Redfield P:N:C observed in nature (Geider & La Roche 2002; Martiny, Pham, et al. 2013; Moreno & Martiny 2018).

The degrees to which phytoplankton P:N:C ratios are affected by stresses depend

both on the cellular stress response mechanisms and the magnitude of the environmental change (e.g., how much temperature increases), as well as temporal variability of environmental drivers. Most types of stress responses can be divided into a stress-specific, primary response and a general secondary response (Brembu, Mühlroth, Alipanah, & Bones 2017): the stress-specific responses are strong, robust and consistently observed across photosynthetic organisms, while secondary responses are variable amongst different organisms. Primary and secondary responses are closely related to acclimation (plasticity response) and adaptation (evolutionary response) respectively. In essence, acclimation refers to environmentally induced trait change of an organism in the absence of any genetic change, while adaptation involves genetic changes driven by natural selection (Collins, Boyd, & Doblin 2020). Since primary responses do not involve genetic adjustment or natural selection, the responses are fast and often commonly shared amongst different marine phytoplankton. For example, changing the nutrient uptake affinity of a lineage within a generation in response to changing nutrient supply is a commonly seen trait across all phytoplankton groups. On the other hand, secondary response depends both on the environmental condition and genotype (Brembu et al. 2017). The secondary responses take longer time (usually up to few hundred generations) and there is typically no single, unique response even when referring to a single species or functional group and a specific environmental driver (Collins et al. 2020).

By adopting this framework, we are able to use the s-factor as a proxy to understand the relative importance of primary responses over secondary responses in altering the P:C and N:C ratios. For example, if the sign of a s-factor is consistent across all the studies for a particular environmental driver-stoichiometry pair, we may deduce that change in elemental ratio is due to a primary response. On the other hand, we can infer that the change in the ratio is due to a secondary response if there are consistent responses across certain species and PFTs but not for all groups. If the P:C and N:C ratios are not significantly affected (i.e. s-factors are close to 0), we would infer that such environmental driver does not perturb the balance between carbon assimilation and growth. In the subsections below, we discuss for each environmental driver whether there are any underlying patterns present amongst different studies and speculate on cellular mechanisms responsible for producing such patterns (see Figure 3.6 for schematic illustration).

3.5.2 Macronutrients (Phosphate and Nitrate)

Overall, we observe consistent trend across all studies where P:C and N:C increases with increase in the supply of phosphate and nitrate respectively (Figure 3.2). Since the direction of change between and X:C and the supply of element X are positively related, $s^{P:C}_{PO_4}$ and $s^{N:C}_{NO_3}$ are both positive. Observations of phosphate/nitrate against particulate organic matter P:C and N:C indeed broadly follow this general trend (Galbraith & Martiny 2015; Tanioka & Matsumoto 2017). Similarly, we observed consistent stoichiometric responses for changes in N:P supply ratio where increase in N:P lead to lower P:C and higher N:C. This makes intuitive sense because higher N:P supply ratio would increase availability of N with respect to availability of P. Positive correlation between X:C with

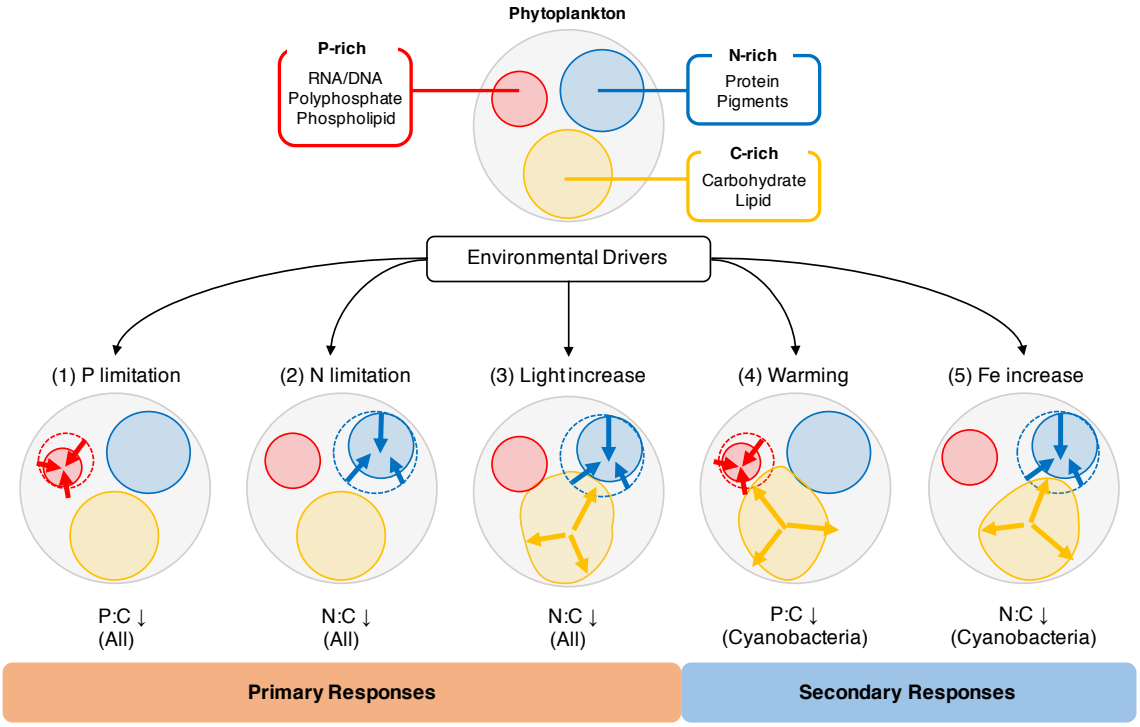

Figure 3.6: Illustration of how the five environmental drivers under a typical future climate scenario affect the cellular allocation of volume between P-rich (red), N-rich (blue), and C-rich (orange) pools. Primary responses ((1)∼(3)) are responses displayed in all the PFTs, while secondary responses ((4) and (5)) are displayed only in certain PFTs. In (3)∼(5), changes in allocation of cellular volume between carbon and other pools could happen separately or simultaneously.

respect to availability of element X across all the species and studies suggest that this is a primary plasticity response and effectively decouples intracellular reserves of element X and carbon from the ambient availability of X.

Phytoplankton can temporally store excess nutrient intracellularly until the rate of carbon assimilation catches up to achieve steady-state balanced growth. Excess phosphorus for example can be stored mainly as polyphosphate (Dyhrman 2016) and excess nitrate can be stored primarily as protein and free amino acids (Liefer et al. 2019; Sterner & Elser 2002). Phytoplankton can consume these internal stores of nutrients (e.g., polyphosphates under P limitation) while maintaining the level of carbon fixation, when the uptake of the nutrients does not meet its demand for growth (Cembella, Antia, Harrison, & Rhee 1984). In addition, phytoplankton can reduce their ribosomes and RNA content under P limitation as RNA typically accounts for 50% of non-storage phosphorus (Hessen et al. 2017; Lin, Litaker, & Sunda 2016) which would conserve phosphorus for other uses in cell resulting in lower P:C ratios. Similarly, cells can reduce synthesis of N-rich protein content under N limitation resulting in lower N:C ratio (Grosse, van Breugel, Brussaard, & Boschker 2017; Liefer et al. 2019). These transient processes controlling the intracellular content of P or N (but not C content as much) likely result in positive correlation between P:C and N:C with macronutrient concentrations.

Although $s_{PO_4}^{P:C}$ and $s_{NO_3}^{N:C}$ are consistently positive across all the studies, they are noticeably higher for diatoms than for other phytoplankton groups (Figure 3.2a, b). There are several hypotheses for explaining this trend. One of the most plausible hypotheses is related to the size and storage capacity difference amongst phytoplankton groups (Edwards, Thomas, Klausmeier, & Litchman 2012; Lomas et al. 2014). Since diatoms are generally larger and possess more storage capacity, they are capable of greater luxury uptake and accumulation of internal P and N reserves when the nutrient is in excess (N. S. Garcia et al. 2018). On the other hand when nutrients are scarce, large cell size of diatoms allow them to increase their carbon content considerably by accumulating excess carbon as polysaccharides and lipids (Liefer et al. 2019; Lin et al. 2016). Another plausible hypothesis concerns variability in acclimation/adaptation strategy at the genetic level (Dyhrman 2016). Recent studies suggests that different phytoplankton groups exhibit different levels of transcriptional responsiveness and have

dissimilar strategies for nitrate (Lampe, Wang, Cassar, & Marchetti 2019) and phosphate (Martiny, Ustick, A. Garcia, & Lomas 2019) uses. In particular, diatoms have superior abilities to uptake and store nutrients by being able to quickly regulate their gene expression patterns required for nutrient uptake compared to other phytoplankton groups (Cáceres et al. 2019; Lampe et al. 2018; 2019). These hypotheses provide plausible explanation for why diatoms have elevated stoichiometry sensitivity to nutrients compared to other phytoplankton groups.

A previous meta-analysis study showed that cellular N:P ratio of phytoplankton is significantly positively correlated with N:P supply ratio of nutrients (Persson et al. 2010), providing a picture that essentially "algae are what they eat". As cellular N:P is effectively a ratio between cellular N:C and P:C, our analysis is consistent with this picture because the mean plasticity of P:C is greater than that of N:C (i.e. the magnitude of $s_{NP}^{P:C}$ is significantly greater than that of $s_{NP}^{N:C}$ with the opposite sign; Figure 3.2c). We would expect $s_{NP}^{P:C}$ and $s_{NP}^{N:C}$ to be more equal in magnitude if cellular N:P ratio was more homeostatic. Cellular N content generally covaries with cellular protein contents (Leonardos & Geider 2004; Liang, Koester, Liefer, Irwin, & Finkel 2019), while cellular P content covaries with macromolecular pools of RNA, DNA, and phospholipids (Liefer et al. 2019). Large stoichiometry sensitivity of P:C over N:C suggest N-uptake and protein synthesis change does not keep pace completely with P-uptake and synthesis of P-rich molecules. This pattern of larger stoichiometric flexibility of P:C over N:C with respect to nutrient availability has also been observed globally in the marine environment (Galbraith & Martiny 2015) consistent with our meta-analysis result.

3.5.3 Irradiance

Light availability affects photoacclimation of phytoplankton and subsequently the cellular allocation of volume between N-rich light-harvesting apparatus, P-rich biosynthetic apparatus, and C-rich energy storage reserves (Falkowski & LaRoche 1991; Moreno & Martiny 2018). At a fixed growth rate and under a nitrogen limited condition, high irradiance should downregulate production of N-rich light harvesting proteins and pigments in order to minimize the risk of photooxidative stress, and excess light energy is stored as C-rich storage compounds such as lipids and polysaccharides (Berman-Frank & Dubinsky 1999). As a result, N:C is expected to decrease under high light. In contrast, under

low light condition, macromolecular composition should favor N-rich light harvesting apparatus over C-rich storage reserves, thus elevating N:C. This line of reasoning would predict negative s-factors for the effect of irradiance on N:C, which is borne out in our meta-analysis (Figure 3.3).

The magnitude of $s_I^{N:C}$ is consistently less than 0.1 and the responses are weak across all PFTs. This result agrees with a previous study which compiled experimental data prior to 1997 (MacIntyre, Kana, Anning, & Geider 2002). It is possible however that s-factor obtained in our meta-analysis is underestimated as there are several methodological factors that may mute the effect of irradiance on N:C ratio of phytoplankton. Firstly, not all studies were carried under nutrient (nitrate) limited condition, hence the downregulation of N-rich light harvesting apparatus was not needed to maintain growth. Secondly, the growth rate was not controlled in all the studies. Ideally, chemostat/turbidostat experiments are most suited for isolating the effect of environmental driver as it allows direct manipulation of growth rate. This is because any change in cellular nutrient:C ratio can be attributed to a specific environmental driver rather than to changes in specific growth rate (Hessen, Faerovig, & Andersen 2002). However, for practical and economic reasons, batch and semi-continuous culture are more commonly used (La Roche, Rost, & Engel 2010). Thirdly, we did not consider the effect of light regimes (i.e. the length of light and dark hours) and diel changes on N:C. Longer light period leads to a more stable N:C over the course of the day as the amount of carbon fixed remains relatively constant, while experiments with longer dark hours leads to larger diel change in N:C (Lopez, Garcia, Talmy, & Martiny 2016; Mohr, Intermaggio, & LaRoche 2010; Ng & Liu 2015; Talmy et al. 2014). We speculate that the lack of diel changes may have muted the underlying photoacclimation responses. Despite these experimental limitations, consistency in the s-factors across all studies indicates irradiance measured by photon flux density is one of the key determinants for N:C. This is consistent with the global observation (Martiny, Vrugt, et al. 2013) and model studies (Arteaga et al. 2014; Talmy et al. 2014; Talmy, Martiny, Hill, Hickman, & Follows 2016) where N:C of phytoplankton is higher in the light-limited polar/subpolar regions than in the light-replete low latitudes.

In contrast to the total cellular C and N quota, P quota should only be affected by change in irradiance if P is the main limiting nutrient (Moreno & Martiny 2018). Under

P limitation, P:C is expected to decrease at increased light level because the total supply of inorganic phosphorus will not be able to keep up with the increase in photosynthetic carbon fixation, leading to decoupled uptake of C and P (Hessen et al. 2002; Hessen, Leu, Færøvig, & Falk Petersen 2008). Conversely, P:C is expected to increase at lower irradiance because carbon fixation decreases while phosphorus uptake remains constant (Urabe & Sterner 1996). We did not observe such P:C responses, as only 1 out of the 17 experiments units used in our meta-analysis was clearly P-limited. We speculate that other experimental conditions such as temperature, growth phase, and nutrition status muted the effects of irradiance on P:C leading to an overall statistically insignificant s-factor.

3.5.4 Temperature

For microorganisms, temperature is arguably the most important environmental factor affecting growth and survival (Madigan et al. 2017). Temperature controls the kinetic responses such as enzyme activity, cell division, and nutrient uptake which all are thought to occur at higher rates with elevated temperatures (Hessen et al. 2017). Also, temperature can alter macromolecular composition, rate of protein synthesis, and storage of elements (Moreno & Martiny 2018). Phytoplankton are able to efficiently grow over a range of temperatures around the optimal growth temperature but their growth at substantially different temperatures can lead to photodamage (Huner et al. 2008), inhibition of protein synthesis (Y.-Y. Li et al. 2019), or the decline in photosynthetic efficiency (Falk, Maxwell, Laudenbach, & Huner 2006). As a result, a growth curve of phytoplankton is unimodal (Boyd et al. 2013; Zhu, Qu, Gale, Fu, & Hutchins 2017) with increasing growth rate from the minimum temperature to the optimum temperature and decreasing growth rate towards the maximum temperature (Madigan et al. 2017).

Broadly, there are two kinds of species, a thermal specialist whose growth rate rapidly drops off as temperature exceeds the optimal temperature, and a thermal generalist whose growth rate remains constant over a wide range of temperatures (Collins et al. 2020). Since the P:C and growth rate are intricately linked (Sterner & Elser 2002), our meta-analysis suggests that cyanobacteria are thermal specialists because an increase in temperature significantly decreased P:C across all studies (Figure 3.4). Although the

underling mechanism for explaining lower P:C at higher temperature is not fully understood, there are three hypotheses (Paul, Matthiessen, & Sommer 2015): (1) increase in metabolic stimulation of inorganic carbon uptake over phosphorus uptake; (2) increase in nutrient use efficiency which enables greater carbon fixation for given nutrient availability; and (3) "translation compensation theory," which predicts that less P-rich ribosomes are required for protein synthesis and growth as the translation process becomes kinetically more efficient (McKew, Metodieva, Raines, Metodiev, & Geider 2015; Toseland et al. 2013; Woods et al. 2003; Xu, Gao, Li, & Hutchins 2014; Zhu et al. 2017). In this meta-analysis, the decrease in P:C in cyanobacteria at elevated temperatures (Figure 3.4) is possibly attributable to a combination of these three hypotheses (F. Fu et al. 2014; Jiang et al. 2018; Martiny, Ma, Mouginot, Chandler, & Zinser 2016), as they are likely not mutually exclusive.

For non-cyanobacteria phytoplankton, their stoichiometric response to changes in temperature was mixed even among closely related phytoplankton lineages (Figure 3.4). This suggests the importance of species-specific adaptive/evolutionary response to warming (Schaum, Buckling, Smirnoff, Studholme, & Yvon-Durocher 2018; Taucher et al. 2015). Another important factor to consider is the interactive effect of temperature with other environmental drivers. Multiple studies suggest that the effect of temperature on growth and metabolic rates are masked out by nutrient and/or light limitations (Marañón, Lorenzo, Cermeño, & Mouriño-Carballido 2018a; 2018b; Qu et al. 2019; Roleda et al. 2013). These factors may explain why, for example, the coccolithophore *Emiliania huxleyi* grown under different supply ratios of inorganic N:P responded differently at different temperatures (Bi, Ismar, Sommer, & Zhao 2018). At a low N:P supply ratio (i.e. under N limited condition), P:C decreased with warming, but the trend reversed and the magnitude of s-factor became smaller under P limited condition. We also cannot rule out the possibility that mixed responses may be an artifact of the experimental methods because the majority of the experiments were carried under batch method where the growth rates are not controlled. This makes it inherently difficult to tease apart the influence of temperature and growth rate on elemental stoichiometry.

A previous meta-analysis (Yvon-Durocher et al. 2015) and this work both support the idea that P:C is more flexible than N:C with respect to change in temperature, which suggest that intracellular P content is more sensitive to change in temperature

than intracellular N content. The two studies differ in that our study did not reveal a clear, overall signal of the temperature effect on P:C except for cyanobacteria (Figure 3.4), whereas the previous study found a statistically significant, overall negative linear relation between temperature and P:C (Yvon-Durocher et al. 2015). An important consideration in this regard is that the previous meta-analysis used studies up to 1996, while the data we included in our meta-analysis were substantially supplemented with data reported after 1996.

3.5.5 Iron

Iron is used in key biochemical processes such as electron transport, respiration, protein synthesis, and N fixation (Marchetti & Maldonado 2016; Twining & Baines 2013). Many of the iron-dependent processes are required for harvesting energy and biochemical intermediates. As energy acquisition is equivalent to light acquisition in phototrophs, it makes sense that s-factors for iron are similar in the signs and magnitudes to those of light. Although the effect of iron on N:C is weak, similar in magnitude to that of light, the s-factor for cyanobacteria is statistically significant where an increase in iron leads to decrease in N:C. This suggests that an increase in the carbon assimilation via photosynthesis and/or a reduction in the formation of nitrogen rich compounds such as porphyrin and phycobiliprotein that are essential for light harvesting (Falkowski & Raven 2007; Twining & Baines 2013). The iron s-factors for diatoms on the other hand are mixed across the studies and the overall mean was not significant. This suggests that change in Fe availability affects cellular C and N proportionally for diatoms (Greene, Geider, & Falkowski 1991; Roche, Geider, Graziano, Murray, & Lewis 1993; Takeda 1998; van Oijen, van Leeuwe, Gieskes, & de Baar 2004). These contrasting results between cyanobacteria and diatoms may be due to differences in growth conditions. For example, temperature, phosphorus, and/or irradiance can moderate how iron affects phytoplankton physiology (Boyd 2019; Bucciarelli, Pondaven, & Sarthou 2010; Mills, Ridame, Davey, La Roche, & Geider 2004; Strzepek, Boyd, & Sunda 2019). In addition, iron requirement is generally higher in nitrogen-fixing cyanobacteria than in non-nitrogen-fixing species (Sunda & Huntsman 1995). There was not enough data on P:C to carry out meta-analysis. Yet a number of laboratory studies, which were excluded from this meta-analysis due to the lack of requisite data (at least 3 per experiment),

have shown that N:C and P:C may decrease (Berman-Frank, Cullen, Shaked, Sherrell, & Falkowski 2001; De La Rocha, Hutchins, Brzezinski, & Zhang 2000; Muggli & Harrison 1996; Price 2005; Sugie & Yoshimura 2013) or increase (Doucette & Harrison 1991; Maldonado & Price 1996; Sakshaug & Holm-Hansen 1977) significantly with increasing Fe-limitation. In future, more studies are needed to provide a more coherent picture on how iron would affect P:C and N:C.

3.6 Implications for global biogeochemical cycles

We can give a first-order estimate of how much the elemental stoichiometry of marine phytoplankton may change in the future given a typical projection of the change in the key environmental drivers and the estimates of the s-factors (Table 3.3; Figure 3.6). Global climate models generally predict a decline in macronutrients and increase in temperature, irradiance and iron as a result of surface warming, increased vertical stratification and reduced mixed layer depth (Bopp et al. 2013; Boyd, Lennartz, Glover, & Doney 2015). Iron concentration in surface is expected to increase as stratification would reduce biological production and leave more iron underutilized at the surface, assuming the same iron input (Boyd et al. 2015). With large projected declines in macronutrients (-28.0% for phosphate, -18.7% for nitrate), we estimate that P:C and N:C for diatoms would decrease by 21.0% and 4.1% respectively in the 2100s (Table 3.3). This translates to increase in C:P and C:N by $\sim$ 30 units (molar) and $\sim$ 0.3 units (molar) assuming the modified Redfield C:N:P of 117:16:1 as the present-day value (L. A. Anderson & Sarmiento 1994). There are additional changes to C:P and C:N by other drivers. In the case of cyanobacteria, C:P increases as temperature rises and decreases as iron increases. The total C:P change is $+10 \sim 33\%$ for all PFTs, with diatoms having the largest increase, followed by cyanobacteria and eukaryotes. For C:N, we estimate an overall increase by $1 \sim 5\%$ with the largest change in diatoms closely followed by eukaryotes. In summary, this simple calculation highlights potentially a large shift in the phytoplankton chemical composition especially for C:P, whose change is predominantly driven by phosphate.

In the real ocean, none of the environmental changes discussed will likely occur in isolation. For example, irradiance, temperature, and nutrient availability are often

Table 3.3: Projected change in C:P (molar) and C:N (molar) between 1981-2000 and 2081-2100 given model-based projected changes in environmental drivers from Boyd et al. (2015). C:N and C:P are calculated separately for each driver with s-factors from Table 3.2 combined with reference C:N:P of 117:16:1 for diatoms and eukaryotes; and C:N:P of 329:45:1 for cyanobacteria, both of which are consistent with the values used by Boyd et al. (2015). Ranges in the estimate are derived from propagating standard error for the s-factors. We used equation (3.2) in the main text for estimating the combined effect of multiple drivers. Values in bracket are respective percent changes in C:P and C:N from the reference values.

Driver	Δ (C:P) (molar)			Δ (C:N) (molar)		
	Diatoms	Eukaryotes	Cyanobacteria	Diatoms	Eukaryotes	Cyanobacteria
P (-28%)	+27∼35	/	+21∼38	/	/	+0.06∼0.1
N (-18.7%)	+1.3∼1.7	+0.9∼1.7	/	+0.3∼0.4	+0.2∼0.3	/
I (+0.7%)	/	/	/	<+0.01	<+0.01	<+0.01
T (+0.9%)	/	/	+14∼36	/	/	/
Fe (+6.5%)	/	/	-6 ∼-2.5	/	/	/
Combined Effects (% change)	+30∼39 (+26∼33%)	+15∼21 (+13∼18%)	+32∼78 (+10∼24%)	+0.3∼0.4 (+4∼5%)	+0.2∼0.3 (+3∼4%)	+0.08∼0.1 (+1%)

linked because the change in light availability will affect sea surface temperature, which in turn will alter vertical stratification in the water column and nutrient upwelling. Indeed, a meta-analysis on the pair-wise effects of environmental drivers on elemental stoichiometry of phytoplankton has shown that interactions of two environmental stressors can impose predominantly non-additive effects to P:C and N:C of phytoplankton, and that the effect of multiple environmental stressors is more than simply the sum of its parts (Villar-Argaiz et al. 2018). In addition, a recent multi-driver study carried for eight different drivers has shown that only a few dominant drivers can explain most of the evolutionary changes in population growth rates (Brennan, Colegrave, & Collins 2017). We are not aware of a similar multi-driver study conducted specifically for phytoplankton stoichiometry, but our results demonstrate that the macronutrients are the dominant controls on P:C and N:C, and thus we believe we have captured the first order behavior of P:N:C.

Similarly, the link between P:N:C of individual phytoplankton cells and of the larger

ecosystem community including heterotrophs is complex, and it is not possible to simply assume that P:N:C ratios of organic matter collected in the ocean reflects the stoichiometry of uptake and production by phytoplankton. In addition to the individual phytoplankton stoichiometry, the bulk organic matter stoichiometry reflects the phytoplankton community composition (Bonachela et al. 2016; Weber & Deutsch 2010) as well as the stoichiometry of organic matter accumulation and remineralization, which can be decoupled from the organic matter production ratio (Schulz et al. 2008). For example, the observed N:C ratio of biogenic sinking organic matter is close to the Redfield ratio even at very low nutrient conditions (Copin-Montegut & Copin-Montegut 1983; Martiny, Vrugt, et al. 2013), which would predict low phytoplankton N:C. This apparent decoupling between phytoplankton N:C and bulk organic matter N:C may reflect the fact that heterotrophic bacteria and grazers that process organic matter derived from phytoplankton are more protein-rich (higher N:C) and homeostatic than phytoplankton (Sterner & Elser 2002). In addition, processes such as viral shunt (Jover, Effler, Buchan, Wilhelm, & Weitz 2014) and preferential remineralization of phytoplankton macromolecules (Frigstad et al. 2011; Kreus, Schartau, Engel, Nausch, & Voss 2015) can also decouple phytoplankton P:N:C from the bulk organic matter P:N:C.

There are some limitations and weaknesses in the current suite of ocean biogeochemistry models in predicting spatial and temporal distribution of essential biogeochemical elements such as nitrogen, phosphorus, and oxygen. For example phosphate concentrations are systematically overestimated in the surface (Martiny, Lomas, et al. 2019) and the global distribution of nitrogen fixation, denitrification, and oxygen minimum zones exhibit substantial variability between models (W. Fu, Primeau, Keith Moore, Lindsay, & Randerson 2018). Recent global biogeochemical models are therefore starting to incorporate a more realistic representation of plankton physiology, which includes flexible phytoplankton P:N:C (e.g., Buchanan, Matear, Chase, Phipps, & Bindoff 2018). Modeling studies with flexible phytoplankton P:N:C have demonstrated that lowering of P:C and N:C in phytoplankton under future climate scenario has the potential to buffer expected future decline in carbon export and net primary productivity caused by increased stratification (Kwiatkowski, Aumont, Bopp, & Ciais 2018; Tanioka & Matsumoto 2017). This buffering effect cannot be simulated by biogeochemical models with fixed phytoplankton P:N:C.

Many of the global models with flexible P:N:C currently employ simple linear models where P:C and N:C are expressed as a function of single macronutrient (phosphate or nitrate). Our meta-analysis showed that temperature and light dependencies are also important for determining P:C and N:C ratios. One way to combine the dependencies of multiple environmental drivers (e.g., P, N, Irradiance, and Temperature) in a single equation is the power-law formulation (Tanioka & Matsumoto 2017):

$$[\mathrm{X:C}] = [\mathrm{X:C}]_0 \left(\frac{[\mathrm{PO_4}]}{[\mathrm{PO_4}]_0}\right)^{s_{\mathrm{PO_4}}^{\mathrm{X:C}}} \left(\frac{[\mathrm{NO_3}]}{[\mathrm{NO_3}]_0}\right)^{s_{\mathrm{NO_3}}^{\mathrm{X:C}}} \left(\frac{\mathrm{I}}{\mathrm{I}_0}\right)^{s_{\mathrm{I}}^{\mathrm{X:C}}} \left(\frac{\mathrm{T}}{\mathrm{T}_0}\right)^{s_{\mathrm{T}}^{\mathrm{X:C}}} (\mathrm{X} = \mathrm{P\ or\ N}) \tag{3.2}$$

where subscript "0" indicates reference values. The s-factors obtained from this meta-analysis are the exponents of equation (3.2) for different PFTs. Within the context of the power law formulation, our results would indicate, for example, that diatoms would have the largest plasticity in P:C and N:C compared to other PFTs. Under future warming, diatoms' high s-factors may thus play an important role in buffering the expected future decline in carbon export and net primary productivity (Kemp & Villareal 2013).

3.6.1 Conclusions

Our meta-analysis represents an important bottom-up approach in predicting on how elemental stoichiometry of phytoplankton may evolve under the climate change. We conclude that macronutrient availability is the most significant and shared environmental driver of P:C and N:C. Changes in P:C and N:C by macronutrients are driven by primary/plasticity responses commonly shared across phytoplankton. In addition, light availability is a key driver for modulating N:C ratio. Our analysis shows that diatoms have the higher stoichiometric plasticity compared to other plankton groups. Diatoms' large stoichiometric flexibility and high intrinsic growth rate can explain their unexpectedly high diversity (Malviya et al. 2016) and large contribution to carbon export globally even in oligotrophic regions (Agusti et al. 2015; Nelson & Brzezinski 1997). The effects of other environmental drivers (temperature and iron) on P:C and N:C were either mixed amongst species and/or weak suggesting that these drivers elicit secondary responses. Future laboratory-based studies focused on exploring the effects of temperature and iron will be useful in filling the gaps to gain more mechanistic views on how

these drivers affect different plankton species. In addition, a further investigation on how multiple environmental drivers would interactively alter the elemental composition of phytoplankton would be needed for a complete understanding.

3.6.2 Acknowledgements

We thank Carolyn Bishoff, Julia Kelly, and Amy Riegelman from University of Minnesota Library for helping out literature search and data selection. We also thank Neil Price, Michael Roleda, Eva Bucciarelli, and Tim van Oijen for providing raw data.

Chapter 4

Phytoplankton stoichiometry and feeding behavior of zooplankton

The contents of this section were originally published in the journal *Ecological Modelling* (Volume 368, Issue 24, 1528-1542) under the title 'Effects of incorporating age-specific traits of zooplankton into a marine ecosystem model'. This work included below is its published form with permission of all authors. See Tanioka and Matsumoto (2018) for details. To view the published article, go to the Science Direct website (`https://www.sciencedirect.com/science/article/pii/S0304380017304866?via%3Dihub`).
Copyright (2017) Elsevier B. V.

4.1 Synopsis

Using a numerical model we investigated how the interactions between zooplankton foraging behavior and stoichiometry of phytoplankton would affect the cycling of nitrogen and phosphorus. Our results suggest that phytoplankton-zooplankton interaction is affected by food quality of phytoplankton as well as aging-related reduction in assimilation rate of zooplankton. We also show that age-specific traits of zooplankton have impacts on nutrient cycling especially on the elemental stoichiometry of large particulate organic matter.

4.2 Introduction

In most multi-species biogeochemical models including those used in the recent phase of Coupled Model Intercomparison Project (CMIP5), zooplankton are represented as two or three "functional groups" upon body size (e.g., Aumont, Ethé, Tagliabue, Bopp, & Gehlen 2015; J. K. Moore et al. 2004). Large zooplankton typically grazes on larger prey and gets coagulated to form large detritus that sinks fast, and likewise for small zooplankton functional types. Although zooplankton classification based upon morphology (e.g., body size) is important and most common, there are non-morphological key traits that are important to account for when assessing their roles in ecosystems. These traits include physiological (e.g., stoichiometric requirement, metabolic rate), behavioral (e.g., feeding mode), and life-history traits (Litchman, Ohman, & Kiørboe 2013). However, such traits of zooplankton are typically not considered in global biogeochemical models, but their importance is strongly suggested by recent modeling results that show including traits such as feeding mode (e.g., mixotrophy) leads to large impacts in marine nutrient cycles and food web (Mitra et al. 2014; Ward & Follows 2016). In fact, representation of zooplankton is one of the most significant factors that result in disparity for determining carbon export (T. R. Anderson, Hessen, Mitra, Mayor, & Yool 2013; Cavan, Henson, Belcher, & Sanders 2017).

A well-known key trait of zooplankton is their nutritional requirement (Hessen, Elser, Sterner, & Urabe 2013). Similar to the way phytoplankton can be limited by phosphorus (P) or nitrogen (N), some zooplankton are known to be more N limited while others require more P for growth (Elser & Urabe 1999). For example, calanoid copepods are typically rich in N and have optimal N:P ratio of 50:1, significantly higher than the canonical Redfield Ratio of 16:1 while Daphnia is more rich in P and has a lower N:P ratio of approximately 14:1 (Andersen & Hessen 1991). In certain environments, zooplankton with high N:P ratios excrete at low N:P ratios leading to N limitation in the ambient waters and thus for phytoplankton; similarly, environments dominated by zooplankton with low N:P ratios can lead to P limitation for phytoplankton (Sterner 1990).

In addition to interspecific variabilities, intraspecific variabilities such as age and sex are also significant for zooplankton (e.g., van Someren Gréve, Almeda, Lindegren,

& Kiørboe 2017). It is well known that copepods go through multiple, complex life stages with five to six naupliar stages followed by five copepodite stages before reaching adulthood (Kiørboe & Sabatini 1995). Each life stage during ontogeny is characterized by different traits. For example, younger nauplii grow faster than older copepodites, and growth rate declines continually in the copepodite stages (Carlotti & Sciandra 1989). Faster growing nauplii are typically richer in P, as higher growth rates are associated with higher P demand according to the growth rate hypothesis (Elser, Dobberfuhl, Mackay, & Schampel 1996). A recent study has also found age-specific variability in food selectivity, where younger nauplii selectively feed on prey with lower N:P ratios, while older copepodites prefer prey with higher N:P when multiple food sources are available (Meunier, Boersma, Wiltshire, & Malzahn 2016).

Here we present simple formulations for incorporating these age-specific traits (body C:N:P, growth rate, and food preference based on food quality) of copepod into an existing state-of-art marine biogeochemical model ERSEM (European Regional Seas Ecosystem Model) (Butenschön et al. 2016). Using this model, we conduct numerical experiments in a 0D chemostat setting to assess the impacts of incorporating these age-specific traits on food web dynamics and nutrient cycling. Previous modeling studies have shown zooplankton's active prey switching based on the food quality of phytoplankton significantly affects both plankton dynamics and nutrient cycling (Mitra & Flynn 2006; Sailley, Polimene, Mitra, Atkinson, & Allen 2014). These studies however did not consider zooplankton cannibalism and zooplankkton-zooplankton grazing, which exists in the ERSEM framework. In this work, we developed a new food selectivity formulation, which includes zooplankton grazing as well as cannibalism. In order to extract age-specific traits, we used data from laboratory experiment of a common marine copepod species *Acartia tonsa* (Meunier et al. 2016).

4.3 Method

ERSEM represents the marine carbon and nutrient cycle with full dynamic stoichiometry (C, N, P, and Chl) in all its functional types including organic matter (Butenschön et al. 2016). The model consists of 4 phytoplankton functional groups (picophytoplankton, nanophytoplankton, microphytoplankton, and diatoms), 3 zooplankton types

(heterotrophic flagellates, microzooplankton, and mesozooplankton), and heterotrophic bacteria (Figure 4.1). These plankton functional types are chiefly based on size and each zooplankton functional types are capable of predating on different prey, including cannibalism, according to size. Details on ERSEM are extensively described elsewhere (Butenschön et al. 2016), so here we describe our new contribution to the model, which is incorporation of age-specific traits (i.e., food quality dependence of body C:N:P, growth rate, and food preference).

Copepods represent the mesozooplankton, which are the top predators in ERSEM. To incorporate their age-specific traits in the model, we formulated: (i) C:N:P ratios; (ii) maximum assimilation rate; and (iii) flexible food preference as a function of mesozooplankton age. (i) and (ii) are obtained directly from the linear regression applied to the experimental data by Meunier et al. (2016), and (iii) is a modified formulation of the active-prey switch model by Fasham, Ducklow, and McKelvie (1990) extended

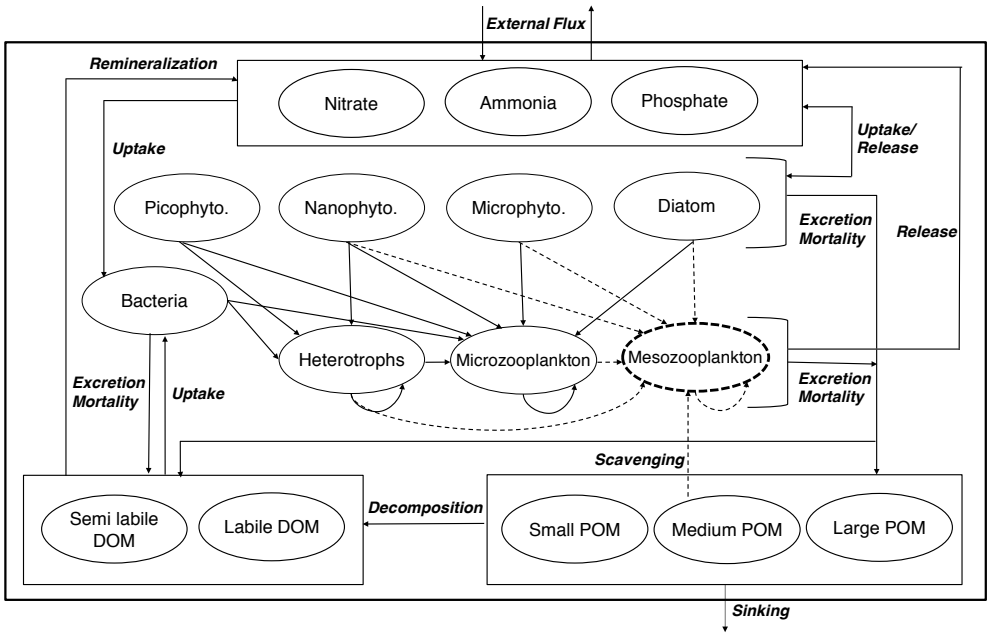

Figure 4.1: Biogeochemical model ERSEM used in simulations. Prey-predator interactions involving mesozooplankton are shown with the dotted lines. In ERSEM, grazing preferences of mesozooplankton are parameterized to a constant value. In the new model presented here, grazing preference is flexible based on food quality (FQ) of each prey types as well as prey biomass.

here to incorporate the food quality of the prey. As explained below, we are not explicitly modeling the age structure of mesozooplankton population in the model. Rather, we are using their C:N:P and maximum growth rate as a proxy for the mean age of the mesozooplankton population. Hence this formulation is fundamentally different from zooplankton models that explicitly model each life-stage (e.g., Carlotti & Sciandra 1989; Fennel 2001; Pinceel, Vanschoenwinkel, Brendonck, & Buschke 2016; Wang, Wei, & Batchelder 2014). Essentially, this study can be interpreted as a sensitivity test on how changes in the C:N:P ratios, the maximum assimilation, and the prey selectivity of mesozooplankton affect marine ecosystem dynamics.

4.3.1 C:N:P as a function of age

All zooplankton functional types in ERSEM have their cellular C, N, and P as the state variables. Source minus sink (SMS) terms are described by the following equations:

$$\mathrm{SMS(C)} = \mathrm{uptake} - \mathrm{excretion} - \mathrm{respiration} - \mathrm{predation} - \mathrm{mortality} \tag{4.1}$$

$$\mathrm{SMS(N,P)} = \mathrm{uptake} - \mathrm{excretion} - \mathrm{release} - \mathrm{predation} - \mathrm{mortality} \tag{4.2}$$

Uptake term for zooplankton takes a Michaelis-Menten form given by a function of maximum assimilation rate ($\mathrm{g_{max}}$), $\mathrm{Q_{10}}$ temperature dependence (T), total food available ($\mathrm{F_{tot}}$), half saturation constant (h), and the zooplankton biomass ($\mathrm{Z_C}$) (Blackford, Allen, & Gilbert 2004; Butenschön et al. 2016):

$$\mathrm{uptake} = \mathrm{g_{max}} \frac{\mathrm{F_{tot}}}{\mathrm{F_{tot}} + \mathrm{h}} \mathrm{T Z_c} \tag{4.3}$$

Total food available $\mathrm{F_{tot}}$ is the sum for each food source ($\mathrm{F_j}$) multiplied by the prescribed food preference of each food source (ϕ_j) and a Michaelis-Menten term utilizing a minimum food parameter ($\mathrm{Z_{minfood}}$):

$$\mathrm{F_{tot}} = \sum_\mathrm{j} \phi_\mathrm{j} \mathrm{F_j} \frac{\mathrm{F_j}}{\mathrm{F_j} + \mathrm{Z_{minfood}}} \tag{4.4}$$

In ERSEM, it is assumed that mesozooplankton have a fixed C:N:P ratio while heterotrophic flagellates ("heterotrophs") and microzooplankton have variable C:N:P ratios. To the extent that the C:N:P ratios in the prey of mesozooplankton deviate from its fixed internal ratio, there is a food or nutritional imbalance. In such a case, mesozooplankton in ERSEM release C, N, and P at different rates so as to maintain its internal ratio. These C, N, and P released as a result of this homeostatic regulation are added to large particulate organic matter pool.

We used the experimental data of Meunier et al. (2016) to obtain a relationship between C:N:P of marine copepod *Acartia tonsa* as a function of age (Figure 4.2). By carrying out standard linear regression, statistically significant ($p < 0.05$) linear equations describing relationship between age and C:N:P are obtained:

$$\mathrm{C:P(molar)} = 5.77 \cdot \mathrm{Age(days)} + 52.6 \tag{4.5}$$

$$\mathrm{N:P(molar)} = 1.94 \cdot \mathrm{Age(days)} + 7.15 \tag{4.6}$$

Between the age of 1 day to 14 days, C:P ratio more than triples from 40 to 130 (Figure 4.2 top) and N:P ratio also increases from 6.5 to 32 (Figure 4.2 bottom). Since we are not explicitly modeling the different life stage of mesozooplankton, these ratios are assumed to reflect the mean C:N:P ratios of mesozooplankton population rather than individual C:N:P. In other words, high N:P means that mesozooplankton population is mostly composed of older copepodites and vice versa for low N:P.

4.3.2 Maximum assimilation rate as a function of age

In their experiment, Meunier et al. (2016) demonstrate a statistically significant relationship ($p < 0.05$) between relative growth rate, age, and body N:P where relative growth rate decrease linearly with age and N:P. Faster growth rates of nauplii are associated with higher P content, in agreement with the growth rate hypothesis (Elser et al. 1996). Their results suggest that the relative growth rate changes by 0.06 d^{-1} for each day of aging (i.e., product of relative growth rate per N:P and the relative change in N:P per age). In our model, we thus assume the same for the maximum assimilation

rate of mesozooplankton (dotted line, Figure 4.2 bottom):

$$g_{max}(d^{-1}) = -0.06 \cdot \text{Age(days)} + 1.36 \tag{4.7}$$

Accordingly, at the age of 6 days, the maximum assimilation rate is exactly 1.0 d^{-1}, which is equal to the predefined value in ERSEM.

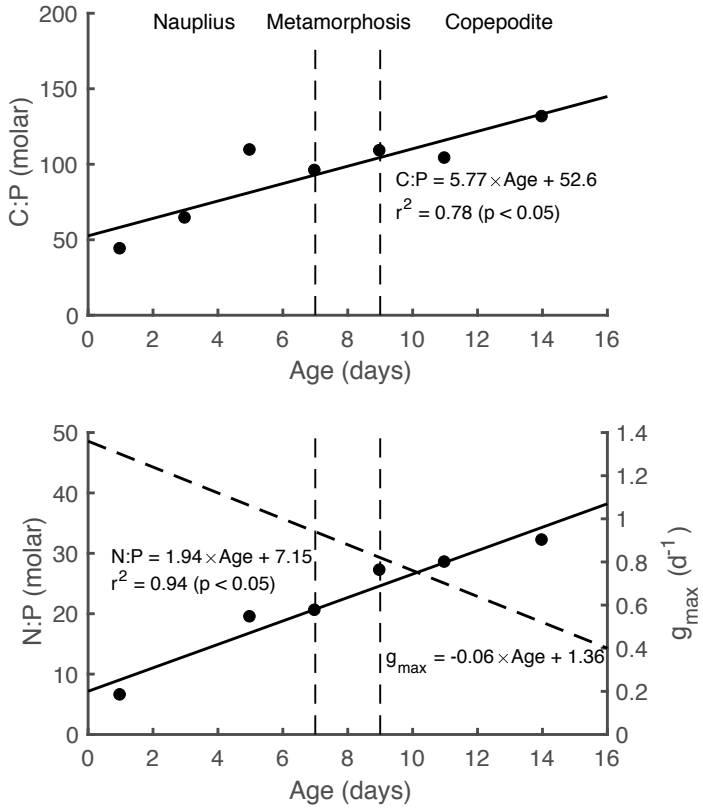

Figure 4.2: C:N:P ratios and maximum assimilation rate during copepod ontogeny. (Top) Molar C:P of *Acartia tonsa* as a function of age. Nauplius stage is between 0-7 days, metamorphosis from nauplius to copepodite stage occurs between 7-9 days, and copepodite stage is from 9 days and beyond. (Bottom) Molar N:P and estimated maximum assimilation rate (g_{max}) during ontogeny. Maximum assimilation rate is inferred from the negative linear relationships between relative growth rate and N:P and between N:P and age (see main text). All C:N:P data are from Meunier et al. (2016).

4.3.3 Flexible grazing preference as a function of age

In the original ERSEM, each zooplankton has a fixed, biomass independent prey preference based on the predator-prey size relationship (Appendix C: Table C.1). For example, mesozooplankton prefers grazing on microzooplankton (0.25) and mesozooplankton (0.25; i.e., cannibalism) the most, followed by diatoms (0.15), microphytoplankton (0.15), scavenging on medium sized POM (0.1), heterotrophic flagellates (0.05), and nanophytoplankton (0.05). The preferences are normalized and add up to 1. Assigning fixed preferences however ignores the fact that some mesozooplankton can preferentially prey on food that best satisfies their nutrient requirement for different life stages (Meunier et al. 2016). The experiment of Meunier et al. (2016) shows that nauplii with lower N:P prefer prey rich in P, while copepodites with higher N:P prefer prey rich in N. As an alternative to ERSEM's original fixed prey preferences, we formulated a new flexible food preference scheme based on the commonly used active predator switch model, known as the "Fasham formulation" (Fasham et al. 1990; Vallina, Ward, Dutkiewicz, & Follows 2014) and extended it to incorporate the dependence on food quality.

The original active predator switch proposed by Fasham et al. (1990) is:

$$\phi_{\mathrm{j}} = \frac{\rho_{\mathrm{j}} \mathrm{p_j}}{\sum_{\mathrm{j}} \rho_{\mathrm{j}} \mathrm{p_j}} \tag{4.8}$$

where ϕ_{j} is the variable preference of prey type j. It is a product of ρ_{j}, the density independent grazing preference for prey j, and $\mathrm{p_j}$, the biomass of prey j. In our formulation, we adopt the default values of ρ_{j} from ERSEM. Fasham's formulation describes how predators preferentially select the most abundant prey, reflecting an increase in capture efficiency as biomass of a given type of prey increases relative to others (Vallina et al. 2014). The constant preference ρ_{j} is related to predator-prey size ratios and the matchup between attack-survival strategies. The product of ρ_{j} and $\mathrm{p_j}$ is normalized, such that the sum of all the prey preference for a given predator adds up to 1.

We modified this original Fasham's formulation to incorporate age-specific food preference by assuming that a predator would preferentially select prey that has a higher

food quality (i.e., N:P ratios that most closely match the predator's nutritional requirement). Equation (4.8) is thus modified as follows:

$$\phi_{\mathrm{j}} = \frac{\rho_{\mathrm{j}} \mathrm{p_j} \cdot \mathrm{FQ_j}}{\sum_{\mathrm{j}} (\rho_{\mathrm{j}} \mathrm{p_j} \cdot \mathrm{FQ_j})} \tag{4.9}$$

where $\mathrm{FQ_j}$ is a food quality of prey j, measured in terms of the deviation from the ideal food N:P:

$$\mathrm{FQ_j} = \frac{1}{\sigma\sqrt{2\pi}} \exp\left[-\frac{1}{2}\left(\frac{\Delta(\mathrm{N:P})_{\mathrm{j}}}{\sigma}\right)^2\right] \tag{4.10}$$

where

$$\Delta(\mathrm{N:P})_{\mathrm{j}} = \frac{\text{ideal food N:P} - \text{food N:P}}{\text{ideal food N:P}} \tag{4.11}$$

As illustrated in Figure 4.3, FQ of each prey ($\mathrm{FQ_j}$) is a Gaussian function of the fractional difference between ideal food's N:P ratio and food's actual N:P ratio and takes the maximum value when that difference is zero. Definition of ideal food N:P follows the threshold elemental ratio (T. R. Anderson, Hessen, Elser, & Urabe 2005; Raubenheimer, Simpson, & Mayntz 2009):

$$\text{ideal food N:P} = \text{consumer N:P} \times \frac{\mathrm{GGE.N}}{\mathrm{GGE.P}} \tag{4.12}$$

where GGE.X is the gross growth efficiency of element X (e.g., if all ingested X leads to growth, GGE.X equals 100%). Experimental results of Meunier et al. (2016) show no statistically significant difference between the N:P of new tissue built and N:P ingested for both nauplii and copepodites. Hence, we assume that both GGE of N and GGE of P equal 100%. This assumption is often made in other studies (T. R. Anderson 1992; Urabe & Watanabe 1992). Therefore, FQ is highest when food N:P equals consumer's N:P. Although FQ would be the highest for cannibalism by this definition, our formulation does not necessarily lead to cannibalism being the most preferred feeding option. This is because food preference is not determined solely on the basis of FQ but is also a function of density independent preference (ρ_{j}) and prey biomass ($\mathrm{p_j}$). However, to prevent excess cannibalism by mesozooplankton, we set an upper bound for preference of cannibalism to be 0.25 (25%), a default value used in the original ERSEM.

As copepod's N:P changes with age (Figure 4.2), the peak of FQ curve shifts with age (Figure 4.3). Nauplii have the peak shifted to the left (i.e., preference for lower N:P) and copepodite has the peak shifted to the right (i.e., preference for higher N:P), reflecting their change in food's ideal N:P. Food quality function is a Gaussian, such that food quality is the same for a positive deviation of food N:P from the predator's N:P as for a negative deviation by the same absolute value. This is based on the observation that excess nutrient as well as lack of nutrients can limit ingestion rate because nutrient excess incurs physiologically significant metabolic costs, a phenomena known as "stoichiometric knife edge" (Boersma & Elser 2006; Bullejos et al. 2014; Laspoumaderes, Modenutti, Elser, & Balseiro 2015). Hence our definition of food quality differs from other zooplankton models which assume that simply an increase in prey nutrient content equal higher food quality (Branco, Stomp, Egas, & Huisman 2010; Zhao, Ramin, Cheng, & Arhonditsis 2008). The parameter σ in equation (4.10) is a measure of the

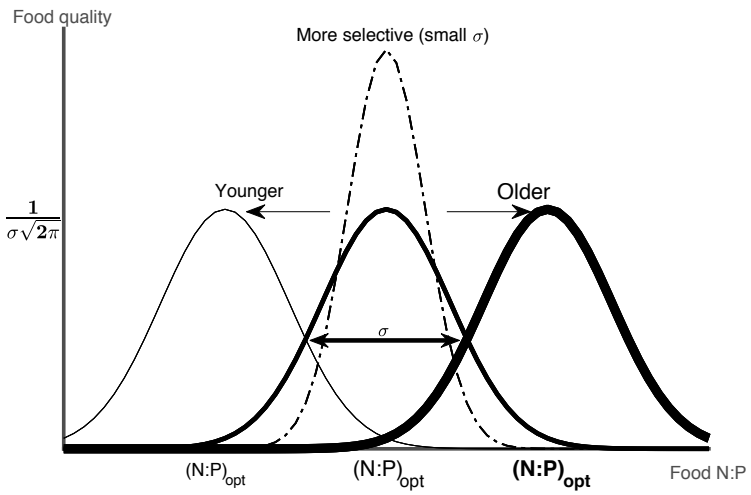

Figure 4.3: Schematic diagram showing the effect of food quality on food preference of copepod (mesozooplankton). Food preference function is a Gaussian function with two parameters, ideal N:P ratio of food ($(\mathrm{N:P})_{\mathrm{opt}}$) and degree of food selectivity (σ). Older copepod prefers food rich in N, giving them high $(\mathrm{N:P})_{\mathrm{opt}}$. shifting curve to the right (thick line). Younger copepod prefers P-rich food giving them lower $(\mathrm{N:P})_{\mathrm{opt}}$ (thin line). More selective copepod with small (σ) has higher peak value but narrower range of preference (dashed-dot). Note that area under the graph is approximately equal in all cases.

strength of food selectivity, where a large σ gives a broad food preference profile indicating weak selectivity of prey based on N:P. In contrast, a small σ indicates a sharp food preference profile and strong selectivity. By changing the value of σ, this formulation can simulate weaker, non-selective feeding behavior of copepod (Isari, Antó, & Saiz 2013) as well as a more strongly selective behavior. For this study, we assumed that the value of σ is constant with age as there is not yet any experimental evidence on how σ changes over the life stages of copepod. Yet, the usage of Gaussian function for describing food quality has a useful property over quadratic function for example, since Gaussian function has only two unknown parameters and that the area under the food quality function is always normalized to 1. Therefore, the effects of food quality and food quantity on food preference can effectively be decoupled.

4.3.4 Experimental setup

Our modified ERSEM was run in a zero dimensional (homogeneously mixed) chemostat setting under constant light (100 W m^{-2}) and temperature (10 °C). There is thus no seasonality. In order to investigate the effects of mesozooplankton's age-specific traits, each set of experiments was run by assuming a different fixed mean age of mesozooplankton between 1 and 14 days. The selection of mean age is reflected in mesozooplankton C:N:P as well as the maximum assimilation rate based on equations (4.5)-(4.7). For each experiment, simulations were run for 5 years, during which the model becomes steady, and the results from the final year were averaged. External nutrient supply rate of N and P is fixed at 0.1 d^{-1}, with N:P stoichiometry of 17:1 (17 mM:1 mM). All living functional types (phytoplankton, zooplankton, and bacteria) are initialized with the biomass of 20 mgC m^{-3} with N and P at the Redfield stoichiometry (molar) of C:N:P = 106:16:1, except for mesozooplankton, which has different C:N:P for each age experiment. Labile DOM was seeded with 80 mgC m^{-3} of carbon, and 1 and 0.1 mmol m^{-3} of N and P respectively. Semi-labile DOM and POM were assumed to be zero initially. All the numerical experiments were carried using MATLAB and the computational codes are available for download from authors GitHub (`http://github.com/tanio003/ERSEM_agemodel`).

4.4 Results

Biomass of mesozooplankton at equilibrium changes with the mean age (i.e., via N:P ratio) and the degree of food selectivity (i.e., σ value) (Figure 4.4). When prey selectivity based on food quality is strong (i.e., small σ, Figure 4.4a), mesozooplankton biomass takes a unimodal pattern where biomass is highest when the mean mesozooplankton age is 4-6 days (body N:P of 12-20). At the younger nauplii stage (age of 1-3 days), N:P ratio of mesozooplankton is 7-10 (Figure 4.2), which is significantly lower than the N:P ratios of most of its prey, that there is not adequate prey that can satisfy nauplii's nutritional requirement. In this case, their choice of diet is limited to cannibalism and few P-rich prey (nanophytoplankton and heterotrophic flagellates) (Figure 4.5a). Although the maximum assimilation rate is highest at the nauplius stage (Figure 4.2), the scarcity of food choice leads to a very low biomass of mesozooplankton. Likewise, at the later copepodite stage (age $>$ 9 days) prey is limited to few N-rich organisms with high N:P. The dearth of prey choices due to large difference between their own N:P and prey's N:P at young (1-4 days) and old age (9-14 days) is a major factor contributing to the unimodal biomass pattern of mesozooplankton when food selectivity is strong. Furthermore, the growth of mesozooplankton at older age is diminished by aging-related reduction in the maximum assimilation rate.

As mesozooplankton's mean age approaches late nauplius to early metamorphosis phase (age of 3-6 days), their body N:P approaches the external nutrient supply flux ratio of 17 and the ratios of most other plankton. As more prey now have N:P ratios close to mesozooplankton's ideal food N:P, mesozooplankton has a greater selection of food (Figure 4.5a). Under this high food selectivity scenario, mesozooplankton prefers feeding on microzooplankton followed by nanophytoplankton, mesozooplankton, medium size POM and heterotrophs. Preference increases for microzooplankton and medium sized POM (mPOM) but decreases for heterotrophs during this life stage, hence we observe concurrent decrease in microzooplankton biomass and increase in biomass of heterotrophs (Figure 4.4a).

As mesozooplankton becomes less selective based on food quality (i.e., larger σ, meaning more generalist in terms of grazing), the window in which mesozooplankton can grow becomes wider (compare Figure 4.4a and b). As σ becomes even larger, the

mesozooplankton response for different values of their internal N:P ratio approaches the Fasham formulation (Figure 4.4c) or the original ERSEM's fixed preference formulation (Figure 4.4d), both of which have no food quality dependence on prey preference. With the Fasham and Fixed preference formulations, mesozooplankton can feed on all prey even during the early nauplius stage and the late copepodite stage (Figure 4.5c and d). This contrasts with the low σ case, where avail- able prey types were limited to one or two prey types (Figure 4.5a). This is a major finding of this study, where the age-dependent food selectivity of mesozooplankton can alter the overall food web dynamics. As evident in Figure 4.4, the total biomass of all plankton functional types was not significantly affected by both the age and the food preference. This suggests that the top down control by the mesozooplankton was not strong in these model runs.

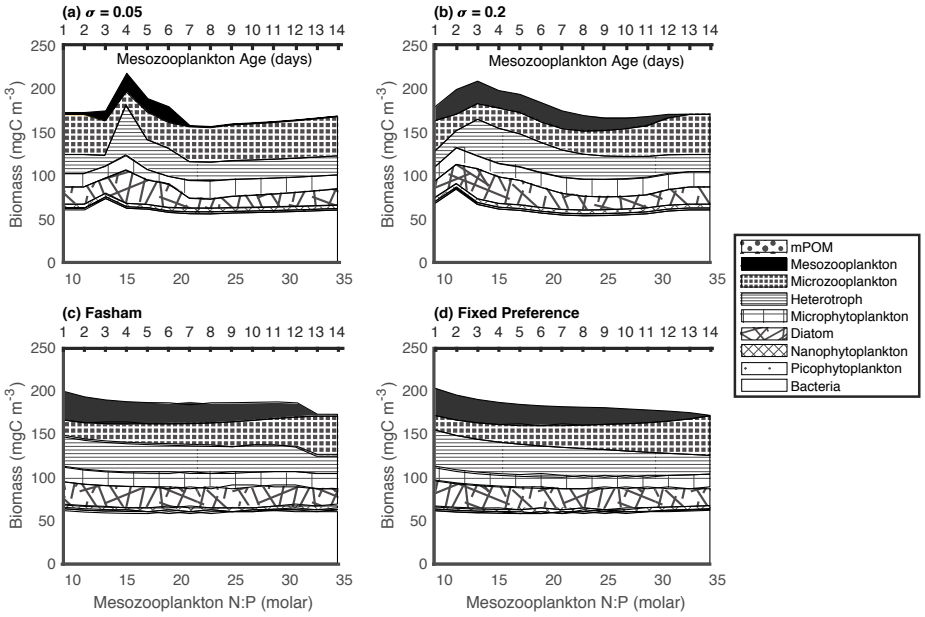

Figure 4.4: Equilibrium biomass of plankton functional types as a function of mesozooplankton N:P ratio. Shown are (a) Food preference model with $\sigma = 0.05$ (highly selective), (b) $\sigma = 0.2$ (moderately selective), (c) Fasham formulation, and (d) Fixed preference. Age of mesozooplankton is directly proportional to N:P shown in the top axis. Different shading patterns indicate different plankton functional types.

Incorporating flexible grazing formulations for microzooplankton and heterotrophs as well could lead to a stronger top down control (Armengol, Franchy, Ojeda, Santana-del Pino, & Hernández-León 2017). Although this is outside the scope of this study, indeed in another set of experiments where we allowed microzooplankton and heterotrophs food preference to be flexible, we did see transition from bottom-up to top-down control with increasing magnitude of σ. Larger σ (i.e., lower food selectivity) allows grazer to forage on phytoplankton even under conditions of nutrient imbalance, which leads to a stronger top-down control.

Age-dependent traits also affect nutrient dynamics (Figure 4.6) in addition to trophic interactions. When food preference is independent of food quality (Fasham and Fixed preference), released N:P deviates substantially from body N:P (Figure 4.6a). During

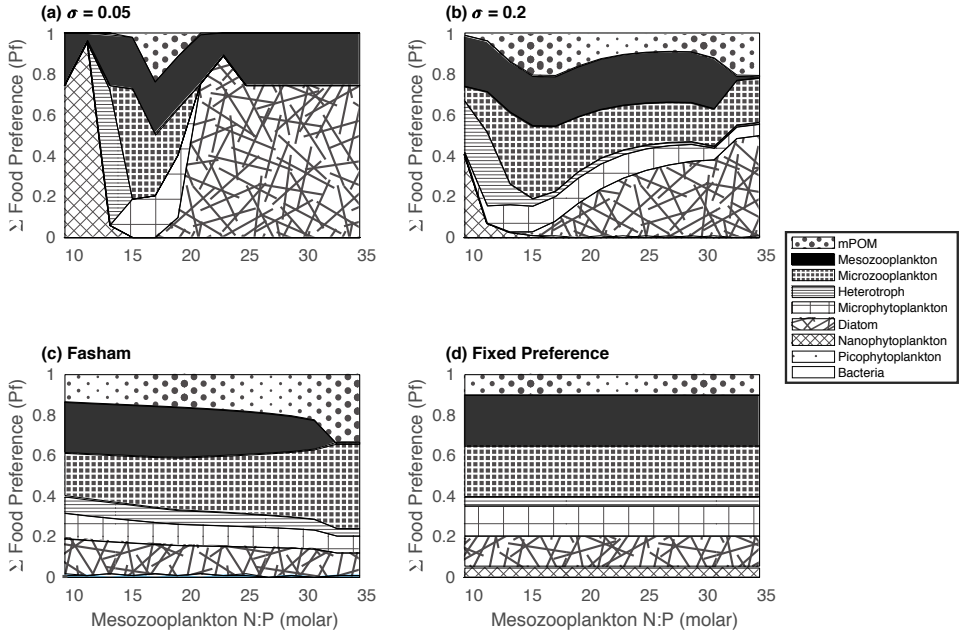

Figure 4.5: Equilibrium food preference of mesozooplankton as a function of mesozooplankton N:P ratio. Shown are (a) Food preference model with $\sigma = 0.05$ (highly selective), (b) $\sigma = 0.2$ (moderately selective), (c) Fasham formulation, and (d) Fixed preference. Shading scheme is same as Figure 4.4 each indicating different plankton functional types. Note that mesozooplankton only feed on nanophytoplankton, diatom, heterotrophs, microzooplankton, mesozooplankton (cannibalism), and medium sized POM.

nauplius stage (low internal N:P), they preferentially release more N compared to P, hence released N:P is above the 1:1 line. During copepodite stage (age > 9 days), body N:P is higher, leading to low N:P release ratio below 1:1 line. This is a typical behavior of copepod as they can release N or P preferentially in order to maintain homeostasis (Sterner 1990). On the other hand, when food quality dependence is high (i.e., low σ), released N:P more closely matches the 1:1 line. At low σ, mesozooplankton's food imbalance is small, so that they have little excess N or P to release. Although the metabolic costs associated with extra release of N and/or P is not explicitly included in the model, this can be an important trait in the actual marine environment (Elser et al. 2016; Plath & Boersma 2001). The trade-off associated with this food selection behavior is that their food choice becomes limited when their ideal food N:P deviates from food's N:P ratio.

Similar relationship holds between N:P ratio of large POM (lPOM) and N:P of mesozooplankton (Figure 4.6b). Since lPOM is mostly made up of released materials

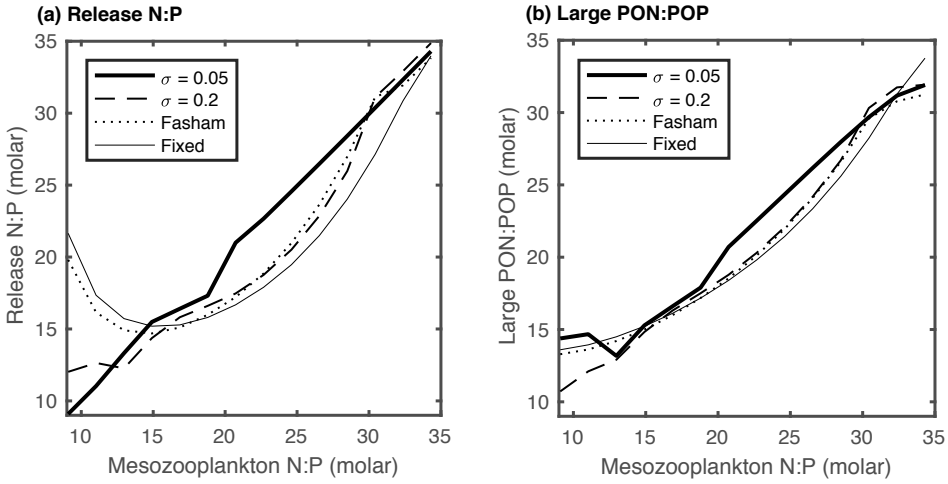

Figure 4.6: N:P ratio of released nutrient and large POM as a function of mesozooplankton N:P ratio. (a) Released N:P of mesozooplankton at equilibrium for different prey selectivity formulations. 1:1 line (not shown) indicates that released N:P equals body N:P. Region above 1:1 is an area of excess release of N, while area below is an area of excess P release over body N:P. (b) N:P ratio of large POM as a function of body N:P for different prey selectivity formulations.

from mesozooplankton, N:P ratio of lPOM is closely tied to released N:P ratio of mesozooplankton except for the fact that lPOM sinks and gets decomposed to DOM. When prey selection is not determined by food quality (Fasham or Fixed), N:P ratio lPOM is higher and lower than body N:P during nauplius and copepodite stage respectively. On the other hand, when prey selection is sensitive to food quality, N:P ratio of lPOM matches N:P ratio of mesozooplankton.

Influences of mesozooplankton nutrient release on the ambient water's inorganic N:P and bulk PON to POP ratio were marginal (not shown) due to the fact that mesozooplankton made up only 10% of the total biomass and that external nutrient supply flux was high enough to keep nutrient concentration replenished, minimizing the top down control. A further study incorporating selective feeding of other zooplankton types (heterotrophs and microzooplankton) may increase the effects of consumer-driven nutrient cycling. Indeed microzooplankton and heterotrophs also appear capable of selectively feeding on prey that most satisfies metabolic needs and to maintain C:N:P homeostasis (Meunier et al. 2012).

4.5 Discussion

For the first time, we introduced age-specific traits of marine zooplankton within the framework of an existing state of the art ecosystem model. Our modeling approach uses mesozooplankton C:N:P ratio as a proxy for the mean age instead of modeling the age structure explicitly. This approach relies on average population age structure of mesozooplankton following a unimodal structure. A unimodal population structure was reported in the North Sea by the classic study of Rakusa-Suszczewski (1967). More recently, Villar-Argaiz, Medina-Sánchez, and Carrillo (2002) observed a unimodal age structure of copepod during the large portion of ice-free period for the calanoid copepod *Mixodiaptomus lacinatus*. The unimodal structure is indicated by the time evolution of the age class abundances of the calanoids. In addition, an individual-based modeling study also predicts a unimodal population structure of copepod *Calanus sinicus* population in Yellow Sea during large portion of the stratified season (Wang et al. 2014).

Our numerical experiments show variations in response of plankton community and

its stoichiometry to changes in mesozooplankton's mean age, age-specific traits (internal C:N:P ratios and growth rate), and food preferences. High food selectivity leads to unimodal biomass distribution of mesozooplankton. Although there are multiple explanations for a unimodal population age structure in nature (Villar-Argaiz et al. 2002), our study indicates that one possible explanation is that young naupliar growth is limited by scarcity of food choice at the same time old copepodite growth is limited by nutrition imbalance and reduction of assimilation rate. These results provide testable and viable hypothesis on how age-specific traits of mesozooplankton modify plankton community structure.

An important future implication of this study is that the increasing N:P supply ratio due to the large addition of anthropogenic nitrogen into the oceans (Beusen, Bouwman, Van Beek, Mogollón, & Middelburg 2016; Bouwman et al. 2017) can significantly impact the age structure of copepod populations and modify the ocean N cycle. For example, nitrogen loading can favor older populations with higher optimal N:P over younger population with lower optimal N:P. In a negative feedback, the increase in abundance of older copepods with a preference for N may lead to a larger N export via large POM (i.e., copepods fecal pellets and excretion) thus ameliorating the excess N condition. Although questions remain on how age-specific traits of zooplankton impact nutrient cycling and food web dynamics on large spatial scales, formulations provided here can easily be incorporated into a wide variety of global biogeochemical models for further studies.

4.6 Acknowledgments

We thank Robert Sterner for providing us feedbacks on manuscript and Cédric Meunier for providing us with data. A prototype of the model was presented in the Ocean Carbon and Biogeochemistry (OCB) meeting at Woods Hole Oceanographic Institute, MA in Summer 2017. We thank multiple comments received during this conference.

Chapter 5

Phytoplankton stoichiometry and organic matter respiration

The contents of this section is currently under review in the journal *Geophysical Research Letters* under the title 'Stability of Marine Organic Matter Respiration Stoichiometry'.

5.1 Synopsis

Most organic carbon produced by phytoplankton in the surface is ocean is decomposed by bacteria using dissolved oxygen. This process is expected to accelerate under global warming leading to a significant loss of oxygen from the marine ecosystem. In order to accurately estimate the total amount of oxygen consumed during decomposition of organic matter, we require information on how much oxygen is required per unit of organic carbon. Here we estimate per-unit-carbon oxygen demand using two independent methods and show that the estimates are nearly constant in large parts of the world ocean. We suggest that this is attributable to the fact that globally, the organic matter is largely made of protein which requires less oxygen than other molecules such as lipid and carbohydrate.

5.2 Introduction

The expansion of oxygen-minimum zones (OMZs) and ocean deoxygenation in general are two of the biggest challenges facing the marine ecosystems as a consequence of higher CO_2 and a warming climate (Oschlies, Brandt, Stramma, & Schmidtko 2018). The global oxygen content has declined by more than 2% over the past five decades (Schmidtko, Stramma, & Visbeck 2017) and climate models predict a further deoxygenation under global warming (Bopp et al. 2013; Keeling, Körtzinger, & Gruber 2010). The decline in gas solubility due to the surface warming explains roughly half of the deoxygenation and the changes in oxygen transport and biological consumption account for the rest (Helm, Bindoff, & Church 2011; Schmidtko et al. 2017). However, teasing apart relative contributions of these factors is difficult and the models often fail to reproduce the temporal variability of oxygen concentrations inferred from time-series data (Long, Deutsch, & Ito 2016).

Biological consumption of dissolved oxygen is particularly difficult to characterize in models (Robinson 2019). Oxygen consumption is influenced by factors such as temperature effects on metabolism (Brewer & Peltzer 2017; Matsumoto 2007), flux of organic matter (Suess 1980), mineral ballast (Hofmann & Schellnhuber 2009), and the elemental composition of organic matter (Laws 1991). Parameterization of organic matter composition alone can lead to a significant uncertainty in reproducing the time-series data of surface oxygen (Andrews, Buitenhuis, Le Quéré, & Suntharalingam 2017). Field studies suggest that future, warmer ocean with higher CO_2 and stronger stratification will favor the production of organic matter rich in carbon (Paul et al. 2015; Riebesell et al. 2007; Yvon-Durocher, Schaum, & Trimmer 2017). Subsequent export of C-rich organic matter from surface to deep ocean can increase oxygen consumption and expand OMZs by 50% (Oschlies, Schulz, Riebesell, & Schmittner 2008). A critical assumption in this projection is that the amount of oxygen consumed per unit organic carbon ($O_2 : C_{rem}$) remains fixed both spatially and temporally (Paulmier, Kriest, & Oschlies 2009). The assumption may be reasonable in the deep ocean, where respiration rates are small and ocean circulation effectively homogenizes tracer concentrations (L. A. Anderson & Sarmiento 1994; DeVries & Deutsch 2014). However, this may not be the case in the upper layer of the ocean where the elemental composition of particulate organic matter

(POM) and dissolved organic matter (DOM) vary spatially (Galbraith & Martiny 2015; Letscher, Moore, Teng, & Primeau 2015; Martiny, Pham, et al. 2013; Martiny, Vrugt, & Lomas 2014).

An accurate determination of $O_2 : C_{rem}$ requires knowing the total numbers of carbon, hydrogen, oxygen, nitrogen, and phosphorus atoms in organic matter. For example, a relatively large amount of O_2 is needed (i.e. high $O_2 : C_{rem}$) to completely oxidize an organic matter rich in hydrogen, nitrogen, and phosphorus, but poor in oxygen (L. A. Anderson 1995; Karl & Grabowski 2017; Laws 1991). Of the three main macromolecules that compromise organic matter, protein has the highest demand for O_2 per mole remineralized, followed by lipid and carbohydrate (L. A. Anderson 1995). Since 1970's there has been significant improvements in the sampling and analysis techniques for accurately determining biochemical compositions of organic matter (Bhavya et al. 2019). In addition, a novel algorithm using satellite ocean color was recently developed to estimate the annual mean macromolecule compositions of phytoplankton (protein, carbohydrate, lipid, and chlorophyll) on the global scale (Roy 2018). In this study, we use two independent methods to determine large scale annual mean $O_2 : C_{rem}$ in the surface ocean using: (1) satellite-derived measurements of phytoplankton macromolecules; and (2) objectively gridded nutrient data. In addition, we determine seasonal changes in $O_2 : C_{rem}$ using local, *in situ* data on macromolecular concentrations in order to demonstrate the potential for $O_2 : C_{rem}$ to vary in the future. A notable strength of our approach in determining the remineralization ratios over previous approaches (Y.-H. Li & Peng 2002; Takahashi, Broecker, & Langer 1985) is that we do not require dissolved inorganic carbon data, thus circumventing the complicating factor of oceanic uptake of anthropogenic CO_2. Since biochemical processes in the ocean are complex and details of key reactions are still uncovered (Garcia-Robledo et al. 2017; Wright, Konwar, & Hallam 2012), we assume complete oxidation of organic matter by oxygen. A reliably estimated surface ocean O_2:C respiration stoichiometry would allow a more complete assessment of how the future oxygen cycle will evolve.

5.3 Methods

5.3.1 Estimating O_2:C from satellite-dericed phytoplankton macromolecular composition

In the first method of estimating the large scale annual mean $O_2 : C_{rem}$, we use remotely sensed estimates of the annually averaged main phytoplankton macromolecules (i.e., protein, lipid, carbohydrate, and chlorophyll) from Roy (2018). Given their molecular composition and knowledge of their mean chemical formulae (L. A. Anderson 1995; Geider & La Roche 2002; see Appendix D: Table D.1), a simple molecular weighted mean yields the remineralization stoichiometry of the bulk organic matter made of phytoplankton.

The macromolecule estimate is based on light-absorption coefficients of phytoplankton (optical property retrievable from ocean color) and allometric relationships between phytoplankton cell size and their cellular macromolecular contents (Roy 2018). In this study, we exclude the coastal and polar regions and bin the open ocean to the 11 oceanographic regions: Subpolar North Atlantic (NADR, GFST), Subpolar North Pacific (PSAW, PSAE, KURO, NPPF), Subtropical North Atlantic (NASW, NASE, NATR), Subtropical North Pacific (NPSW, NPTG), Tropical Atlantic (WTRA, ETRA), Tropical Pacific (WARM, PNEC, PEQD), North Indian (MONS), South Indian (ISSG), Subtropical South Atlantic (SATL), Subtropical South Pacific (SPSG), and Subantarctic (SANT). Names in brackets correspond to the oceanographic provinces of Longhurst (1995). In calculating the elemental composition of bulk phytoplankton biomass, we assume fixed elemental compositions for protein, lipid, carbohydrate, and chlorophyll in terms of C, H, O, N, P (Appendix D: Table D.1). Lipid is further split into two pools, 2/3 to the P-free lipid pool and 1/3 to phospholipid (Finkel et al. 2016). We calculate C, H, O, N, and P content of the bulk organic matter (sum of all the macromolecules) and then compute O_2:C remineralization ratio assuming complete aerobic oxidation of organic matter (L. A. Anderson 1995):

$$O_2 : C_{rem} = 1.00 + 0.25(H : C) - 0.5(O : C) + 1.25(N : C) + 1.25(P : C) \tag{5.1}$$

Roy (2018) does not provide the estimate of the nucleic acid content (DNA and RNA),

which typically make up 5-15% of phytoplankton by weight (Geider & La Roche 2002). We therefore estimate the weight % of nucleic acid that is required to meet the C:P export ratios from a previous inverse modeling study (Teng et al. 2014).

5.3.2 Estimating O_2:C from the vertical gradient method of dissolved nutrients and oxygen

We calculate $O_2 : C_{rem}$ from $N : P_{exp}$, $C : P_{exp}$, and $O_2 : P_{rem}$ using a method previously developed to estimate $CaCO_3$:Organic carbon, N:P, and Si:N export ratios (Dunne et al. 2007; Henson, Sanders, & Madsen 2012; Sarmiento et al. 2002; Sarmiento, Gruber, Brzezinski, & Dunne 2004). N:P export ratio is estimated from the vertical gradients of NO_3^- and PO_4^{3-} from 1x1 degree 2013 World Ocean Atlas (WOA) (H. E. Garcia et al. 2013) between the surface layer and the deep layer which approximately corresponds to the thermocline:

$$N : P_{exp} = \frac{(NO_3^-)_{deep} - (NO_3^-)_{surf}}{(PO_4^{3-})_{deep} - (PO_4^{3-})_{surf}}. \tag{5.2}$$

Similarly, $O_2 : P_{rem}$ is calculated from the apparent oxygen utilization (AOU) in the subsurface layer and the vertical gradient of PO_4^{3-}:

$$O_2 : P_{rem} = \frac{AOU_{deep}}{(PO_4^{3-})_{deep} - (PO_4^{3-})_{surf}}. \tag{5.3}$$

We calculate $N : P_{exp}$ and $O_2 : P_{rem}$ in each WOA grid box using the Ferret program of NOAA's Pacific Marine Environmental Laboratory (`http://ferret.pmel.noaa.gov/Ferret/`). All tracers concentrations are normalized to salinity of 35. In other words, for a given tracer, its concentration is multiplied by 35 and divided by the local salinity to account for the effects of evaporation and precipitation. We separate ocean boundaries based on the 0.3 μM contour of the annually mean NO_3^- concentrations in the top 100 m. We use the bootstrap method to estimate the regional $N : P_{exp}$ and $O_2 : P_{rem}$ by constructing 10000 trial datasets from the original dataset by random selection with replacement and taking the median of all the individual estimates as the best estimate. The 95% confidence interval comes from the 2.5% and 97.5% tails of the resulting distribution. We exclude waters poleward of subtropical gyres and marginal seas as this method of determining export/remineralization ratio inherently assume that

the lateral transport is much smaller than the vertical tracer transport (Sarmiento et al. 2002). See Appendices D.3 and D.4 for details on the vertical gradient method.

We carry out our calculations for three choices of surface and deep layer: "0-100-200" (units in m), "0-200-400", "0-MLD-200", where MLD is the spatially variable mixed layer depth defined by the temperature difference criterion of $\Delta T = 0.8$ °C from 10 m (Kara, Rochford, & Hurlburt 2003). In addition, we also consider the effects of seasonal variability by using summer-averaged values and winter-averaged values from the WOA. These combinations yield 9 different calculations of the vertical gradients (3 different depth ranges and x3 temporal averages) and we report ensemble mean and standard deviation of $N : P_{exp}$ and $O_2 : P_{rem}$ from 9 sensitivity experiments.

C:P export ratio is calculated using equation (5.4) derived by Peng and Broecker (1987):

$$O_2 : P_{rem} = (1 + f)C : P_{exp} + 2N : P_{exp} \tag{5.4}$$

where parameter f is a measure of dissolved oxygen needed to oxidize excess hydrogen atoms bound to organic matter. The derivation for equation (5.4) is described in the Appendix D.2. We assume a fixed f value of 0.11 in applying equation (5.4) and this assumption is supported by two lines of evidence. First, we obtain $f = 0.11$ by applying equation (5.4) to mean algal composition ($C_{106}H_{175}O_{42}N_{16}P$) and mean O_2:P remineralization ratio of 150 based on various observations and model studies (L. A. Anderson 1995; DeVries & Deutsch 2014). Mean algal composition ($C_{106}H_{175}O_{42}N_{16}P$) is composed of 54.4% protein, 25.5% carbohydrate, 16.1% lipid, and 4.0% nucleic acid by organic dry weight (L. A. Anderson 1995). Second, regression of $PO_4{}^{3-}$, $NO_3{}^-$, $\Sigma\ CO_2$, and alkalinity along isopycnal horizons in deep Indian sea waters free of fossil fuel CO_2 yields f of 0.1 (Peng & Broecker 1987).

5.3.3 Estimating O_2:C from laboratory and *in situ* measurements of phytoplankton macromolecules

We use data from Finkel et al. (2016), who summarized 1562 observations of macromolecule composition (protein, lipid, carbohydrate, RNA, DNA, Chlorophyll-a, and

Ash) for marine and freshwater microalgae across 7 major microalgae phyla (Cyanobacteria, Chlorophyta, Cryptophyta, Bacillariophyta, Haptophyta, Ochrophyta, and Dinophyta) from 130 publications. Of the 1562 total observations, we select observations which all three of protein, lipid, and carbohydrate estimates are given as dry weight per cell (n = 420). We estimate the elemental content (C, H, N, O, P) of the 420 data by summing the contributions from three major macromolecular pools (protein, lipid, carbohydrate) weighted by their chemical composition (Appendix D: Table D.1) and calculate remineralization O_2:C ratio using equation (5.1). We do not include contributions from nucleic acid and chlorophyll because there are very few observations of them compared to those of protein, lipid, and carbohydrate.

Phytoplankton macromolecule concentrations from various global oceans are compiled by Bhavya et al. (2019). Of 25 datasets they have collected and tabulated, we select 10 that cover the timespan of at least 6 months continuously. When the dataset covers multiple sampling stations across different depths and geographic locations we take a simple average across all the stations to calculate the mean macromolecule concentrations. We use GraphClick software (Arizona software, 2010) to extract numbers from graphs and figures when data were not explicitly listed in the results. We estimate the elemental composition and remineralization ratios of the bulk organic matter from the concentrations of the 3 main macromolecules (protein, lipid, and carbohydrate) using the method described already. As uncertainties in measured macromolecules are not available at all sites, we calculate $O_2 : C_{rem}$ at each site by taking concentrations of each macromolecule at face value.

5.3.4 Monte Carlo simulation

We carry out Monte Carlo simulation by randomly changing the relative proportions of protein, lipid, and carbohydrate to assess the sensitivity of $O_2 : C_{rem}$ to different macromolecular compositions. Unless otherwise stated, all mathematical simulations are done in MATLAB R2018b (MathWorks). We generate 10,000 sets of three pseudo random numbers with uniform distribution between 0 and 1. The three numbers correspond to the relative abundance of protein, carbohydrate, and lipid. For each set, the three numbers are normalized so that their sum is $1 - \alpha$, where α is the relative abundance of nucleic acid. For the default case, we assume α of 5%. For each of the 10,000 sets,

we compute the elemental stoichiometry of the bulk organic matter using the method outlined in the previous sections by using well characterized elemental compositions of protein, carbohydrate, lipid, and nucleic acid. A nonparametric estimate of probability density function (pdf) for 10,000 sets is generated using the kernel density estimator. Median value and the 95% confidence interval are derived from the resulting cumulative density function. We run three end-member simulations (i.e., three 10,000 sets) to illustrate how $O_2 : C_{rem}$ and the confidence intervals vary with the change in the macromolecular composition. In the first simulation, protein is always assigned the largest of the three pseudo random numbers with no constraint on the remaining two numbers for lipid and carbohydrate. This protein-dominant composition pattern is the most commonly observed pattern for marine and freshwater phytoplankton (Hedges et al. 2002). In the second simulation, the relative proportions of protein, carbohydrate, and lipid are assigned randomly, so that any one of them could be the first, second, or the third largest element. In the third simulation, carbohydrate is always assigned the largest pseudo random number with no constraint on the remaining two numbers for protein and lipid. We explore the effects of nucleic acid in determining the shape of $O_2 : C_{rem}$ pdf by changing α from 0% (no nucleic acid) to 10% of the total mass.

5.4 Results and Discussion

Phytoplankton macromolecules show a clear pattern with high total concentrations in the nutrient rich waters and low concentrations in subtropical gyres and other oligotrophic regions (Figure 5.1a). Protein makes up the largest portion, followed by lipid, carbohydrate, and chlorophyll. Despite the large systematic variability in the total macromolecular content of phytoplankton our analysis yields a fairly tight $O_2 : C_{rem}$ of 1.4-1.5 (Figure 5.1b). The uncertainty in $O_2 : C_{rem}$ reflects the uncertainty associated with the remote sensing algorithm used to estimate macromolecular content (Roy 2018) (Appendix D.1). For example, the relative uncertainty is high in nutrient rich, productive regions and low in oligotrophic regions (Appendix D: Table D.2). The inferred nucleic acid fraction in the ocean is as low as few percent in the oligotrophic regions to as high as 18% in the subarctic regions (Figure 5.1a). This spatial variability is consistent with the growth rate hypothesis, which posits that fast growing phytoplankton in the

nutrient rich waters allocate a larger fraction of their biomass to nucleic acid resulting in low cellular C:P (Sterner & Elser 2002).

$O_2 : C_{rem}$ estimated from the vertical gradient method shows a spatially constant value of ∼1.4 in the large parts of the tropical and subtropical oceans (Figure 5.2a), consistent with the results from the first method (Figure 5.1b). The magnitude of $O_2 : C_{rem}$ is dependent on the balance between $N : P_{exp}$ and $O_2 : P_{rem}$ (Appendix D.2). In most regions, $N : P_{exp}$ and $O_2 : P_{rem}$ are well correlated despite large scale variabilities (Figure 5.2b, c), so that $O_2 : C_{rem}$ remains close to the mean value of ∼1.4. For example, high $N : P_{exp}$ is compensated by high $O_2 : P_{rem}$ in the North Atlantic subtropical gyre, so that $O_2 : C_{rem}$ remains close to 1.4. Similarly, low $O_2 : P_{rem}$ is compensated by low $N : P_{exp}$ in the South Indian Ocean. Noticeable positive deviation of $O_2 : C_{rem}$ in the South Atlantic Ocean is caused by significantly small $O_2 : P_{rem}$. Oxygen consumption suggested by subsurface apparent oxygen utilization (AOU) is smaller than implied by the vertical gradient of PO_4^{3-}, suggesting that oxygen consumption and phosphate remineralization may be somewhat decoupled or that the assumption inherent in AOU is violated. The decoupling can, for example, be achieved during hydrolysis of organic

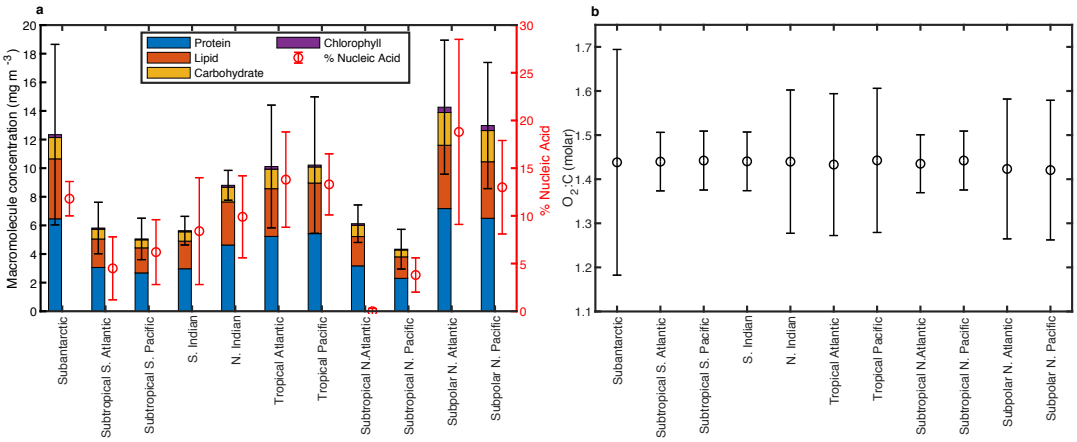

Figure 5.1: Satellite-derived annually averaged phytoplankton macromolecular content and O_2:C remineralization ratio binned into 11 oceanographic regions. (a) Bar graph of protein, lipid, carbohydrate, and chlorophyll content based on the ocean color. Error bar is the sum of algorithm uncertainty for each macromolecule. Red indicates inferred % nucleic acid required to meet previously estimated $C : P_{exp}$ ratios (Teng et al. 2014) given the remotely sensed macromolecular content; (b) O_2:C remineralization ratio estimated from the total macromolecule content.

phosphoric acid esters, the process that releases phosphate in the water column but does not consume oxygen (Thomas 2002). In addition, O_2 disequilibrium caused by seasonal ice, deep winter convection and heat loss can decouple AOU from the true remineralization signal (Ito, Follows, & Boyle 2004). Our analysis shows this decoupling is most prominent in the summer months when $O_2 : C_{rem}$ exceeds ~1.7 (Appendix D: Table D.5). Unfortunately, the number of currently available observations needed to assess this decoupling mechanism is limited, leaving significantly high $O_2 : C_{rem}$ in our results.

The two independent methods employed in this study both indicate that O_2:C remineralization ratio is approximately 1.4 in much of the global ocean. We suggest two mechanisms for explaining this relatively stable pattern. The first is an argument based on the macromolecular composition of phytoplankton. Satellite-derived measurements (Figure 5.1a) and the laboratory-based measurements of phytoplankton macromolecular content (Figure 5.3a) show that protein makes up the largest fraction followed by lipid and carbohydrate. Despite large variability in the total macromolecular concentration, this compositional pattern is consistent across all oceanographic regions and across major phyla. In nutrient rich regions, such as subpolar and upwelling regions, protein synthesis is favored by high abundance of essential nutrients such as nitrates (Liefer et

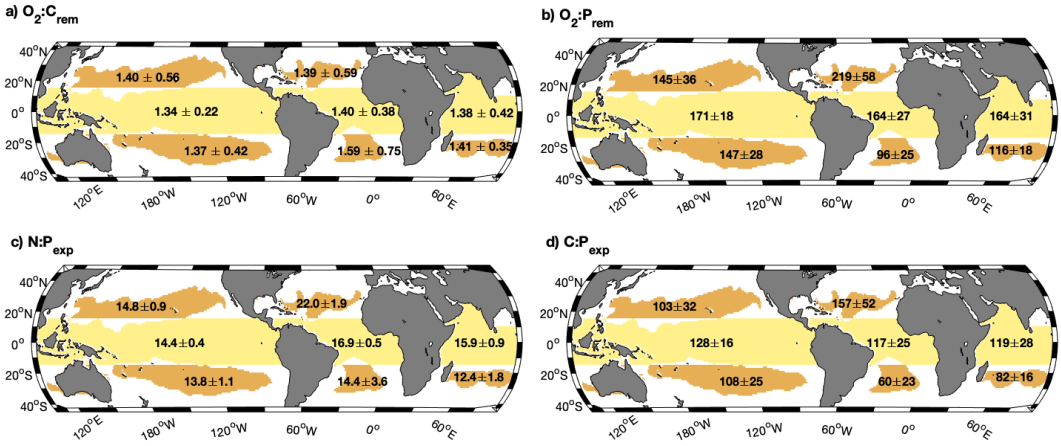

Figure 5.2: Export and remineralization ratios determined from the vertical gradient method. The mean ($\pm 1\sigma$) (a) $O_2 : C_{rem}$, (b) $O_2 : P_{rem}$, (c) $N : P_{exp}$, and (d) $C : P_{exp}$ at the bottom of the surface layer within regions defined by 0.3 μM contour of the annually averaged NO_3^- concentrations. Subtropical gyres = Orange, Tropical and upwelling regions = Yellow.

al. 2019). Protein synthesis is also favored in the warm temperature (Fanesi, Wagner, Birarda, Vaccari, & Wilhelm 2019; Toseland et al. 2013) thereby resulting in high protein fraction in tropics and subtropics. Phylum averaged $O_2 : C_{rem}$ based on laboratory measurements are tightly clustered around the global mean value of 1.4 (Figure 5.3a). A Monte Carlo simulation with an ensemble of 10,000 randomly generated biomass composition confirms that $O_2 : C_{rem}$ is confined to the 95% confidence interval between 1.34 and 1.50 when protein is the largest fraction of the three main macromolecules (Figure 5.3b) and this result is not affected by the amount of nucleic acid.

The second mechanism that can help maintain $O_2 : C_{rem}$ of $\sim$1.4 involves zooplankton and higher trophic level interactions. Compared to autotrophic organisms, heterotrophs are known to be more homeostatic and capable of regulating their elemental composition (Meunier, Malzahn, & Boersma 2014). In addition, the biomass of heterotrophs including bacteria and zooplankton is typically richer in protein and poorer in carbohydrates compared to phytoplankton biomass (Kirchman 2018). Observations and modeling studies have shown that trophic level interactions can regulate ecosystem C:N ratio even when food quality of phytoplankton is low under the nutrient limited conditions (Martiny, Vrugt, et al. 2013; Talmy et al. 2016). As $O_2 : C_{rem}$ is strongly related to C:N ratio of organic matter, the stability of the latter leads to the stability of the former.

There are some limitations in the methods we used to determine large scale $O_2 : C_{rem}$. One limitation is that both the satellite-derived and the vertical gradient methods do not extend to depths below the thermocline. For example, preferential remineralization of organic nitrogen over carbon could lead to a lower $O_2 : C_{rem}$ at depth. On the global level, there is a systematic increase in C:N ratio of particulate organic matter with depth at a rate of approximately 0.2 units per 1000 m (Schneider, Schlitzer, Fischer, Nothig, & Nöthig 2003). This change in C:N translates to a modest 0.004 per 1000 m change in $O_2 : C_{rem}$, assuming a linear relationship between C:N and $O_2 : C_{rem}$ and C:N of $\sim$6.6 in the surface. Unless there are significant accompanying changes in oxygen and hydrogen content of organic matter, $O_2 : C_{rem}$ is thus unlikely to be affected by preferential remineralization of nitrogen. Isopycnal analysis of remineralization stoichiometry of the deep ocean ($>$ 400 m) also indicates relatively constant ratios at depths (L. A. Anderson & Sarmiento 1994). However as the elemental composition and their

characteristics of organic matter below mesopelagic zone is still largely uncharacterized (Karl & Grabowski 2017; C. Lee, Wakeham, & Arnosti 2004), further studies would be

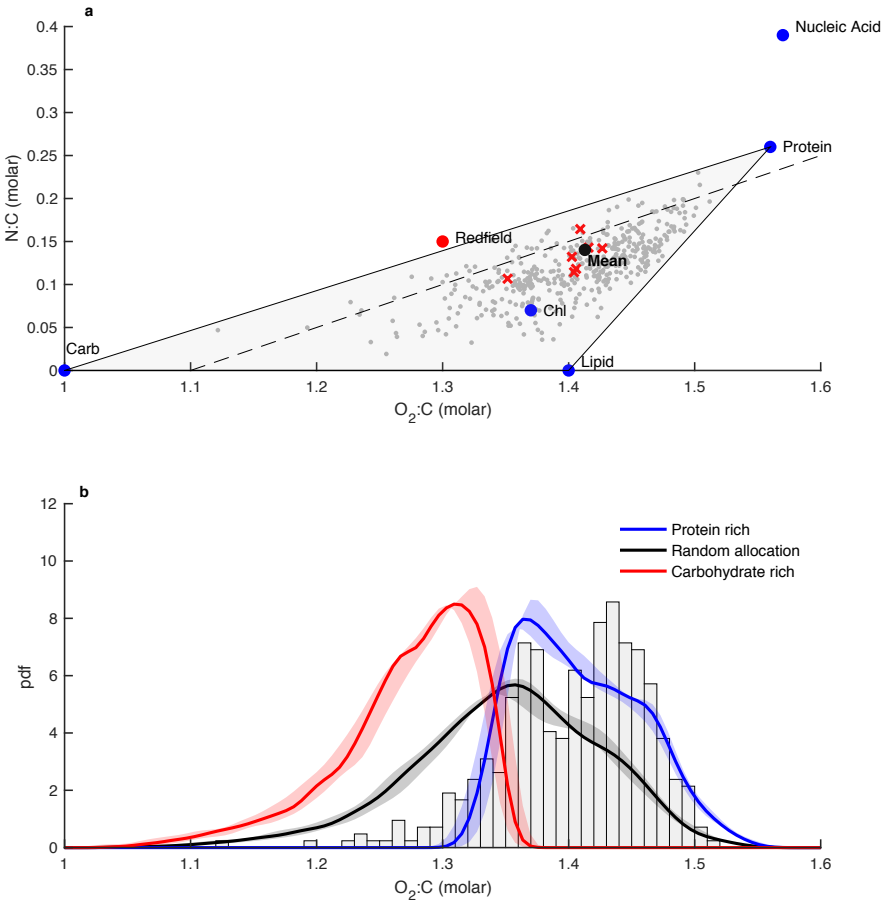

Figure 5.3: $O_2 : C_{rem}$ estimated from laboratory-based measurements of phytoplankton macromolecule content. (a) Grey dots: N:C and $O_2 : C_{rem}$ calculated from 420 observations of marine and freshwater microalgae (Finkel et al. 2016). Blue dots: Macromolecule endmembers. Red crosses: Phylum specific ratios for 7 different phyla (Cyanobacteria, Chlorophyta, Cryptophyta, Bacillariophyta, Haptophyta, Ochrophyta, Dinophyta). The black dotted line is $O_2 : C_{rem} = 1.11 + 2$N:C, a first order estimate of $O_2 : C_{rem}$ as a function of N:C (Appendix D.2); (b) Probability density function (pdf) of $O_2 : C_{rem}$ obtained from Monte Carlo ensemble simulation. The thick lines assume that nucleic acid makes up 5%. Shades show the effect of varying nucleic acid content between 0 and 10%. Histogram: $O_2 : C_{rem}$ of aquatic microalgae shown in (a) binned at a fixed interval of 0.01.

needed to accurately determine $O_2 : C_{rem}$ in the deep ocean.

Another limitation is that we do not consider the effects of denitrification on the stoichiometry of organic matter respiration. Subsurface water column denitrification would reduce the vertical gradient of NO_3^- and this may help explain somewhat low N:P export ratios in subtropical gyres (Figure 5.2c). This N:P underestimation would in turn lead to underestimation of $O_2 : C_{rem}$. However, this error may not be significant on the global scale, because denitrification tends to be local and its effect would be smoothed out over a large spatial scale (Y.-H. Li, Karl, Winn, Mackenzie, & Gans 2000). In addition, the decrease in N:P due to denitrification should be compensated partly in terms of $O_2 : C_{rem}$ by an associated increase in $O_2 : P_{rem}$ as remineralized PO_4^{3-} from aerobic remineralization becomes smaller. Indeed a previous study has shown that accounting for denitrification increases global estimate of $O_2 : P_{rem}$ by approximately 3 to 5 units (DeVries & Deutsch 2014).

5.5 Implications for the Future Marine Oxygen Cycle

While our analysis indicates that global annual mean $O_2 : C_{rem}$ is stable today, *in situ* measurements of phytoplankton macromolecular composition show a noticeable temporal shift for example in the coastal waters of East/Japan Sea (Jo et al. 2017) (Site 3, Figure 5.4) where the relative fraction of carbohydrate increases to $\sim$70% during late spring. This increase translates to $O_2 : C_{rem}$ of $\sim$1.16, which is almost 20% lower than the global mean. A similar seasonal trend of high carbohydrate/low protein during spring was observed in the Bedford Basin, Arctic Ocean (Site 1) and Princess Astrid Coast in Antarctica (Site 10). Increase in the relative abundance of carbohydrate over protein in late spring is likely to be caused by nutrient-depleted condition following spring bloom. Alternatively, a change in the phytoplankton community composition from protein rich to carbohydrate rich taxonomic group may have caused such chemical shift in the bulk composition. No significant seasonal trend in macromolecule compositions was observed in the Mediterranean (Sites 5-8), where climate is generally mild, and in the regions where nutrient concentrations are high throughout the year (Sites 2 and 9) suggesting strong spatial variability on the regional scale. These local studies thus demonstrate that phytoplankton is potentially capable of adapting to low nutrient condition by shifting

their macromolecular composition from protein rich to carbohydrate rich. However, a further study would be required to assess the temporal variability of $O_2 : C_{rem}$ on the global scale.

In summary, estimated O_2:C remineralization in the surface ocean today is roughly ~1.4 with little spatial variability despite large spatial variabilities in C:N:P ratios of

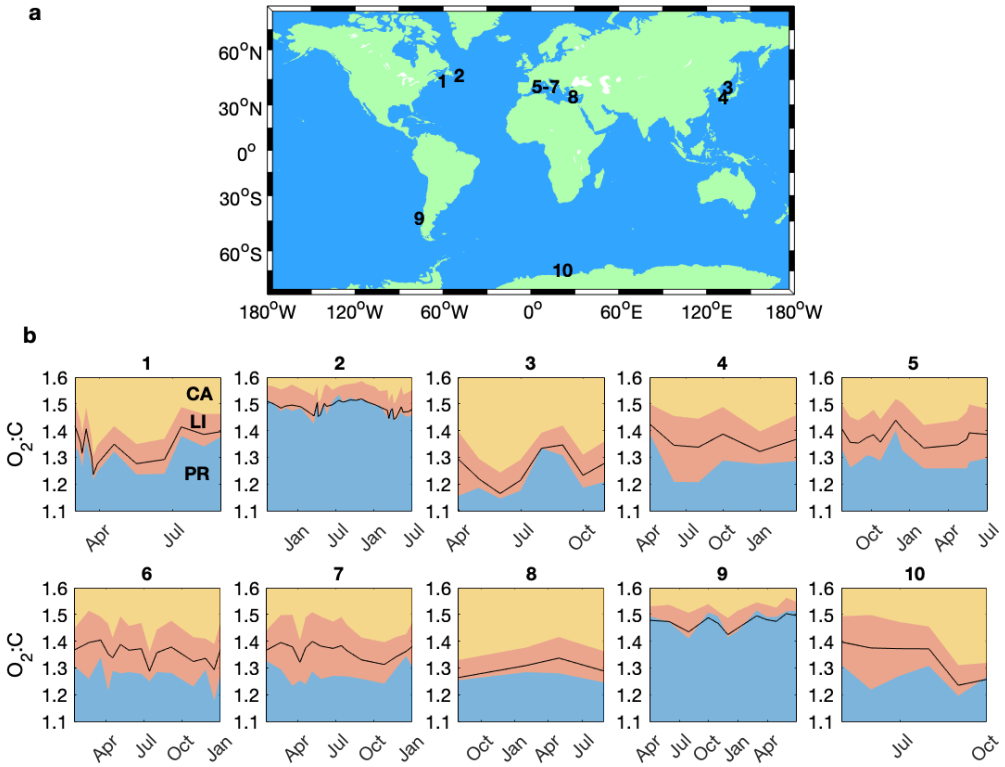

Figure 5.4: $O_2 : C_{rem}$ in various marine ecosystems estimated from biochemical composition of phytoplankton. (a) Locations in which macromolecule composition investigations have been conducted for at least 6 months period. 1 = Bedford Basin (Mayzaud et al. 1989); 2 = Logy Bay (Navarro & Thompson 1995); 3 = Southwestern East/Japan Sea (Jo et al. 2017); 4 = Gwangyang Bay (J. H. Lee et al. 2017); 5 = W. Mediterranean submarine cave (Fichez 1991); 6 = Mediterranean seagrass system (Danovaro et al. 1998); 7 = Ligurian Sea (Danovaro & Fabiano 1997); 8 = Cretan Sea (Danovaro et al. 2000); 9 = Yaldad Bay (Navarro et al. 1993); 10 = Princess Astrid Coast (Dhargalkar et al. 1996); (b) Seasonal $O_2 : C_{rem}$ estimated from the total macromolecule content and the relative fractions of major phytoplankton macromolecules (shaded, PR = Protein, LI = Lipid, CA = Carbohydrate).

organic matter. This pattern is explained by the characteristic macromolecule allocation of phytoplankton where cellular nucleic acid fraction (P content) is highly variable depending on the growth condition and the relative fraction of protein content is universally higher over lipid and carbohydrate. Current biogeochemical models including those used in the CMIP5 experiments assume constant $O_2 : C_{rem}$ of 1.4 -1.5 (Buchanan et al. 2018; Paulmier et al. 2009) obtained from previous local field observations (L. A. Anderson & Sarmiento 1994; Körtzinger, Hedges, & Quay 2001; Takahashi et al. 1985) and generalized theories (L. A. Anderson 1995; Fraga, Ríos, Pèrez, & Figueiras 1998; Laws 1991). Our results indicate that a fixed O_2:C remineralization ratio of 1.4 in models remains to be valid assumption at least in the tropics and subtropics.

Future warming and climate change are expected to increase remineralization and the production of C-rich organic matter which in combination could accelerate deoxygenation through positive feedback involving the production of greenhouse N_2O via denitrification and anaerobic respiration of organic matter (Keeling et al. 2010; Oschlies et al. 2008). If $O_2 : C_{rem}$ decreases, as carbohydrate becomes the dominant macromolecule in phytoplankton or as the algal community shifts in favor of more carbohydrate-rich phytoplankton, our study would predict that ocean deoxygenation could be ameliorated. In the absence of such amelioration, oxygen deoxygenation driven by biological consumption of oxygen is likely to continue unabated with potentially detrimental impacts on the survival of marine organisms.

5.6 Acknowledgments

We thank Pearce Buchanan for fruitful discussions. Satellite-derived phytoplankton macromolecule data are available from Roy (2018). Ocean tracer data used to calculate vertical gradients are available from World Ocean Atlas 2013 (`https://www.nodc.noaa.gov/OC5/woa13/woa13data.html`). Phytoplankton macromolecule dataset used in Figure 5.3 is available from the Macromolecular database (`https://doi.org/10.1371/journal.pone.0155977.s001`) (Finkel et al. 2016). Timeseries data of phytoplankton macromolecules used in Figure 5.4 are provided in the Zenodo repository (`https://doi.org/10.5281/zenodo.3462575`).

Chapter 6

Concluding Remarks

The work presented in this dissertation establishes a robust framework for linking phytoplankton stoichiometry and global ocean biogeochemical dynamics. The synthesis on how different environmental drivers modify elemental composition of marine phytoplankton (Chapter 3) is a significant advancement over previous efforts that were either qualitative or did not cover wide array of published studies. I have shown that both C:N and C:P ratios are expected to increase under future climate scenario as the ocean becomes warmer and vertically stratified. I also showed that diatoms have the greatest flexibility in elemental stoichiometry compared to other phytoplankton types. This has an important implication for future ocean biogeochemical dynamics as we often overlook the plasticity of diatoms in marine ecosystem and assume that there will be a shift toward smaller phytoplankton in the nutrient-poor, vertically stratified ocean following the basic principles of Margalef's Mandala (Margalef 1978). I propose that high stoichiometric plasticity of diatoms as well as a general shift toward C-rich composition of phytoplankton would buffer an expected decline in export production of carbon (Chapters 2, 3). I also showed in the final chapter the shift in chemical composition of phytoplankton, from protein-rich to carbohydrate-rich, can reduce per-unit-carbon consumption of oxygen significantly and that this can ameliorate ongoing open ocean deoxygenation (Chapter 5). In summary, I conclude that elemental stoichiometry of phytoplankton is flexible as a function of environmental drivers and that change in elemental stoichiometry will play important roles in future ocean global biogeochemical dynamics.

To end this dissertation, I will discuss some key topics that are of potential interest for the future study:

- *Including our insights from meta-analysis into 3D Earth System Models*: Our work in this dissertation is largely theoretical and the future predictions of ocean biogeochemistry are based on the simple first-order arguments. In order to test how flexible stoichiometry of phytoplankton affect ocean global biogeochemical dynamic more accurately, we need to incorporate our meta-analysis results into Earth System Models. I have already shown in Chapter 2 the preliminary results using MESMO, an Earth System Model of Intermediate Complexity. In the future, I will be incorporating our C:N:P power-law model into fully coupled Earth System Models such as CESM (J. K. Moore, Lindsay, Doney, Long, & Misumi 2013). A notable strength of our power-law model over other cellular stoichiometry models (e.g., Pahlow, Dietze, & Oschlies 2013) is that our model is relatively straight forward and computationally efficient while it is still capable of capturing the key nonlinear aspects of phytoplankton physiology.

- *Investigating the roles of zooplankton, heterotrophic bacteria, and virus in determining elemental composition of organic mater*: I have mentioned in Chapter 3 already that elemental composition of organic matter simply does not equal uptake ratio of phytoplankton but are largely affected by subsequent recycling processes. In this effort, I started exploring in Chapter 4 the roles of zooplankton in determining the elemental composition of particulate organic matter using a zero-dimensional model. In the future this work could be expanded to include more realistic physical settings for example by coupling to a 1D diffusion-advection model.

- *Using latest insights from molecular and systems biology in predicting elemental composition of marine phytoplankton*: One promising method for predicting phytoplankton cellular composition more accurately is to use the publicly available genome-scale metabolic models of marine phytoplankton. Essentially, each genome scale models contain cellular information on all known chemical reactions, metabolites, and genes for the particular organisms (O'Brien, Monk, & Palsson 2015). There are currently over 20 metabolic reconstructions publicly available for

marine microorganisms including all major phytoplankton groups (Fondi & Fani 2017). By using these genome-scale models, we can explicitly and deterministically relate phytoplankton physiology to elemental composition.

References

Agusti, S., González-Gordillo, J. I., Vaqué, D., Estrada, M., Cerezo, M. I., Salazar, G., ... Duarte, C. M. (2015). Ubiquitous healthy diatoms in the deep sea confirm deep carbon injection by the biological pump. *Nature Communications*, *6*(1), 7608.

Andersen, T., & Hessen, D. O. (1991). Carbon, nitrogen, and phosphorus content of freshwater zooplankton. *Limnology and Oceanography*, *36*(4), 807–814.

Anderson, L. A. (1995). On the hydrogen and oxygen content of marine phytoplankton. *Deep-Sea Research Part I*, *42*(9), 1675–1680.

Anderson, L. A., & Sarmiento, J. L. (1994). Redfield ratios of remineralization determined by nutrient data analysis. *Global Biogeochemical Cycles*, *8*(1), 65–80.

Anderson, T. R. (1992). Modelling the influence of food C:N ratio, and respiration on growth and nitrogen excretion in marine zooplankton and bacteria. *Journal of Plankton Research*, *14*(12), 1645–1671.

Anderson, T. R., Hessen, D. O., Elser, J. J., & Urabe, J. (2005). Metabolic Stoichiometry and the Fate of Excess Carbon and Nutrients in Consumers. *The American Naturalist*, *165*(1), 1–15.

Anderson, T. R., Hessen, D. O., Mitra, A., Mayor, D. J., & Yool, A. (2013). Sensitivity of secondary production and export flux to choice of trophic transfer formulation in marine ecosystem models. *Journal of Marine Systems*, *125*(September), 41–53.

Andrews, O., Buitenhuis, E., Le Quéré, C., & Suntharalingam, P. (2017). Biogeochemical modelling of dissolved oxygen in a changing ocean. *Philosophical Transactions of the Royal Society A: Mathematical, Physical and Engineering Sciences*, *375*(2102).

Armengol, L., Franchy, G., Ojeda, A., Santana-del Pino, Á., & Hernández-León, S. (2017). Effects of copepods on natural microplankton communities: do they exert top-down control? *Marine Biology*, *164*(6), 1–13.

Arteaga, L., Pahlow, M., & Oschlies, A. (2014). Global patterns of phytoplankton nutrient and light colimitation inferred from an optimality-based model. *Global Biogeochemical Cycles*, *28*(7), 648–661.

Aumont, O., Ethé, C., Tagliabue, A., Bopp, L., & Gehlen, M. (2015). PISCES-v2: An ocean biogeochemical model for carbon and ecosystem studies. *Geoscientific Model Development*, *8*(8), 2465–2513.

Béchemin, C., Grzebyk, D., Hachame, F., Hummert, C., & Maestrini, S. (1999). Effect of different nitrogen/phosphorus nutrient ratios on the toxin content in Alexandrium minutum. *Aquatic Microbial Ecology*, *20*(2), 157–165.

Behrenfeld, M. J., & Falkowski, P. G. (1997). Photosynthetic rates derived from satellite-based chlorophyll concentration. *Limnology and Oceanography*, *42*(1), 1–20.

Berges, J., Varela, D., & Harrison, P. (2002). Effects of temperature on growth rate, cell composition and nitrogen metabolism in the marine diatom Thalassiosira pseudonana (Bacillariophyceae). *Marine Ecology Progress Series*, *225*(February 2014), 139–146.

Berman-Frank, I., Cullen, J. T., Shaked, Y., Sherrell, R. M., & Falkowski, P. G. (2001). Iron availability, cellular iron quotas, and nitrogen fixation in Trichodesmium. *Limnology and Oceanography*, *46*(6), 1249–1260.

Berman-Frank, I., & Dubinsky, Z. (1999). Balanced Growth in Aquatic Plants: Myth or Reality? *BioScience*, *49*, 29–37.

Beusen, A. H. W., Bouwman, A. F., Van Beek, L. P. H., Mogollón, J. M., & Middelburg, J. J. (2016). Global riverine N and P transport to ocean increased during the 20th century despite increased retention along the aquatic continuum. *Biogeosciences*, *13*(8), 2441–2451.

Bhavya, P. S., Kim, B. K., Jo, N., Kim, K., Kang, J. J., Lee, J. H., ... Lee, S. H. (2019). A Review on the Macromolecular Compositions of Phytoplankton and the Implications for Aquatic Biogeochemistry. *Ocean Science Journal*, *54*(1), 1–14.

Bi, R., Ismar, S., Sommer, U., & Zhao, M. (2017). Environmental dependence of the correlations between stoichiometric and fatty acid-based indicators of phytoplankton nutritional quality. *Limnology and Oceanography*, *62*(1), 334–347.

Bi, R., Ismar, S. M., Sommer, U., & Zhao, M. (2018). Simultaneous shifts in elemental stoichiometry and fatty acids of Emiliania huxleyi in response to environmental changes. *Biogeosciences*, *15*(4), 1029–1045.

Bittar, T. B., Lin, Y., Sassano, L. R., Wheeler, B. J., Brown, S. L., Cochlan, W. P., & Johnson, Z. I. (2013). Carbon allocation under light and nitrogen resource gradients in two model marine phytoplankton 1. *Journal of Phycology*, *49*(3), 523–535.

Blackford, J. C., Allen, J. I., & Gilbert, F. J. (2004). Ecosystem dynamics at six contrasting sites: A generic modelling study. *Journal of Marine Systems*, *52*(1-4), 191–215.

Blanco-Ameijeiras, S., Moisset, S. A. M., Trimborn, S., Campbell, D. A., Heiden, J. P., & Hassler, C. S. (2018). Elemental Stoichiometry and Photophysiology Regulation of Synechococcus sp. PCC7002 Under Increasing Severity of Chronic Iron Limitation. *Plant and Cell Physiology*, *59*(9), 1803–1816.

Boersma, M., & Elser, J. J. (2006). Too much of a good thing: On stoichiometrically balanced diets and maximal growth. *Ecology*, *87*(5), 1325–1330.

Bonachela, J. A., Klausmeier, C. A., Edwards, K. F., Litchman, E., & Levin, S. A. (2016). The role of phytoplankton diversity in the emergent oceanic stoichiometry. *Journal of Plankton Research*, *38*(4), 1021–1035.

Bopp, L., Resplandy, L., Orr, J. C., Doney, S. C., Dunne, J. P., Gehlen, M., ... Vichi, M. (2013). Multiple stressors of ocean ecosystems in the 21st century: projections with CMIP5 models. *Biogeosciences*, *10*(10), 6225–6245.

Bouwman, A. F., Beusen, A. H. W., Lassaletta, L., van Apeldoorn, D. F., van Grinsven, H. J. M., Zhang, J., & Ittersum van, M. K. (2017). Lessons from temporal and spatial

patterns in global use of N and P fertilizer on cropland. *Scientific Reports*, *7*(January), 40366.

Boyd, P. W. (2019). Physiology and iron modulate diverse responses of diatoms to a warming Southern Ocean. *Nature Climate Change*, *9*(2), 148–152.

Boyd, P. W., Lennartz, S. T., Glover, D. M., & Doney, S. C. (2015). Biological ramifications of climate-change-mediated oceanic multi-stressors. *Nature Climate Change*, *5*(1), 71–79.

Boyd, P. W., Rynearson, T. A., Armstrong, E. A., Fu, F., Hayashi, K., Hu, Z., ... Thomas, M. K. (2013). Marine Phytoplankton Temperature versus Growth Responses from Polar to Tropical Waters – Outcome of a Scientific Community-Wide Study. *PLoS ONE*, *8*(5), e63091.

Boyd, P. W., Strzepek, R., Fu, F., & Hutchins, D. A. (2010). Environmental control of open-ocean phytoplankton groups: Now and in the future. *Limnology and Oceanography*, *55*(3), 1353–1376.

Branco, P., Stomp, M., Egas, M., & Huisman, J. (2010). Evolution of Nutrient Uptake Reveals a Trade-Off in the Ecological Stoichiometry of Plant-Herbivore Interactions. *The American Naturalist*, *176*(6), E162–E176.

Brauer, V. S., Stomp, M., Rosso, C., van Beusekom, S. A., Emmerich, B., Stal, L. J., & Huisman, J. (2013). Low temperature delays timing and enhances the cost of nitrogen fixation in the unicellular cyanobacterium Cyanothece. *The ISME Journal*, *7*(11), 2105–2115.

Brembu, T., Mühlroth, A., Alipanah, L., & Bones, A. M. (2017). The effects of phosphorus limitation on carbon metabolism in diatoms. *Philosophical Transactions of the Royal Society B: Biological Sciences*, *372*(1728), 20160406.

Brennan, G. L., Colegrave, N., & Collins, S. (2017). Evolutionary consequences of multidriver environmental change in an aquatic primary producer. *Proceedings of the National Academy of Sciences of the United States of America*, *114*(37), 9930–9935.

Brewer, P. G., & Peltzer, E. T. (2017). Depth perception: The need to report ocean biogeochemical rates as functions of temperature, not depth. *Philosophical Transactions of the Royal Society A: Mathematical, Physical and Engineering Sciences*, *375*(2102), 20160319.

Broecker, W. S. (1982). Ocean chemistry during glacial time. *Geochimica et Cosmochimica Acta*, *46*(10), 1689–1705.

Bucciarelli, E., Pondaven, P., & Sarthou, G. (2010). Effects of an iron-light co-limitation on the elemental composition (Si, C, N) of the marine diatoms Thalassiosira oceanica and Ditylum brightwellii. *Biogeosciences*, *7*(2), 657–669.

Buchanan, P. J., Matear, R. J., Chase, Z., Phipps, S. J., & Bindoff, N. L. (2018). Dynamic Biological Functioning Important for Simulating and Stabilizing Ocean Biogeochemistry. *Global Biogeochemical Cycles*, *32*(4), 565–593.

Bullejos, F. J., Carrillo, P., Gorokhova, E., Medina-Sánchez, J. M., Gabriel Balseiro, E., & Villar-Argaiz, M. (2014). Shifts in food quality for herbivorous consumer growth: Multiple golden means in the life history. *Ecology*, *95*(5), 1272–1284.

Butenschön, M., Clark, J., Aldridge, J. N., Icarus Allen, J., Artioli, Y., Blackford, J., ... Torres, R. (2016). ERSEM 15.06: A generic model for marine biogeochemistry and the ecosystem dynamics of the lower trophic levels. *Geoscientific Model Development*, *9*(4), 1293–1339.

Cabré, A., Marinov, I., & Leung, S. (2015). Consistent global responses of marine ecosystems to future climate change across the IPCC AR5 earth system models. *Climate Dynamics*, *45*(5-6), 1253–1280.

Cáceres, C., Spatharis, S., Kaiserli, E., Smeti, E., Flowers, H., & Bonachela, J. A. (2019). Temporal phosphate gradients reveal diverse acclimation responses in phytoplankton phosphate uptake. *The ISME Journal*, *13*(11), 2834–2845.

Carlotti, F., & Sciandra, A. (1989). Population dynamics model of Euterpina acutifrons (Copepoda: Harpacticoida) coupling individual growth and larval development. *Marine Ecology Progress Series*, *56*, 225–242.

Cavan, E. L., Henson, S. A., Belcher, A., & Sanders, R. (2017). Role of zooplankton in determining the efficiency of the biological carbon pump. *Biogeosciences*, *14*(January), 177–186.

Cembella, A. D., Antia, N. J., Harrison, P. J., & Rhee, G.-Y. (1984). The Utilization of Inorganic and Organic Phosphorous Compounds as Nutrients by Eukaryotic Microalgae: A Multidisciplinary Perspective: Part 2. *CRC Critical Reviews in Microbiology*, *11*(1), 13–81.

Chavez, F. P., & Barber, R. T. (1987). An estimate of new production in the equatorial Pacific. *Deep Sea Research Part A, Oceanographic Research Papers*, *34*(7), 1229–1243.

Claquin, P., Martin-Jezequel, V., Kromkamp, J. C., Veldhuis, M. J. W., & Kraay, G. W. (2002). UNCOUPLING OF SILICON COMPARED WITH CARBON AND NITROGEN METABOLISMS AND THE ROLE OF THE CELL CYCLE IN CONTINUOUS CULTURES OF THALASSIOSIRA PSEUDONANA (BACILLARIOPHYCEAE) UNDER LIGHT, NITROGEN, AND PHOSPHORUS CONTROL1. *Journal of Phycology*, *38*(5), 922–930.

Collins, S., Boyd, P. W., & Doblin, M. A. (2020). Evolution, Microbes, and Changing Ocean Conditions. *Annual Review of Marine Science*, *12*(1), annurev–marine–010318–095311.

Copin-Montegut, C., & Copin-Montegut, G. (1983). Stoichiometry of carbon, nitrogen, and phosphorus in marine particulate matter. *Deep Sea Research Part A. Oceanographic Research Papers*, *30*(1), 31–46.

Danovaro, R., Croce, N. D., & Fabiano, M. (1998). Biochemical composition of particulate organic matter and bacterial dynamics at the sediment-water interface in a Mediterranean seagrass system. *Hydrobiologia*, *363*, 241–251.

Danovaro, R., Dell'Anno, A., Pusceddu, A., Marrale, D., Della Croce, N., Fabiano, M., & Tselepides, A. (2000). Biochemical composition of pico-, nano- and micro-particulate organic matter and bacterioplankton biomass in the oligotrophic Cretan Sea (NE Mediterranean). *Progress in Oceanography*, *46*(2-4), 279–310.

Danovaro, R., & Fabiano, M. (1997). Seasonal changes in quality and quantity of food available for benthic suspension-feeders in the Golfo Marconi (North-western Mediterranean). *Estuarine, Coastal and Shelf Science*, *44*(6), 723–736.

De La Rocha, C., Hutchins, D., Brzezinski, M., & Zhang, Y. (2000). Effects of iron and zinc deficiency on elemental composition and silica production by diatoms. *Marine Ecology Progress Series*, *195*, 71–79.

DeVries, T., & Deutsch, C. (2014). Large-scale variations in the stoichiometry of marine organic matter respiration. *Nature Geoscience*, *7*(12), 890–894.

Dhargalkar, V. K., Matondkar Prabhu, S. G., & Verlencar, X. N. (1996). *Seasonal variations in carbon budget in water column off Princess Astrid Coast, Antarctica* (Tech. Rep.).

Doucette, G. J., & Harrison, P. J. (1991). Aspects of iron and nitrogen nutrition in the red tide dinoflagellateGymnodinium sanguineum. *Marine Biology*, *110*(2), 175–182.

Dunne, J. P., Armstrong, R. A., Gnnadesikan, A., & Sarmiento, J. L. (2005). Empirical and mechanistic models for the particle export ratio. *Global Biogeochemical Cycles*, *19*(4).

Dunne, J. P., John, J. G., Shevliakova, E., Stouffer, R. J., Krasting, J. P., Malyshev, S. L., ... Zadeh, N. (2013). GFDL's ESM2 Global Coupled Climate–Carbon Earth System Models. Part II: Carbon System Formulation and Baseline Simulation Characteristics*. *Journal of Climate*, *26*(7), 2247–2267.

Dunne, J. P., Sarmiento, J. L., & Gnanadesikan, A. (2007). A synthesis of global particle export from the surface ocean and cycling through the ocean interior and on the seafloor. *Global Biogeochemical Cycles*, *21*(4).

Dyhrman, S. T. (2016). Nutrients and Their Acquisition: Phosphorus Physiology in Microalgae. In *The physiology of microalgae* (pp. 155–183). Cham: Springer International Publishing.

Edwards, K. F., Thomas, M. K., Klausmeier, C. A., & Litchman, E. (2012). Allometric scaling and taxonomic variation in nutrient utilization traits and maximum growth rate of phytoplankton. *Limnology and Oceanography*, *57*(2), 554–566.

Elser, J. J., Dobberfuhl, D. R., Mackay, N. a., & Schampel, J. H. (1996). Organism Size, Life History, and N:P Stoichiometry: Toward a unified view of cellular and ecosystem processes. *BioScience*, *46*(9), 674–684.

Elser, J. J., Kyle, M., Learned, J., McCrackin, M. L., Peace, A. L., & Steger, L. (2016). Life on the stoichiometric knife-edge: Effects of high and low food C: P ratio on growth, feeding, and respiration in three Daphnia species. *Inland Waters*, *6*(2), 136–146.

Elser, J. J., & Urabe, J. (1999). The stoichiometry of consumer-driven nutrient recycling: Theory, observations, and consequences. *Ecology*, *80*(3), 735–751.

Eppley, R. W., & Peterson, B. J. (1979). Particulate organic matter flux and planktonic new production in the deep ocean. *Nature*, *282*(5740), 677–680.

Eppley, R. W., Renger, E. H., & Betzer, P. R. (1983). The residence time of particulate organic carbon in the surface layer of the ocean. *Deep Sea Research Part A, Oceanographic Research Papers*, *30*(3), 311–323.

Fábregas, J., Patiño, M., Vecino, E., Cházaro, F., & Otero, A. (1995). Productivity and biochemical composition of cyclostat cultures of the marine microalga Tetraselmis suecica. *Applied Microbiology and Biotechnology*, *43*(4), 617–621.

Falk, S., Maxwell, D. P., Laudenbach, D. E., & Huner, N. P. A. (2006). Photosynthetic Adjustment to Temperature. In N. R. Baker (Ed.), *Photosynthesis and the environment* (pp. 367–385). Dordrecht: Kluwer Academic Publishers.

Falkowski, P. G., & LaRoche, J. (1991). ACCLIMATION TO SPECTRAL IRRADIANCE IN ALGAE. *Journal of Phycology*, *27*(1), 8–14.

Falkowski, P. G., & Raven, J. A. (2007). *Aquatic Photosynthesis* (2nd editio ed.). Princeton, NJ: Princeton University Press.

Falkowski, P. G., Scholes, R. J., Boyle, E., Canadell, J., Canfield, D., Elser, J. J., ... Steffen, W. (2000). The global carbon cycle: a test of our knowledge of earth as a system. *Science*, *290*(5490), 291–296.

Fanesi, A., Wagner, H., Birarda, G., Vaccari, L., & Wilhelm, C. (2019). Quantitative macromolecular patterns in phytoplankton communities resolved at the taxonomical level by single-cell Synchrotron FTIR-spectroscopy. *BMC Plant Biology*, *19*(1), 142.

Fasham, M. J. R., Ducklow, H. W., & McKelvie, S. M. (1990). A nitrogen-based model of plankton dynamics in the oceanic mixed layer. *Journal of Marine Research*, *48*(3), 591–639.

Feng, Y., Roleda, M. Y., Armstrong, E., Law, C. S., Boyd, P. W., & Hurd, C. L. (2018). Environmental controls on the elemental composition of a Southern Hemisphere strain of the coccolithophore <i>Emiliania huxleyi</i>. *Biogeosciences*, *15*(2), 581–595.

Fennel, W. (2001). Modeling of copepods with links to circulation models. *Journal of Plankton Research*, *23*(11), 1217–1232.

Fichez, R. (1991). Suspended particulate organic matter in a Mediterranean submarine cave. *Marine Biology*, *108*(1), 167–174.

Finkel, Z. V., Beardall, J., Flynn, K. J., Quigg, A., Rees, T. A. V., & Raven, J. A. (2010). Phytoplankton in a changing world: cell size and elemental stoichiometry. *Journal of Plankton Research*, *32*(1), 119–137.

Finkel, Z. V., Follows, M. J., Liefer, J. D., Brown, C. M., Benner, I., & Irwin, A. J. (2016). Phylogenetic diversity in the macromolecular composition of microalgae. *PLoS ONE*, *11*(5), e0155977.

Finkel, Z. V., Quigg, A., Raven, J. A., Reinfelder, J. R., Schofield, O. E., & Falkowski, P. G. (2006). Irradiance and the elemental stoichiometry of marine phytoplankton. *Limnology and Oceanography*, *51*(6), 2690–2701.

Flynn, K. J. (2008). Use, abuse, misconceptions and insights from quota models - The droop cell quota model 40 years on. *Oceanography and Marine Biology*, *46*, 1–23.

Flynn, K. J. (2010). Ecological modelling in a sea of variable stoichiometry: Dysfunctionality and the legacy of Redfield and Monod. *Progress in Oceanography*, *84*(1-2), 52–65.

Flynn, K. J., Raven, J. A., Rees, T. A. V., Finkel, Z., Quigg, A., & Beardall, J. (2010). IS THE GROWTH RATE HYPOTHESIS APPLICABLE TO MICROALGAE?1. *Journal of Phycology*, *46*(1), 1–12.

Fondi, M., & Fani, R. (2017). *Constraint-based metabolic modelling of marine microbes and communities* (Vol. 34).

Fraga, F., Ríos, A. F., Pèrez, F. F., & Figueiras, F. G. (1998). Theoretical limits of oxygen:carbon and oxygen:nitrogen ratios during photosynthesis and mineralisation of organic matter in the sea. *Scientia Marina*, *62*(1-2), 161–168.

Frigstad, H., Andersen, T., Hessen, D. O., Naustvoll, L.-J., Johnsen, T. M., & Bellerby, R. G. J. (2011). Seasonal variation in marine C:N:P stoichiometry: can the composition of seston explain stable Redfield ratios? *Biogeosciences*, *8*(10), 2917–2933.

Fu, F., Yu, E., Garcia, N., Gale, J., Luo, Y., Webb, E., & Hutchins, D. (2014). Differing responses of marine N2 fixers to warming and consequences for future diazotroph community structure. *Aquatic Microbial Ecology*, *72*(1), 33–46.

Fu, F.-X., Zhang, Y., Bell, P. R. F., & Hutchins, D. A. (2005). PHOSPHATE UPTAKE AND GROWTH KINETICS OF TRICHODESMIUM (CYANOBACTERIA) ISOLATES FROM THE NORTH ATLANTIC OCEAN AND THE GREAT BARRIER REEF, AUSTRALIA. *Journal of Phycology*, *41*(1), 62–73.

Fu, F.-X., Zhang, Y., Feng, Y., & Hutchins, D. A. (2006). Phosphate and ATP uptake and growth kinetics in axenic cultures of the cyanobacterium Synechococcus CCMP 1334. *European Journal of Phycology*, *41*(1), 15–28.

Fu, W., Primeau, F., Keith Moore, J., Lindsay, K., & Randerson, J. T. (2018). Reversal of Increasing Tropical Ocean Hypoxia Trends With Sustained Climate Warming. *Global Biogeochemical Cycles*, *32*(4), 551–564.

Fu, W., Randerson, J. T., & Moore, J. K. (2016). Climate change impacts on net primary production (NPP) and export production (EP) regulated by increasing stratification and phytoplankton community structure in the CMIP5 models. *Biogeosciences*, *13*(18), 5151–5170.

Galbraith, E. D., & Martiny, A. C. (2015). A simple nutrient-dependence mechanism for predicting the stoichiometry of marine ecosystems. *Proceedings of the National Academy of Sciences*, *112*(27), 8199–8204.

Garcia, C. A., Baer, S. E., Garcia, N. S., Rauschenberg, S., Twining, B. S., Lomas, M. W., & Martiny, A. C. (2018). Nutrient supply controls particulate elemental concentrations and ratios in the low latitude eastern Indian Ocean. *Nature Communications*, *9*(1), 4868.

Garcia, H. E., Locarnini, R. A., Boyer, T. P., Antonov, J. I., Baranova, O. K., Zweng, M. M., ... Johnson, D. R. (2013). WORLD OCEAN ATLAS 2013 Volume 4: Dissolved Inorganic Nutrients (phosphate, nitrate, silicate). *Technical Ed. NOAA Atlas NESDIS*, *75*(September), 25.

Garcia, N. S., Fu, F.-X., Breene, C. L., Bernhardt, P. W., Mulholland, M. R., Sohm, J. A., & Hutchins, D. A. (2011). INTERACTIVE EFFECTS OF IRRADIANCE AND CO2 ON CO2 FIXATION AND N2 FIXATION IN THE DIAZOTROPH TRICHODESMIUM ERYTHRAEUM (CYANOBACTERIA)1. *Journal of Phycology*, *47*(6), 1292–1303.

Garcia, N. S., Sexton, J., Riggins, T., Brown, J., Lomas, M. W., & Martiny, A. C. (2018). High Variability in Cellular Stoichiometry of Carbon, Nitrogen, and Phosphorus Within Classes of Marine Eukaryotic Phytoplankton Under Sufficient Nutrient Conditions. *Frontiers in Microbiology*, *9*, 543.

Garcia-Robledo, E., Padilla, C. C., Aldunate, M., Stewart, F. J., Ulloa, O., Paulmier, A., ... Revsbech, N. P. (2017). Cryptic oxygen cycling in anoxic marine zones. *Proceedings of the National Academy of Sciences*, *114*(31), 8319–8324.

Geider, R., & La Roche, J. (2002). Redfield revisited: variability of C:N:P in marine microalgae and its biochemical basis. *European Journal of Phycology*, *37*(1), 1–17.

Giovagnetti, V., Cataldo, M. L., Conversano, F., & Brunet, C. (2012). Growth and photophysiological responses of two picoplanktonic Minutocellus species, strains RCC967 and RCC703 (Bacillariophyceae). *European Journal of Phycology*, *47*(4), 408–420.

Goldman, J. C. (1979). Temperature effects on steady-state growth, phosphorus uptake, and the chemical composition of a marine phytoplankter. *Microbial Ecology*, *5*(3), 153–166.

Goldman, J. C., McCarthy, J. J., & Peavey, D. G. (1979). Growth rate influence on the chemical composition of phytoplankton in oceanic waters. *Nature*, *279*(5710), 210–215.

Goldman, J. C., & Ryther, J. H. (1976). Temperature-influenced species competition in mass cultures of marine phytoplankton. *Biotechnology and Bioengineering*, *18*(8), 1125–1144.

Greene, R. M., Geider, R. J., & Falkowski, P. G. (1991). Effect of iron limitation on photosynthesis in a marine diatom. *Limnology and Oceanography*, *36*(8), 1772–1782.

Grosse, J., van Breugel, P., Brussaard, C. P. D., & Boschker, H. T. S. (2017). A biosynthesis view on nutrient stress in coastal phytoplankton. *Limnology and Oceanography*, *62*(2), 490–506.

Gruber, N., & Galloway, J. N. (2008). An Earth-system perspective of the global nitrogen cycle. *Nature*, *451*(7176), 293–296.

Gurevitch, J., Koricheva, J., Nakagawa, S., & Stewart, G. (2018). Meta-analysis and the science of research synthesis. *Nature*, *555*(7695), 175–182.

Hedges, J. I., Baldock, J. A., Gélinas, Y., Lee, C., Peterson, M. L., & Wakeham, S. G. (2002). The biochemical and elemental compositions of marine plankton: A NMR perspective. *Marine Chemistry*, *78*(1), 47–63.

Heiden, J. P., Bischof, K., & Trimborn, S. (2016). Light Intensity Modulates the Response of Two Antarctic Diatom Species to Ocean Acidification. *Frontiers in Marine Science*, *3*, 260.

Helm, K. P., Bindoff, N. L., & Church, J. A. (2011). Observed decreases in oxygen content of the global ocean. *Geophysical Research Letters*, *38*(23).

Henson, S. A., Sanders, R., & Madsen, E. (2012). Global patterns in efficiency of particulate organic carbon export and transfer to the deep ocean. *Global Biogeochemical Cycles*, *26*(1).

Henson, S. A., Yool, A., & Sanders, R. (2015). Variability in efficiency of particulate organic carbon export: A model study. *Global Biogeochemical Cycles*, *29*(1), 33–45.

Hessen, D. O., Elser, J. J., Sterner, R. W., & Urabe, J. (2013). Ecological stoichiometry: An elementary approach using basic principles. *Limnology and Oceanography*, *58*(6), 2219–2236.

Hessen, D. O., Faerovig, P. J., & Andersen, T. (2002). Light, Nutrients, and P:C Ratios in Algae: Grazer Performance Related to Food Quality and Quantity. *Ecology*, *83*(7), 1886.

Hessen, D. O., Hafslund, O. T., Andersen, T., Broch, C., Shala, N. K., & Wojewodzic, M. W. (2017). Changes in Stoichiometry, Cellular RNA, and Alkaline Phosphatase Activity of Chlamydomonas in Response to Temperature and Nutrients. *Frontiers in Microbiology*, *8*, 18.

Hessen, D. O., Leu, E., Færøvig, P. J., & Falk Petersen, S. (2008). Light and spectral properties as determinants of C:N:P-ratios in phytoplankton. *Deep Sea Research Part II: Topical Studies in Oceanography*, *55*(20-21), 2169–2175.

Hillebrand, H., Steinert, G., Boersma, M., Malzahn, A., Meunier, C. L., Plum, C., & Ptacnik, R. (2013). Goldman revisited: Faster-growing phytoplankton has lower N : P and lower stoichiometric flexibility. *Limnology and Oceanography*, *58*(6), 2076–2088.

Hofmann, M., & Schellnhuber, H.-J. (2009). Oceanic acidification affects marine carbon pump and triggers extended marine oxygen holes. *Proceedings of the National Academy of Sciences*, *106*(9), 3017–3022.

Huner, N. P. A., Maxwell, D. P., Gray, G. R., Savitch, L. V., Krol, M., Ivanov, A. G., & Falk, S. (2008). Sensing environmental temperature change through imbalances between

energy supply and energy consumption: Redox state of photosystem II. *Physiologia Plantarum*, *98*(2), 358–364.

Ilyina, T., Six, K. D., Segschneider, J., Maier-Reimer, E., Li, H., & Núñez-Riboni, I. (2013). Global ocean biogeochemistry model HAMOCC: Model architecture and performance as component of the MPI-Earth system model in different CMIP5 experimental realizations. *Journal of Advances in Modeling Earth Systems*, *5*(2), 287–315.

Irwin, A. J., Finkel, Z. V., Müller-Karger, F. E., & Troccoli Ghinaglia, L. (2015). Phytoplankton adapt to changing ocean environments. *Proceedings of the National Academy of Sciences*, *112*(18), 5762–5766.

Isari, S., Antó, M., & Saiz, E. (2013). Copepod foraging on the basis of food nutritional quality: Can copepods really choose? *PLoS ONE*, *8*(12), e84742.

Ito, T., Follows, M. J., & Boyle, E. A. (2004). Is AOU a good measure of respiration in the oceans? *Geophysical Research Letters*, *31*(17), 1–4.

Jacq, V., Ridame, C., L'Helguen, S., Kaczmar, F., & Saliot, A. (2014). Response of the Unicellular Diazotrophic Cyanobacterium Crocosphaera watsonii to Iron Limitation. *PLoS ONE*, *9*(1), e86749.

Jiang, H.-B., Fu, F.-X., Rivero-Calle, S., Levine, N. M., Sañudo-Wilhelmy, S. A., Qu, P.-P., ... Hutchins, D. A. (2018). Ocean warming alleviates iron limitation of marine nitrogen fixation. *Nature Climate Change*, *8*(8), 709–712.

Jo, N., Kang, J. J., Park, W. G., Lee, B. R., Yun, M. S., Lee, J. H., ... Lee, S. H. (2017). Seasonal variation in the biochemical compositions of phytoplankton and zooplankton communities in the southwestern East/Japan Sea. *Deep-Sea Research Part II: Topical Studies in Oceanography*, *143*, 82–90.

Johansson, N., & Granéli, E. (1999). Cell density, chemical composition and toxicity of Chrysochromulina polylepis (Haptophyta) in relation to different N:P supply ratios. *Marine Biology*, *135*(2), 209–217.

Jover, L. F., Effler, T. C., Buchan, A., Wilhelm, S. W., & Weitz, J. S. (2014). The elemental composition of virus particles: implications for marine biogeochemical cycles. *Nature Reviews Microbiology*, *12*(7), 519–528.

Kara, A. B., Rochford, P. A., & Hurlburt, H. (2003). Mixed layer depth variability over the global ocean. *Journal of Geophysical Research*, *108*(C3), 3079.

Karl, D. M., Björkman, K. M., Dore, J. E., Fujieki, L., Hebel, D. V., Houlihan, T., ... Tupas, L. M. (2001). Ecological nitrogen-to-phosphorus stoichiometry at station ALOHA. *Deep Sea Research Part II: Topical Studies in Oceanography*, *48*(8-9), 1529–1566.

Karl, D. M., & Grabowski, E. (2017). The Importance of H in Particulate Organic Matter Stoichiometry, Export and Energy Flow. *Frontiers in Microbiology*, *8*(MAY), 826.

Keeling, R. E., Körtzinger, A., & Gruber, N. (2010). Ocean deoxygenation in a warming world. *Annual review of marine science*, *2*(1), 199–229.

Kemp, A. E., & Villareal, T. A. (2013). High diatom production and export in stratified waters – A potential negative feedback to global warming. *Progress in Oceanography*, *119*, 4–23.

Kiørboe, T., & Sabatini, M. (1995). *Scaling of fecundity, growth and development in marine planktonic copepods* (Vol. 120) (No. 1-3).

Kirchman, D. L. (2018). *Processes in Microbial Ecology* (2nd ed., Vol. 1). Oxford University Press.

Klausmeier, C. A., Litchman, E., Daufresne, T., & Levin, S. A. (2004). Optimal nitrogen-to-phosphorus stoichiometry of phytoplankton. *Nature*, *429*(6988), 171–174.

Klausmeier, C. A., Litchman, E., & Levin, S. A. (2004). Phytoplankton growth and stoichiometry under multiple nutrient limitation. *Limnology and Oceanography*, *49*(4part2), 1463–1470.

Körtzinger, A., Hedges, J. I., & Quay, P. D. (2001). Redfield ratios revisited: Removing the biasing effect of anthropogenic CO2. *Limnology and Oceanography*, *46*(4), 964–970.

Kreus, M., Schartau, M., Engel, A., Nausch, M., & Voss, M. (2015). Variations in the elemental ratio of organic matter in the central Baltic Sea: Part I—Linking primary production to remineralization. *Continental Shelf Research*, *100*, 25–45.

Kudo, I., & Harrison, P. J. (1997). EFFECT OF IRON NUTRITION ON THE MARINE CYANOBACTERIUM SYNECHOCOCCUS GROWN ON DIFFERENT N SOURCES AND IRRADIANCES1. *Journal of Phycology*, *33*(2), 232–240.

Kwiatkowski, L., Aumont, O., Bopp, L., & Ciais, P. (2018). The Impact of Variable Phytoplankton Stoichiometry on Projections of Primary Production, Food Quality, and Carbon Uptake in the Global Ocean. *Global Biogeochemical Cycles*, *32*(4), 516–528.

La Roche, J., Rost, B., & Engel, A. (2010). Bioassays, batch culture and chemostat experimentation. In *Approaches and tools to manipulate the carbonate chemistry., guide for best practices in ocean acidification research and data reporting. in: Riebesell u., fabry vj, hansson l., gattuso j.-p.(eds.)* (pp. 81–94). Office for Official Publications of the European Communities.

Lampe, R. H., Cohen, N. R., Ellis, K. A., Bruland, K. W., Maldonado, M. T., Peterson, T. D., ... Marchetti, A. (2018). Divergent gene expression among phytoplankton taxa in response to upwelling. *Environmental Microbiology*, *20*(8), 3069–3082.

Lampe, R. H., Wang, S., Cassar, N., & Marchetti, A. (2019). Strategies among phytoplankton in response to alleviation of nutrient stress in a subtropical gyre. *The ISME Journal*.

Laspoumaderes, C., Modenutti, B., Elser, J. J., & Balseiro, E. (2015). Does the stoichiometric carbon:phosphorus knife edge apply for predaceous copepods? *Oecologia*, *178*(2), 557–569.

Laufkötter, C., Vogt, M., Gruber, N., Aita-Noguchi, M., Aumont, O., Bopp, L., ... Völker, C. (2015). Drivers and uncertainties of future global marine primary production in marine ecosystem models. *Biogeosciences*, *12*(23), 6955–6984.

Laufkötter, C., Vogt, M., Gruber, N., Aumont, O., Bopp, L., Doney, S. C., ... Völker, C. (2016). Projected decreases in future marine export production: The role of the carbon flux through the upper ocean ecosystem. *Biogeosciences*, *13*(13), 4023–4047.

Laws, E. A. (1991). Photosynthetic quotients, new production and net community production in the open ocean. *Deep Sea Research Part A, Oceanographic Research Papers*, *38*(1), 143–167.

Laws, E. A., Ducklow, H., & McCarthy, J. J. (2000). Temperature effects on export production in the open ocean. *Global Biogeochemical Cycles*, *14*(4), 1231–1246.

Le Quéré, C., Andrew, R. M., Canadell, J. G., Sitch, S., Korsbakken, J. I., Peters, G. P., ... Zaehle, S. (2016). Global Carbon Budget 2016. *Earth System Science Data Discussions*, *8*(2), 1–3.

Lee, C., Wakeham, S., & Arnosti, C. (2004). Particulate organic matter in the sea: the composition conundrum. *Ambio*, *33*(8), 565–75.

Lee, J. H., Lee, D., Kang, J. J., Joo, H. T., Lee, J. H., Lee, H. W., ... Lee, S. H. (2017). The effects of different environmental factors on the biochemical composition of particulate organic matter in Gwangyang Bay, South Korea. *Biogeosciences*, *14*(7), 1903–1917.

Lenton, T. M., & Watson, A. J. (2000). Redfield revisited: 1. Regulation of nitrate, phosphate, and oxygen in the ocean. *Global Biogeochemical Cycles*, *14*(1), 225–248.

Leonardos, N., & Geider, R. J. (2004). Responses of elemental and biochemical composition of Chaetoceros muelleri to growth under varying light and nitrate : phosphate supply ratios and their influence on critical N: P. *Limnology and Oceanography*, *49*(6), 2105–2114.

Leonardos, N., & Geider, R. J. (2005). ELEMENTAL AND BIOCHEMICAL COMPOSITION OF RHINOMONAS RETICULATA (CRYPTOPHYTA) IN RELATION TO LIGHT AND NITRATE-TO-PHOSPHATE SUPPLY RATIOS1. *Journal of Phycology*, *41*(3), 567–576.

Leong, S. C. Y., Maekawa, M., & Taguchi, S. (2010). Carbon and nitrogen acquisition by the toxic dinoflagellate Alexandrium tamarense in response to different nitrogen sources and supply modes. *Harmful Algae*, *9*(1), 48–58.

Leong, S. C. Y., & Taguchi, S. (2004). Response of the dinoflagellate Alexandrium tamarense to a range of nitrogen sources and concentrations: Growth rate, chemical carbon and nitrogen, and pigments. *Hydrobiologia*, *515*(1-3), 215–224.

Letscher, R., Moore, J. K., Teng, Y.-c., & Primeau, F. (2015). Variable C : N : P stoichiometry of dissolved organic matter cycling in the Community Earth System Model. *Biogeosciences*, *12*(1), 209–221.

Li, G., & Campbell, D. A. (2013). Rising CO2 Interacts with Growth Light and Growth Rate to Alter Photosystem II Photoinactivation of the Coastal Diatom Thalassiosira pseudonana. *PLoS ONE*, *8*(1), e55562.

Li, G., & Campbell, D. A. (2017). Interactive effects of nitrogen and light on growth rates and RUBISCO content of small and large centric diatoms. *Photosynthesis Research*, *131*(1), 93–103.

Li, W. K. W. (1980). Temperature Adaptation in Phytoplankton: Cellular and Photosynthetic Characteristics. In *Primary productivity in the sea* (pp. 259–279). Boston, MA: Springer US.

Li, Y.-H., Karl, D. M., Winn, C. D., Mackenzie, F. T., & Gans, K. (2000). Remineralization Ratios in the Subtropical North Pacific Gyre. *Aquatic Geochemistry*, *6*(1), 65–85.

Li, Y.-H., & Peng, T.-H. (2002). Latitudinal change of remineralization ratios in the oceans and its implication for nutrient cycles. *Global Biogeochemical Cycles*, *16*(4), 77–1–77–16.

Li, Y.-Y., Chen, X.-H., Xue, C., Zhang, H., Sun, G., Xie, Z.-X., ... Wang, D.-Z. (2019). Proteomic Response to Rising Temperature in the Marine Cyanobacterium Synechococcus Grown in Different Nitrogen Sources. *Frontiers in Microbiology*, *10*.

Li, Z., Wu, Y., & Beardall, J. (2018). Physiological and biochemical responses of Thalassiosira punctigera to nitrate limitation. *Diatom Research*, *33*(2), 135–143.

Liang, Y., Koester, J. A., Liefer, J. D., Irwin, A. J., & Finkel, Z. V. (2019). Molecular mechanisms of temperature acclimation and adaptation in marine diatoms. *The ISME Journal*, *13*(10), 2415–2425.

Liefer, J. D., Garg, A., Fyfe, M. H., Irwin, A. J., Benner, I., Brown, C. M., ... Finkel, Z. V. (2019). The Macromolecular Basis of Phytoplankton C:N:P Under Nitrogen Starvation. *Frontiers in Microbiology*, *10*, 763.

Lin, S., Litaker, R. W., & Sunda, W. G. (2016). Phosphorus physiological ecology and molecular mechanisms in marine phytoplankton. *Journal of Phycology*, *52*(1), 10–36.

Litchman, E., Ohman, M. D., & Kiørboe, T. (2013). Trait-based approaches to zooplankton communities. *Journal of Plankton Research*, *35*(3), 473–484.

Liu, J., Weinbauer, M., Maier, C., Dai, M., & Gattuso, J. (2010). Effect of ocean acidification on microbial diversity and on microbe-driven biogeochemistry and ecosystem functioning. *Aquatic Microbial Ecology*, *61*(3), 291–305.

Lomas, M. W., Bonachela, J. A., Levin, S. A., & Martiny, A. C. (2014). Impact of ocean phytoplankton diversity on phosphate uptake. *Proceedings of the National Academy of Sciences*, *111*(49), 17540–17545.

Long, M. C., Deutsch, C. A., & Ito, T. (2016). Finding forced trends in oceanic oxygen. *Global Biogeochemical Cycles*, *30*(2), 381–397.

Longhurst, A. (1995). Seasonal cycles of pelagic production and consumption. *Progress in Oceanography*, *36*(2), 77–167.

Lopez, J. S., Garcia, N. S., Talmy, D., & Martiny, A. C. (2016). Diel variability in the elemental composition of the marine cyanobacterium Synechococcus. *Journal of Plankton Research*, *38*(4), 1052–1061.

Lu, Y., Wen, Z., Shi, D., Chen, M., Zhang, Y., Bonnet, S., ... Kao, S.-J. (2018). Effect of light on N₂ fixation and net nitrogen release of <i>Trichodesmium</i> in a field study. *Biogeosciences*, *15*(1), 1–12.

Luo, Y. W., Lima, I. D., Karl, D. M., Deutsch, C. A., & Doney, S. C. (2014). Data-based assessment of environmental controls on global marine nitrogen fixation. *Biogeosciences*, *11*(3), 691–708.

Lyons, T. W., Reinhard, C. T., & Planavsky, N. J. (2014). The rise of oxygen in Earth's early ocean and atmosphere. *Nature*, *506*(7488), 307–15.

MacIntyre, H. L., Kana, T. M., Anning, T., & Geider, R. J. (2002). PHOTOACCLIMATION OF PHOTOSYNTHESIS IRRADIANCE RESPONSE CURVES AND PHOTOSYNTHETIC PIGMENTS IN MICROALGAE AND CYANOBACTERIA1. *Journal of Phycology*, *38*(1), 17–38.

Madigan, M. T., Martinko, J. M., Parker, J., & Others. (2017). *Brock biology of microorganisms* (Vol. 13). New York: Pearson.

Mahowald, N. M., Kohfeld, K., Hansson, M., Balkanski, Y., Harrison, S. P., Prentice, I. C., ... Rodhe, H. (1999). Dust sources and deposition during the last glacial maximum and current climate: A comparison of model results with paleodata from ice cores and marine sediments. *Journal of Geophysical Research*, *104*(D13), 15895–15916.

Maldonado, M., & Price, N. (1996). Influence of N substrate on Fe requirements of marine centric diatoms. *Marine Ecology Progress Series*, *141*(1-3), 161–172.

Malviya, S., Scalco, E., Audic, S., Vincent, F., Veluchamy, A., Poulain, J., ... Bowler, C. (2016). Insights into global diatom distribution and diversity in the world's ocean. *Proceedings of the National Academy of Sciences*, *113*(11), E1516–E1525.

Marañón, E., Lorenzo, M. P., Cermeño, P., & Mouriño-Carballido, B. (2018a). Nutrient limitation suppresses the temperature dependence of phytoplankton metabolic rates. *The ISME Journal*, *12*(7), 1836–1845.

Marañón, E., Lorenzo, M. P., Cermeño, P., & Mouriño-Carballido, B. (2018b). Nutrient limitation suppresses the temperature dependence of phytoplankton metabolic rates. *The ISME Journal*, *12*(7), 1836–1845.

Marchetti, A., & Maldonado, M. T. (2016). Iron. In *The physiology of microalgae* (pp. 233–279). Cham: Springer International Publishing.

Margalef, R. (1978). Life-forms of phytoplankton as survival alternatives in an unstable environment. *Oceanologica Acta*, *1*(4), 493–509.

Mari, X. (1999). Carbon content and C:N ratio of transparent exopolymeric particles (TEP) produced by bubbling exudates of diatoms. *Marine Ecology Progress Series*, *183*(2), 59–71.

Marinov, I., Doney, S. C., & Lima, I. D. (2010). Response of ocean phytoplankton community structure to climate change over the 21st century: Partitioning the effects of nutrients, temperature and light. *Biogeosciences*, *7*(12), 3941–3959.

Martiny, A. C., Lomas, M. W., Fu, W., Boyd, P. W., Chen, Y.-l. L., Cutter, G. A., ... Moore, J. K. (2019). Biogeochemical controls of surface ocean phosphate. *Science Advances*, *5*(8), eaax0341.

Martiny, A. C., Ma, L., Mouginot, C., Chandler, J. W., & Zinser, E. R. (2016). Interactions between Thermal Acclimation, Growth Rate, and Phylogeny Influence Prochlorococcus Elemental Stoichiometry. *PLOS ONE*, *11*(12), e0168291.

Martiny, A. C., Pham, C. T. A., Primeau, F. W., Vrugt, J. A., Moore, J. K., Levin, S. A., & Lomas, M. W. (2013). Strong latitudinal patterns in the elemental ratios of marine plankton and organic matter. *Nature Geoscience*, *6*(4), 279–283.

Martiny, A. C., Ustick, L., A. Garcia, C., & Lomas, M. W. (2019). Genomic adaptation of marine phytoplankton populations regulates phosphate uptake. *Limnology and Oceanography*, lno.11252.

Martiny, A. C., Vrugt, J. A., & Lomas, M. W. (2014). Concentrations and ratios of particulate organic carbon, nitrogen, and phosphorus in the global ocean. *Scientific data*, *1*, 140048.

Martiny, A. C., Vrugt, J. A., Primeau, F. W., & Lomas, M. W. (2013). Regional variation in the particulate organic carbon to nitrogen ratio in the surface ocean. *Global Biogeochemical Cycles*, *27*(3), 723–731.

Matsumoto, K. (2007). Biology-mediated temperature control on atmospheric pCO2 and ocean biogeochemistry. *Geophysical Research Letters*, *34*(20), 1–5.

Matsumoto, K., Tokos, K., Chikamoto, M., & Ridgwell, A. (2010). Characterizing post-industrial changes in the ocean carbon cycle in an Earth system model. *Tellus B*, *62*(4), 296–313.

Matsumoto, K., Tokos, K., Huston, A., & Joy-Warren, H. (2013). MESMO 2: A mechanistic marine silica cycle and coupling to a simple terrestrial scheme. *Geoscientific Model Development*, *6*(2), 477–494.

Matsumoto, K., Tokos, K., Price, A. R., & Cox, S. J. (2008). First description of the Minnesota Earth System Model for Ocean biogeochemistry (MESMO 1.0). *Geoscientific Model Development*, *1*(1), 1–15.

Mayzaud, P., Chanut, J. P., & Ackman, R. G. (1989). Seasonal changes of the biochemical composition of marine particulate matter with special reference to fatty acids and sterols. *Marine Ecology Progress Series*, *56*(1), 189–204.

McKew, B. A., Metodieva, G., Raines, C. A., Metodiev, M. V., & Geider, R. J. (2015). Acclimation of E miliania huxleyi (1516) to nutrient limitation involves precise modification of the proteome to scavenge alternative sources of N and P. *Environmental Microbiology*, *17*(10), 4050–4062.

Meinshausen, M., Smith, S. J., Calvin, K., Daniel, J. S., Kainuma, M. L. T., Lamarque, J.-F., ... van Vuuren, D. P. P. (2011). The RCP greenhouse gas concentrations and their extensions from 1765 to 2300. *Climatic Change*, *109*(1), 213–241.

Meunier, C. L., Boersma, M., Wiltshire, K. H., & Malzahn, A. M. (2016). Zooplankton eat what they need: Copepod selective feeding and potential consequences for marine systems. *Oikos*, *125*(1), 50–58.

Meunier, C. L., Hantzsche, F. M., Cunha-Dupont, A. Ö., Haafke, J., Oppermann, B., Malzahn, A. M., & Boersma, M. (2012). Intraspecific selectivity, compensatory feeding and flexible homeostasis in the phagotrophic flagellate Oxyrrhis marina: Three ways to handle food quality fluctuations. *Hydrobiologia*, *680*(1), 53–62.

Meunier, C. L., Malzahn, A. M., & Boersma, M. (2014). A new approach to homeostatic regulation: Towards a unified view of physiological and ecological concepts. *PLoS ONE*, *9*(9), 3–9.

Meyerink, S. W., Ellwood, M. J., Maher, W. A., Dean Price, G., & Strzepek, R. F. (2017). Effects of iron limitation on silicon uptake kinetics and elemental stoichiometry in two Southern Ocean diatoms, Eucampia antarctica and Proboscia inermis , and the temperate diatom Thalassiosira pseudonana. *Limnology and Oceanography*, *62*(6), 2445–2462.

Mills, M. M., Ridame, C., Davey, M., La Roche, J., & Geider, R. J. (2004). Iron and phosphorus co-limit nitrogen fixation in the eastern tropical North Atlantic. *Nature*, *429*(6989), 292–294.

Mitra, A., & Flynn, K. J. (2006). Accounting for variation in prey selectivity by zooplankton. *Ecological Modelling*, *199*(1), 82–92.

Mitra, A., Flynn, K. J., Burkholder, J. M., Berge, T., Calbet, A., Raven, J. A., ... Zubkov, M. V. (2014). The role of mixotrophic protists in the biological carbon pump. *Biogeosciences*, *11*(4), 995–1005.

Mohr, W., Intermaggio, M. P., & LaRoche, J. (2010). Diel rhythm of nitrogen and carbon metabolism in the unicellular, diazotrophic cyanobacterium Crocosphaera watsonii WH8501. *Environmental Microbiology*, *12*(2), 412–421.

Moore, C. M., Mills, M. M., Arrigo, K. R., Berman-Frank, I., Bopp, L., Boyd, P. W., ... Ulloa, O. (2013). Processes and patterns of oceanic nutrient limitation. *Nature Geoscience*, *6*(9), 701–710.

Moore, J. K., & Doney, S. C. (2007). Iron availability limits the ocean nitrogen inventory stabilizing feedbacks between marine denitrification and nitrogen fixation. *Global Biogeochemical Cycles*, *21*(2), n/a–n/a.

Moore, J. K., Doney, S. C., & Lindsay, K. (2004). Upper ocean ecosystem dynamics and iron cycling in a global three-dimensional model. *Global Biogeochemical Cycles*, *18*(4), n/a–n/a.

Moore, J. K., Lindsay, K., Doney, S. C., Long, M. C., & Misumi, K. (2013). Marine ecosystem dynamics and biogeochemical cycling in the community earth system model [CESM1(BGC)]: Comparison of the 1990s with the 2090s under the RCP4.5 and RCP8.5 scenarios. *Journal of Climate*, *26*(23), 9291–9312.

Morel, F. M. M. (1987). Kinetics of Nutrient Uptake and Growth in Phytoplankton. *Journal of Phycology*, *23*(1), 137–150.

Moreno, A. R., & Martiny, A. C. (2018). Ecological Stoichiometry of Ocean Plankton. *Annual Review of Marine Science*, *10*(1), 43–69.

Mortensen, S. H., Børsheim, K. Y., Rainuzzo, J., & Knutsen, G. (1988). Fatty acid and elemental composition of the marine diatom Chaetoceros gracilis Schütt. Effects of silicate deprivation, temperature and light intensity. *Journal of Experimental Marine Biology and Ecology*, *122*(2), 173–185.

Mou, S., Zhang, Y., Li, G., Li, H., Liang, Y., Tang, L., ... Jiao, N. (2017). Effects of elevated CO2 and nitrogen supply on the growth and photosynthetic physiology of a marine cyanobacterium, Synechococcus sp. PCC7002. *Journal of Applied Phycology*, *29*(4), 1755–1763.

Mouginot, C., Zimmerman, A. E., Bonachela, J. A., Fredricks, H., Allison, S. D., Van Mooy, B. A. S., & Martiny, A. C. (2015). Resource allocation by the marine cyanobacterium S ynechococcus WH8102 in response to different nutrient supply ratios. *Limnology and Oceanography*, *60*(5), 1634–1641.

Muggli, D., & Harrison, P. (1996). Effects of nitrogen source on the physiology and metal nutrition of Emiliania huxleyi grown under different iron and light conditions. *Marine Ecology Progress Series*, *130*(1-3), 255–267.

Navarro, J. M., Clasing, E., Urrutia, G., Asencio, G., Stead, R., & Herrera, C. (1993). Biochemical composition and nutritive value of suspended particulate matter over a tidal flat of Southern Chile. *Estuarine, Coastal and Shelf Science*, *37*(1), 59–73.

Navarro, J. M., & Thompson, R. J. (1995). Seasonal fluctuations in the size spectra, biochemical composition and nutritive value of the seston available to a suspension-feeding bivalve in a subarctic environment. *Marine Ecology Progress Series*, *125*(1-3), 95–106.

Nelson, D. M., & Brzezinski, M. A. (1997). Diatom growth and productivity in an oligotrophic midocean gyre: A 3-yr record from the Sargasso Sea near Bermuda. *Limnology and Oceanography*, *42*(3), 473–486.

Ng, W. H. A., & Liu, H. (2015). Diel variation of the cellular carbon to nitrogen ratio of Chlorella autotrophica (Chlorophyta) growing in phosphorus- and nitrogen-limited continuous cultures. *Journal of Phycology*, *51*(1), 82–92.

Nielsen, M. (1996). Growth and chemical composition of the toxic dinoflagellate Gymnodinium galatheanum in relation to irradiance, temperature and salinity. *Marine Ecology Progress Series*, *136*, 205–211.

Nielsen, M. V. (1992). Irradiance and daylength effects on growth and chemical composition of Gyrodinium aureolum Hulburt in culture. *Journal of Plankton Research*, *14*(6), 811–820.

Nielsen, M. V., & Tønseth, C. P. (1991). Temperature and salinity effect on growth and chemical composition of Gyrodinium aureolum Hulburt in culture. *Journal of Plankton Research*, *13*(2), 389–398.

O'Brien, E. J., Monk, J. M., & Palsson, B. O. (2015). Using genome-scale models to predict biological capabilities. *Cell*, *161*(5), 971–987.

Omta, A. W., Bruggeman, J., Kooijman, S. A. L. M., & Dijkstra, H. A. (2006). Biological carbon pump revisited: Feedback mechanisms between climate and the Redfield ratio. *Geophysical Research Letters*, *33*(14), L14613.

Oschlies, A., Brandt, P., Stramma, L., & Schmidtko, S. (2018). Drivers and mechanisms of ocean deoxygenation. *Nature Geoscience*, *11*(7), 467–473.

Oschlies, A., Schulz, K. G., Riebesell, U., & Schmittner, A. (2008). Simulated 21st century's increase in oceanic suboxia by CO2-enhanced biotic carbon export. *Global Biogeochemical Cycles*, *22*(4), 1–10.

Otero, A., Dominguez, A., Lamela, T., Garcia, D., & Fábregas, J. (1998). Steady-states of semicontinuous cultures of a marine diatom: Effect of saturating nutrient concentrations. *Journal of Experimental Marine Biology and Ecology*, *227*(1), 23–33.

Pahlow, M., Dietze, H., & Oschlies, A. (2013). Optimality-based model of phytoplankton growth and diazotrophy. *Marine Ecology Progress Series*, *489*, 1–16.

Passow, U., & Laws, E. (2015). Ocean acidification as one of multiple stressors: growth response of Thalassiosira weissflogii (diatom) under temperature and light stress. *Marine Ecology Progress Series*, *541*(1), 75–90.

Paul, C., Matthiessen, B., & Sommer, U. (2015). Warming, but not enhanced CO2 concentration, quantitatively and qualitatively affects phytoplankton biomass. *Marine Ecology Progress Series*, *528*, 39–51.

Paulmier, A., Kriest, I., & Oschlies, A. (2009). Stoichiometries of remineralisation and denitrification in global biogeochemical ocean models. *Biogeosciences*, *6*(5), 923–935.

Peng, T.-H., & Broecker, W. S. (1987). C/P ratios in marine detritus. *Global Biogeochemical Cycles*, *1*(2), 155–161.

Persson, J., Fink, P., Goto, A., Hood, J. M., Jonas, J., & Kato, S. (2010). To be or not to be what you eat: regulation of stoichiometric homeostasis among autotrophs and heterotrophs. *Oikos*, *119*(5), 741–751.

Pinceel, T., Vanschoenwinkel, B., Brendonck, L., & Buschke, F. (2016). Modelling the sensitivity of life history traits to climate change in a temporary pool crustacean. *Scientific reports*, *6*, 29451.

Plath, K., & Boersma, M. (2001). Mineral limitation of zooplankton: Stoichiometric constraints and optimal foraging. *Ecology*, *82*(5), 1260–1269.

Polimene, L., Mitra, A., Sailley, S., Ciavatta, S., Widdicombe, C., Atkinson, A., & Allen, J. (2015). Decrease in diatom palatability contributes to bloom formation in the Western English Channel. *Progress in Oceanography*, *137*, 484–497.

Price, N. M. (2005). The elemental stoichiometry and composition of an iron-limited diatom. *Limnology and Oceanography*, *50*(4), 1159–1171.

Qu, P., Fu, F., & Hutchins, D. A. (2018). Responses of the large centric diatom Coscinodiscus sp. to interactions between warming, elevated CO 2 , and nitrate availability. *Limnology and Oceanography*, *63*(3), 1407–1424.

Qu, P., Fu, F.-X., Kling, J. D., Huh, M., Wang, X., & Hutchins, D. A. (2019). Distinct Responses of the Nitrogen-Fixing Marine Cyanobacterium Trichodesmium to a Thermally Variable Environment as a Function of Phosphorus Availability. *Frontiers in Microbiology*, *10*(JUN), 1282.

R Core Team. (2018). *R: A Language and Environment for Statistical Computing.* Vienna, Austria.

Rabouille, S., Semedo Cabral, G., & Pedrotti, M. (2017). Towards a carbon budget of the diazotrophic cyanobacterium Crocosphaera: effect of irradiance. *Marine Ecology Progress Series*, *570*, 29–40.

Rakusa-Suszczewski, S. (1967). The Use of Chaetognath and Copepod Population Age-Structures as an Indication of Similarity between Water Masses. *Journal du Conseil*, *31*(1), 46–55.

Rasdi, N. W., & Qin, J. G. (2015). Effect of N:P ratio on growth and chemical composition of Nannochloropsis oculata and Tisochrysis lutea. *Journal of Applied Phycology*, *27*(6), 2221–2230.

Raubenheimer, D., Simpson, S. J., & Mayntz, D. (2009). Nutrition, ecology and nutritional ecology: Toward an integrated framework. *Functional Ecology*, *23*(1), 4–16.

Raven, J. A., & Geider, R. J. (1988). Temperature and algal growth. *New Phytologist*, *110*(4), 441–461.

Redfield, A. (1958). The biological control of chemical factors in the environment. *American scientist*, *46*(3), 205–221.

Redfield, A., Ketchum, B., & Richards, F. (1963). The influence of organisms on the composition of Seawater. In M. N. Hill (Ed.), *The composition of seawater: Comparative and descriptive oceanography. the sea: ideas and observations on progress in the study of the seas* (Vol. 2, pp. 26–77). New York: Interscience Publishers.

Riebesell, U., Schulz, K. G., Bellerby, R. G. J., Botros, M., Fritsche, P., Meyerhöfer, M., ... Zöllner, E. (2007). Enhanced biological carbon consumption in a high CO2 ocean. *Nature*, *450*(7169), 545–548.

Robinson, C. (2019). Microbial Respiration, the Engine of Ocean Deoxygenation. *Frontiers in Marine Science*, *5*, 533.

Roche, J., Geider, R. J., Graziano, L. M., Murray, H., & Lewis, K. (1993). INDUCTION OF SPECIFIC PROTEINS IN EUKARYOTIC ALGAE GROWN UNDER IRON-, PHOSPHORUS-, OR NITROGEN-DEFICIENT CONDITIONS1. *Journal of Phycology*, *29*(6), 767–777.

Roleda, M. Y., Slocombe, S. P., Leakey, R. J., Day, J. G., Bell, E. M., & Stanley, M. S. (2013). Effects of temperature and nutrient regimes on biomass and lipid production by six oleaginous microalgae in batch culture employing a two-phase cultivation strategy. *Bioresource Technology*, *129*, 439–449.

Roy, S. (2018). Distributions of phytoplankton carbohydrate, protein and lipid in the world oceans from satellite ocean colour. *ISME Journal*, *12*(6), 1457–1472.

Sailley, S. F., Polimene, L., Mitra, A., Atkinson, A., & Allen, J. I. (2014). Impact of zooplankton food selectivity on plankton dynamics and nutrient cycling. *Journal of Plankton Research*, *37*(3), 519–529.

Saito, H., & Tsuda, A. (2003). Influence of light intensity on diatom physiology and nutrient dynamics in the Oyashio region. *Progress in Oceanography*, *57*(3-4), 251–263.

Sakshaug, E., & Andresen, K. (1986). Effect of light regime upon growth rate and chemical composition of a clone of Skeletonema costatum from the Trondheimsfjord, Norway. *Journal of Plankton Research*, *8*(4), 619–637.

Sakshaug, E., Andresen, K., Myklestad, S., & Olsen, Y. (1983). Nutrient status of phytoplankton communities in Norwegian waters (marine, brackish, and fresh) as revealed by their chemical composition. *Journal of Plankton Research*, *5*(2), 175–196.

Sakshaug, E., & Holm-Hansen, O. (1977). Chemical composition of Skeletonema costatum (Grev.) Cleve And Pavlova (monochrysis) Lutheri (droop) green as a function of nitrate-, phosphate-, and iron-limited growth. *Journal of Experimental Marine Biology and Ecology*, *29*(1), 1–34.

Sarmiento, J. L., Dunne, J., Gnanadesikan, A., Key, R. M., Matsumoto, K., & Slater, R. (2002). A new estimate of the CaCO 3 to organic carbon export ratio. *Global Biogeochemical Cycles*, *16*(4), 54–1–54–12.

Sarmiento, J. L., & Gruber, N. (2006). *Ocean Biogeochemical Dynamics*. Princeton, NJ: Princeton University Press.

Sarmiento, J. L., Gruber, N., Brzezinski, M. A., & Dunne, J. P. (2004). High-latitude controls of thermocline nutrients and low latitude biological productivity. *Nature*, *427*(6969), 56–60.

Savageau, M. A. (1976). *Biochemical systems analysis. A study of function and design in molecular biology*. Reading, MA: Addison–Wesley.

Schaum, C.-E., Buckling, A., Smirnoff, N., Studholme, D. J., & Yvon-Durocher, G. (2018). Environmental fluctuations accelerate molecular evolution of thermal tolerance in a marine diatom. *Nature Communications*, *9*(1), 1719.

Schlitzer, R. (2004). Export production in the equatorial and North Pacific derived from dissolved oxygen, nutrient and carbon data. *Journal of Oceanography*, *60*(3), 53–62.

Schmidtko, S., Stramma, L., & Visbeck, M. (2017). Decline in global oceanic oxygen content during the past five decades. *Nature*, *542*(7641), 335–339.

Schneider, B., Schlitzer, R., Fischer, G., Nothig, E., & Nöthig, E.-M. (2003). Depth-dependent elemental compositions of particulate organic matter (POM) in the ocean. *Global Biogeochemical Cycles*, *17*(2), 1032.

Schulz, K. G., Riebesell, U., Bellerby, R. G. J., Biswas, H., Meyerhöfer, M., Müller, M. N., ... Zöllner, E. (2008). Build-up and decline of organic matter during PeECE III. *Biogeosciences*, *5*(3), 707–718.

Shoman, N. Y. (2015). The dynamics of the intracellular contents of carbon, nitrogen, and chlorophyll a under conditions of batch growth of the diatom Phaeodactylum tricornutum (Bohlin, 1897) at different light intensities. *Russian Journal of Marine Biology*, *41*(5), 356–362.

Singh, A., Baer, S. E., Riebesell, U., Martiny, A. C., & Lomas, M. W. (2015). C : N : P stoichiometry at the Bermuda Atlantic Time-series Study station in the North Atlantic Ocean. *Biogeosciences*, *12*(21), 6389–6403.

Six, C., Thomas, J., Brahamsha, B., Lemoine, Y., & Partensky, F. (2004). Photophysiology of the marine cyanobacterium Synechococcus sp. WH8102, a new model organism. *Aquatic Microbial Ecology*, *35*(1), 17–29.

Spilling, K., Ylöstalo, P., Simis, S., & Seppälä, J. (2015). Interaction Effects of Light, Temperature and Nutrient Limitations (N, P and Si) on Growth, Stoichiometry and Photosynthetic Parameters of the Cold-Water Diatom Chaetoceros wighamii. *PLOS ONE*, *10*(5), e0126308.

Staehr, P., Henriksen, P., & Markager, S. (2002). Photoacclimation of four marine phytoplankton species to irradiance and nutrient availability. *Marine Ecology Progress Series*, *238*, 47–59.

Sterner, R. W. (1990). The Ratio of Nitrogen to Phosphorus Resupplied by Herbivores: Zooplankton and the Algal Competitive Arena. *The American Naturalist*, *136*(2), 209.

Sterner, R. W., Andersen, T., Elser, J. J., Hessen, D. O., Hood, J. M., McCauley, E., & Urabe, J. (2008). Scale-dependent Carbon:Nitrogen:Phosphorus Seston Stoichiometry in Marine and Freshwaters. *Limnology and Oceanography*, *53*(3), 1169–1180.

Sterner, R. W., & Elser, J. J. (2002). *Ecological stoichiometry: the biology of elements from molecules to the biosphere*. Princeton, NJ: Princeton University Press.

Strzepek, R. F., Boyd, P. W., & Sunda, W. G. (2019). Photosynthetic adaptation to low iron, light, and temperature in Southern Ocean phytoplankton. *Proceedings of the National Academy of Sciences*, *116*(10), 4388–4393.

Suess, E. (1980). Particulate organic carbon flux in the oceans - Surface productivity and oxygen utilization. *Nature*, *288*(5788), 260–263.

Sugie, K., & Yoshimura, T. (2013). Effects of p CO 2 and iron on the elemental composition and cell geometry of the marine diatom Pseudo-nitzschia pseudodelicatissima (Bacillariophyceae) 1. *Journal of Phycology*, *49*(3), 475–488.

Sunda, W., & Huntsman, S. (1995). Iron uptake and growth limitation in oceanic and coastal phytoplankton. *Marine Chemistry*, *50*(1-4), 189–206.

Sunda, W., & Huntsman, S. (2003). Effect of pH, light, and temperature on Fe–EDTA chelation and Fe hydrolysis in seawater. *Marine Chemistry*, *84*(1-2), 35–47.

Takahashi, T., Broecker, W. S., & Langer, S. (1985). Redfield ratios based on chemcial data from isopycnal surfaces. *J. Geophys. Res.*, *90*, 6907–6924.

Takeda, S. (1998). Influence of iron availability on nutrient consumption ratio of diatoms in oceanic waters. *Nature*, *393*(6687), 774–777.

Talarmin, A., Lomas, M. W., Bozec, Y., Savoye, N., Frigstad, H., Karl, D. M., & Martiny, A. C. (2016). Seasonal and long-term changes in elemental concentrations and ratios of marine particulate organic matter. *Global Biogeochemical Cycles*, *30*(11), 1699–1711.

Talmy, D., Blackford, J., Hardman-Mountford, N. J., Polimene, L., Follows, M. J., & Geider, R. J. (2014). Flexible C : N ratio enhances metabolism of large phytoplankton when resource supply is intermittent. *Biogeosciences*, *11*(17), 4881–4895.

Talmy, D., Martiny, A. C., Hill, C., Hickman, A. E., & Follows, M. J. (2016). Microzooplankton regulation of surface ocean POC:PON ratios. *Global Biogeochemical Cycles*, *30*(2), 311–332.

Tanioka, T., & Matsumoto, K. (2017). Buffering of Ocean Export Production by Flexible Elemental Stoichiometry of Particulate Organic Matter. *Global Biogeochemical Cycles*, *31*(10), 1528–1542.

Tanioka, T., & Matsumoto, K. (2018). Effects of incorporating age-specific traits of zooplankton into a marine ecosystem model. *Ecological Modelling*, *368*(24), 257–264.

Taucher, J., Jones, J., James, A., Brzezinski, M. A., Carlson, C. A., Riebesell, U., & Passow, U. (2015). Combined effects of CO 2 and temperature on carbon uptake

and partitioning by the marine diatoms Thalassiosira weissflogii and Dactyliosolen fragilissimus. *Limnology and Oceanography*, *60*(3), 901–919.

Teng, Y.-C., Primeau, F. W., Moore, J. K., Lomas, M. W., & Martiny, A. C. (2014). Global-scale variations of the ratios of carbon to phosphorus in exported marine organic matter. *Nature Geoscience*, *7*(12), 895–898.

Terry, K. L., Hirata, J., & Laws, E. A. (1983). Light-limited growth of two strains of the marine diatom Phaeodactylum tricornutum Bohlin: Chemical composition, carbon partitioning and the diel periodicity of physiological processes. *Journal of Experimental Marine Biology and Ecology*, *68*(3), 209–227.

Thomas, H. (2002). Remineralization ratios of carbon, nutrients, and oxygen in the North Atlantic Ocean: A field databased assessment. *Global Biogeochemical Cycles*, *16*(3), 24–1–24–12.

Thompson, P. (1999). THE RESPONSE OF GROWTH AND BIOCHEMICAL COMPOSITION TO VARIATIONS IN DAYLENGTH, TEMPERATURE, AND IRRADIANCE IN THE MARINE DIATOM THALASSIOSIRA PSEUDONANA (BACILLARIOPHYCEAE). *Journal of Phycology*, *35*(6), 1215–1223.

Thompson, P. A., Guo, M., Harrison, P. J., & Whyte, J. N. C. (1992). EFFECTS OF VARIATION IN TEMPERATURE. II. ON THE FATTY ACID COMPOSITION OF EIGHT SPECIES OF MARINE PHYTOPLANKTON1. *Journal of Phycology*, *28*(4), 488–497.

Thompson, P. A., Levasseur, M. E., & Harrison, P. J. (1989). Light-limited growth on ammonium vs. nitrate: What is the advantage for marine phytoplankton? *Limnology and Oceanography*, *34*(6), 1014–1024.

Thrane, J.-E., Hessen, D. O., & Andersen, T. (2016). The impact of irradiance on optimal and cellular nitrogen to phosphorus ratios in phytoplankton. *Ecology Letters*, *19*(8), 880–888.

Toseland, A., Daines, S. J., Clark, J. R., Kirkham, A., Strauss, J., Uhlig, C., ... Mock, T. (2013). The impact of temperature on marine phytoplankton resource allocation and metabolism. *Nature Climate Change*, *3*(11), 979–984.

Twining, B. S., & Baines, S. B. (2013). The Trace Metal Composition of Marine Phytoplankton. *Annual Review of Marine Science*, *5*(1), 191–215.

Tyrrell, T. (1999). The relative influences of nitrogen and phosphorus on oceanic primary production. *Nature*, *400*(6744), 525–531.

Urabe, J., & Sterner, R. W. (1996). Regulation of herbivore growth by the balance of light and nutrients. *Proceedings of the National Academy of Sciences*, *93*(16), 8465–8469.

Urabe, J., & Watanabe, Y. (1992). Possibility of N-Limitation or P-Limitation for Planktonic Cladocerans - an Experimental Test. *Limnology and Oceanography*, *37*(2), 244–251.

Uronen, P., Lehtinen, S., Legrand, C., Kuuppo, P., & Tamminen, T. (2005). Haemolytic activity and allelopathy of the haptophyte Prymnesium parvum in nutrient-limited and balanced growth conditions. *Marine Ecology Progress Series*, *299*, 137–148.

Vallina, S. M., Ward, B. A., Dutkiewicz, S., & Follows, M. J. (2014). Maximal feeding with active prey-switching: A kill-the-winner functional response and its effect on global diversity and biogeography. *Progress in Oceanography*, *120*, 93–109.

van Someren Gréve, H., Almeda, R., Lindegren, M., & Kiørboe, T. (2017). Gender-specific feeding rates in planktonic copepods with different feeding behavior. *Journal of Plankton Research*, *10*(4), 1–14.

van de Waal, D. B., Verschoor, A. M., Verspagen, J. M., van Donk, E., & Huisman, J. (2010). Climate-driven changes in the ecological stoichiometry of aquatic ecosystems. *Frontiers in Ecology and the Environment*, *8*(3), 145–152.

van Oijen, T., van Leeuwe, M. A., Gieskes, W. W., & de Baar, H. J. (2004). Effects of iron limitation on photosynthesis and carbohydrate metabolism in the Antarctic diatom Chaetoceros brevis (Bacillariophyceae). *European Journal of Phycology*, *39*(2), 161–171.

Viechtbauer, W. (2010). Conducting Meta-Analyses in R with the metafor Package. *Journal of Statistical Software*, *36*(3), 1–48.

Villar-Argaiz, M., Medina-Sánchez, J. M., Biddanda, B. A., & Carrillo, P. (2018). Predominant Non-additive Effects of Multiple Stressors on Autotroph C:N:P Ratios Propagate in Freshwater and Marine Food Webs. *Frontiers in Microbiology*, *9*(JAN), 69.

Villar-Argaiz, M., Medina-Sánchez, J. M., & Carrillo, P. (2002). Linking life history strategies and ontogeny in crustacean zooplankton: Implications for homeostasis. *Ecology*, *83*(7), 1899–1914.

Voit, E. O. (2013). Biochemical Systems Theory: A Review. *ISRN Biomathematics*, *2013*, 1–53.

Wang, L., Wei, H., & Batchelder, H. P. (2014). Individual-based modelling of Calanus sinicus population dynamics in the Yellow Sea. *Marine Ecology Progress Series*, *503*, 75–97.

Ward, B. A., & Follows, M. J. (2016). Marine mixotrophy increases trophic transfer efficiency, mean organism size, and vertical carbon flux. *Proceedings of the National Academy of Sciences of the United States of America*, *113*(11), 2958–63.

Weber, T. S., & Deutsch, C. A. (2010). Ocean nutrient ratios governed by plankton biogeography. *Nature*, *467*(7315), 550–554.

Wood, G. J., & Flynn, K. J. (1995). GROWTH OF HETEROSIGMA CARTERAE (RAPHIDOPHYCEAE) ON NITRATE AND AMMONIUM AT THREE PHOTON FLUX DENSITIES: EVIDENCE FOR N STRESS IN NITRATE-GROWING CELLS1. *Journal of Phycology*, *31*(6), 859–867.

Woods, H. A., Makino, W., Cotner, J. B., Hobbie, S. E., Harrison, J. F., Acharya, K., & Elser, J. J. (2003). Temperature and the chemical composition of poikilothermic organisms. *Functional Ecology*, *17*(2), 237–245.

Wright, J. J., Konwar, K. M., & Hallam, S. J. (2012). Microbial ecology of expanding oxygen minimum zones. *Nature Reviews Microbiology*, *10*(6), 381–394.

Xu, J., Gao, K., Li, Y., & Hutchins, D. (2014). Physiological and biochemical responses of diatoms to projected ocean changes. *Marine Ecology Progress Series*, *515*, 73–81.

Yoder, J. A. (1979). EFFECT OF TEMPERATURE ON LIGHT-LIMITED GROWTH AND CHEMICAL COMPOSITION OF SKELETONEMA COSTATUM (BACILLARIOPHYCEAE). *Journal of Phycology*, *15*(4), 362–370.

Yvon-Durocher, G., Dossena, M., Trimmer, M., Woodward, G., & Allen, A. P. (2015). Temperature and the biogeography of algal stoichiometry. *Global Ecology and Biogeography*, *24*(5), 562–570.

Yvon-Durocher, G., Schaum, C.-E., & Trimmer, M. (2017). The Temperature Dependence of Phytoplankton Stoichiometry: Investigating the Roles of Species Sorting and Local Adaptation. *Frontiers in Microbiology*, *8*(October), 1–14.

Zhao, J., Ramin, M., Cheng, V., & Arhonditsis, G. B. (2008). Plankton community patterns across a trophic gradient: The role of zooplankton functional groups. *Ecological Modelling*, *213*(3-4), 417–436.

Zhu, Z., Qu, P., Gale, J., Fu, F., & Hutchins, D. A. (2017). Individual and interactive effects of warming and CO2 on Pseudo-nitzschia subcurvata and Phaeocystis antarctica, two dominant phytoplankton from the Ross Sea, Antarctica. *Biogeosciences*, *14*(23), 5281–5295.

Appendix A

Supporting Information For Chapter 2

This supporting information includes the Figures A.1 and A.2.

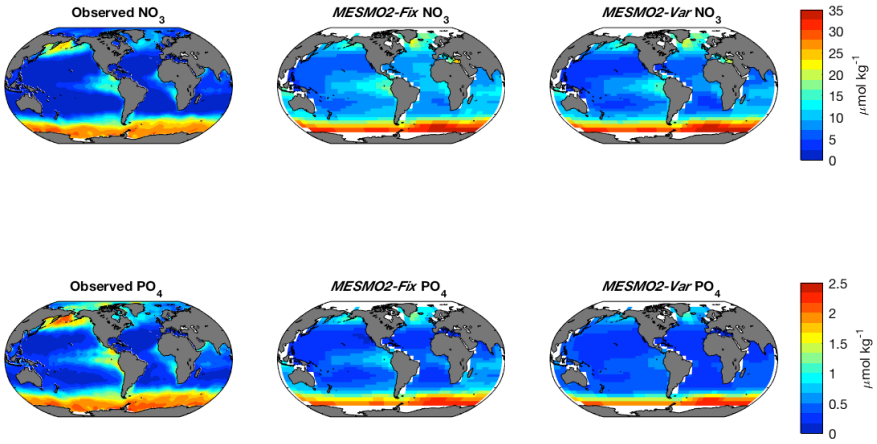

Figure A.1: Observed (H. E. Garcia et al. 2013) and modeled global annual mean surface (0-100 m) nutrient distributions.

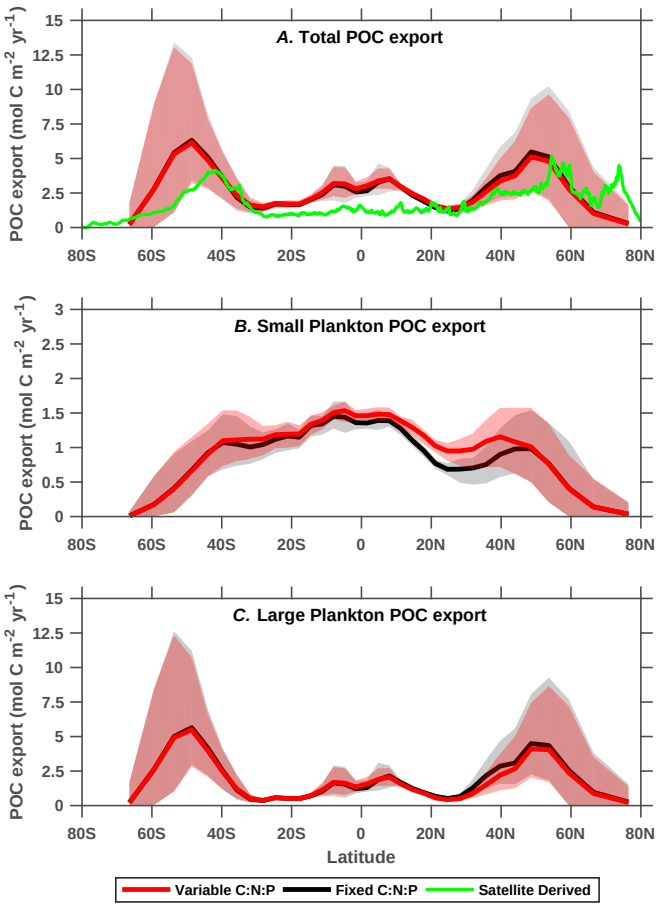

Figure A.2: Zonal averages of POC export in units of mol C m^{-2} yr^{-1}. Thick red line is the modeled annual mean EP with MESMO2-*Var* under preindustrial condition. Thick black line is the annual mean EP with MESMO2-*Fix*. Red shaded and black shaded areas represent seasonal variability of EP with MESMO2-*Var* and MESMO2-*Fix* respectively. (a) Total EP which is a sum of EP by small plankton (b) and large plankton (c). Green line in (a) is a satellite derived annual mean EP using monthly MODIS data from 2009-2013 calculated with empirical algorithms (Behrenfeld & Falkowski 1997; Dunne et al. 2005).

Appendix B

Supporting Information For Chapter 3

Table B.1: List of 64 studies used in the meta-analysis. Abbreviations of the studies used in figures are listed on the left-hand column. All the studies here are included in the main bibliography.

Study	Reference
Bechemin99	Béchemin, Grzebyk, Hachame, Hummert, and Maestrini (1999)
Berges02	Berges, Varela, and Harrison (2002)
Bi17	Bi et al. (2017)
Bi18	Bi et al. (2018)
Bittar13	Bittar et al. (2013)
BlancoAmeijeiras18	Blanco-Ameijeiras et al. (2018)
Brauer13	Brauer et al. (2013)
Bucciarelli10	Bucciarelli et al. (2010)
Claquin02	Claquin, Martin-Jezequel, Kromkamp, Veldhuis, and Kraay (2002)
Fabregas95	Fábregas, Patiño, Vecino, Cházaro, and Otero (1995)
Feng18	Feng et al. (2018)
Finkel06	Finkel et al. (2006)
Fu05	F.-X. Fu, Zhang, Bell, and Hutchins (2005)
Fu06	F.-X. Fu, Zhang, Feng, and Hutchins (2006)
Fu14	F. Fu et al. (2014)
Garcia11	N. S. Garcia et al. (2011)
Giovagnetti12	Giovagnetti, Cataldo, Conversano, and Brunet (2012)
Goldman76	Goldman and Ryther (1976)
Goldman79	Goldman (1979)
Heiden16	Heiden, Bischof, and Trimborn (2016)
Jacq14	Jacq, Ridame, L'Helguen, Kaczmar, and Saliot (2014)

Jiang18	Jiang et al. (2018)
Johansson99	Johansson and Granéli (1999)
Kudo97	Kudo and Harrison (1997)
Leonardos04	Leonardos and Geider (2004)
Leonardos05	Leonardos and Geider (2005)
Leong04	Leong and Taguchi (2004)
Leong10	Leong, Maekawa, and Taguchi (2010)
Li13	G. Li and Campbell (2013)
Li17	G. Li and Campbell (2017)
Li18	Z. Li, Wu, and Beardall (2018)
Li80	W. K. W. Li (1980)
Lu18	Lu et al. (2018)
Mari99	Mari (1999)
Martiny16	Martiny et al. (2016)
Meyerink17	Meyerink, Ellwood, Maher, Dean Price, and Strzepek (2017)
Mortensen88	Mortensen, Børsheim, Rainuzzo, and Knutsen (1988)
Mou17	Mou et al. (2017)
Mouginot15	Mouginot et al. (2015)
Nielsen91	M. V. Nielsen and Tønseth (1991)
Nielsen92	M. V. Nielsen (1992)
Nielsen96	M. Nielsen (1996)
Otero98	Otero, Dominguez, Lamela, Garcia, and Fábregas (1998)
Passow15	Passow and Laws (2015)
Qu18	Qu, Fu, and Hutchins (2018)
Rabouille17	Rabouille, Semedo Cabral, and Pedrotti (2017)
Rasdi15	Rasdi and Qin (2015)
Saito03	Saito and Tsuda (2003)
Sakshaug83	Sakshaug, Andresen, Myklestad, and Olsen (1983)
Sakshaug86	Sakshaug and Andresen (1986)
Schaum18	Schaum et al. (2018)
Shoman15	Shoman (2015)
Six04	Six, Thomas, Brahamsha, Lemoine, and Partensky (2004)
Spilling15	Spilling, Ylöstalo, Simis, and Seppälä (2015)
Staehr02	Staehr, Henriksen, and Markager (2002)
Sugie13	Sugie and Yoshimura (2013)
Terry83	Terry, Hirata, and Laws (1983)
Thompson89	P. A. Thompson, Levasseur, and Harrison (1989)
Thompson92	P. A. Thompson, Guo, Harrison, and Whyte (1992)
Thompson99	P. Thompson (1999)
Uronen05	Uronen, Lehtinen, Legrand, Kuuppo, and Tamminen (2005)
Wood95	Wood and Flynn (1995)
Yoder79	Yoder (1979)
Zhu17	Zhu et al. (2017)

Appendix C

Supporting Information For Chapter 4

This supporting information includes the Table C.1.

Table C.1: Default food preference of mesozooplankton in the original ERSEM model (Butenschön et al. 2016).

From	To Mesozooplankton
Bacteria	-
Picophytoplankton	-
Nanophytoplankton	0.05
Diatoms	0.15
Microphytoplankton	0.15
Heterotrophic flagellates (Heterotrophs)	0.05
Microzooplankton	0.25
Mesozooplankton	0.25
Medium sized POM (mPOM)	0.1

Appendix D

Supporting Information For Chapter 5

This supporting information includes supplementary methods and discussion related to Chapter 5. Supporting information contains detailed discussion of methods used to calculate remineralization stoichiometry (Sections D.1-D.4). In particular, we describe sensitivity tests carried out to test the robustness of the vertical gradient method. We also give derivation of the equation (5.4) in the main text.

Figures D.1 to D.7 are related to the sensitivity analysis. Table D.1 gives the literature values for the elemental composition of phytoplankton macromolecules used in this study. Tables D.2 to D.4 are related to the satellite-derived estimate of macromolecules and uncertainties associated with them. Table D.5 shows the result of 9 sensitivity analyses used to make Figure 5.2 in the main text. A compiled dataset of phytoplankton macromolecules from various oceanographic regions used to create Figure 5.4 in the main text are available from the Zenodo data repository (`https://doi.org/10.5281/zenodo.3462575`).

D.1 Uncertainties associated with O_2:C remineralization ratio calculated from the satellite-derived estimate of macromolecules

Roy (2018) conducted sensitivity tests to show that relative uncertainties (algorithm uncertainties) is highest in the upwelling and productive regions (30-45% for carbohydrates, 30-40% for protein, and 35-50% for lipid) and modest in the oligotrophic and less productive regions (<15% for carbohydrate and protein; and <25% for lipid). For our analysis, we further combined 11 oceanographic regions into 4 regions (Subarctic, Subtropical gyres, Equatorial upwelling regions, and Subantarctic) and assigned fixed % uncertainty values for each region (Table D.2).

Ocean color based algorithm does not provide the estimate of the nucleic acid content (DNA and RNA), which typically make up 5-15% of phytoplankton by weight (Geider & La Roche 2002). We carry out sensitivity analysis by varying the percentage of nucleic acid ranging from 0 to 15% in all of the 11 oceanographic regions (Table D.3). Since $O_2 : C_{rem}$ of nucleic acid is larger compared to that of other main macromolecules (Figure 5.3a), $O_2 : C_{rem}$ increases by 0.01-0.02 when nucleic acid fraction increases from 0% to 15%. This change does not alter the values for $O_2 : C_{rem}$ significantly relative to the relative uncertainty. However, our sensitivity analysis shows that cellular C:P, N:P as well as $O_2 : P_{rem}$ are sensitive to the changes in nucleic acid content, because over 75% of the total cellular phosphorus content come from nucleic acid (Finkel et al. 2016). We therefore estimated the weight % of nucleic acid that is required to meet the C:P export ratios from a previous inverse modeling study (Teng et al. 2014).

D.2 Derivation of equation(5.4) in the main text

First, we consider a complete oxidation reaction of organic matter:

$$(CH_xO_y)_\alpha(NH_3)_\beta(H_3PO_4) + \gamma O_2 = \alpha CO_2 + \beta HNO_3 + H_3PO_4 + \lambda H_2O \qquad (D.1)$$

In this remineralization reaction, we make three implicit assumptions regarding the number of hydrogen and oxygen atoms that accompany carbon, nitrogen, and phosphorus

atoms:

(1) Carbon exists in a repeating molecular chain of CH_xO_y: for every C atom in the organic matter, there is x number of H atoms and y number of O atoms. H ("excess hydrogen") and O content change independently from C, but H and O content are coupled by the parameter f (described later). Excess hydrogen is assumed to come from lipids, polysaccharides, and/or proteins.

(2) Nitrogen exists in a repeating molecular chain of ammonia (NH_3): for every N atom, there are 3 H atoms.

(3) Phosphorus is bound in phosphoric acid (H_3PO_4): for every P atom, there are 3 H atoms and 4 O atoms.

By using these three assumptions and balancing the number of atoms on both sides of equation (D.1), we obtain:

$$O_2 : P_{rem} = C : P + 0.25(H : P) - 0.5(O : P) + 1.25(N : P) + 1.25 \quad (D.2)$$

$$H : P = x(C : P) + 3(N : P) + 3 \quad (D.3)$$

$$O : P = y(C : P) + 4 \quad (D.4)$$

Inserting equations (D.3) and (D.4) into equation (D.2) yields equation (5.4) in the main text ($O_2 : P_{rem} = (1+f)C : P_{exp} + 2N : P_{exp}$) where $f = x/4 - y/2$. The parameter f is thus a measure of externally sourced oxygen needed to oxidize hydrogen atoms in excess of oxygen atoms in organic matter. Finally, note that if we divide both sides of equation (5.4) by C:P, we obtain

$$O_2 : C_{rem} = (1 + f) + 2N : C = (1 + f)[1 + 2N : P/(O_2 : P_{rem} - 2N : P)]. \quad (D.5)$$

Equation (D.5) shows that $O_2 : C_{rem}$ increases if the difference between $O_2 : P_{rem}$ and N:P decreases and/or N:P increases. Further, $O_2 : C_{rem}$ is proportional to N:C.

D.3 Assumptions and limitations of the vertical gradient method

In adopting the vertical gradient method, we make the inherent assumption that the lateral tracer transport is much smaller than the vertical tracer transport. This assumption is based on the basin-wide observation that vertical mixing processes generally occurs on timescale of weeks to months while lateral exchange has a much longer timescale on the order of years (Sarmiento et al. 2002). In particular, the assumption holds in the tropics and subtropics where the isopycnal surfaces are flat and extensive. However, the assumption becomes less tenable in polar and subpolar regions, where isopycnal surfaces are steeper and mixed layers are deeper. For this reason, we exclude waters poleward of subtropical gyres. We also neglected from our analysis grid points where vertical gradients of $PO_4{}^{3-}$, $NO_3{}^{-}$, and AOU are below threshold values of 0.02, 0.2, and 0.8 μM respectively. We assessed the accuracy of vertical gradient method by comparing our results to the previous estimates of C:N:P:O_2 export/remineralization ratios (Figure D.1) and by applying it to the model "data" for which we know exactly the $N : P_{exp}$ and $O_2 : P_{rem}$ ratios (Buchanan et al. 2018) (Figures D.2-D.7). Our method is capable of making a quantitative estimate within 95% confidence interval except in polar and subpolar waters, which we have removed from our results in the main section. In addition, implementing equation (5.4) assumes steady state such that organic matter remineralization ratios equal export ratios. Therefore, we do not consider organic matter inputs from land and loss to sediments.

D.4 Validating the vertical gradient method

We assessed the $N : P_{exp}$ and $O_2 : P_{rem}$ results from the vertical gradient method by applying it to synthetic ocean data for which we know exactly the actual export ratios. The "data" in this case are tracer distributions generated by ocean general circulation model (OGCM) simulations. The OGCM we used is CSIRO Mk3L ocean circulation + the ocean biogeochemical model forced with six different realizations (i.e. surface boundary conditions) of the preindustrial climate (Buchanan et al. 2018). These preindustrial

climatologies of ocean physical states are taken from the Climate Model Intercomparison Project phase 5 (CMIP5) multimodel ensemble comprising of GFDL-ESM2G ("GFDL"), HadGEM2-CC ("HadGEM"), IPSL-CM5A-MR ("IPSL"), MPI-ESM-MR ("MPI"), MRI-CGCM3 ("MRI"), and CSIRO-Mk3L ("Mk3L"). We emphasize that all the ocean physical states were generated using the same OGCM physics model but were forced by different initial surface boundary conditions taken from CMIP5. For our validation analyses, we used biogeochemical model outputs from Variable Elemental Ratios (V_{ele}) model, where C:N:P ratios of organic matter and $O_2 : P_{rem}$ are variable as a function of ambient surface PO_4^{3-} and NO_3^- (Galbraith & Martiny 2015). As the biogeochemical model does not consider the preferential remineralization of any element over other elements, C:N:P and $O_2 : P_{rem}$ ratios are constant throughout the water column. The annual mean model outputs of the 6 different preindustrial climatologies are downloaded from Australian National Computational Infrastructure data portal (`https://doi.org/10.4225/41/5a1b6aa448c32`).

Using the annual mean model "data" of potential temperature, salinity, dissolved O_2, PO_4^{3-}, and NO_3^-, we estimated vertical gradients of NO_3^-:PO_4^{3-} and AOU:PO_4^{3-} using equations (5.2) and (5.3) from the main text at each of the 2.8 degrees by 1.6 degrees grid point. Vertical gradients are then averaged over large oceanographic regions delineated based on the latitude and major ocean basin. These 11 regions are: Southern Ocean ($<$ 45 °S), South Atlantic (45°S - 15°S), South Pacific (45°S - 15°S), South Indian Ocean (45°S - 15°S), North Indian Ocean ($>$ 15°S), Equatorial Atlantic (15°S - 15°N), Equatorial Pacific (15°S - 15°N), North Atlantic (15°N - 45°N), North Pacific (15°N - 45°N), Subarctic Atlantic ($>$ 45°N), and Subarctic Pacific ($>$ 45°N). We did not separate oceanographic regions based on NO_3^- concentration of 0.3 μM because the surface NO_3^- concentrations in the models consistently exceed 0.3 μM even in the oligotrophic subtropical gyres.

We have conducted three sets of sensitivity analyses in estimating vertical gradients by changing the boundaries of the surface and deep layer boxes. In the first set, we employed the original vertical gradient method (Sarmiento et al. 2002), which assumes the depth of 100 m for both the surface and deep box ("0-100-200"). In the second set, we have calculated the vertical gradients with the box depth of 200 m ("0-200-400"), hence doubling the dimensions of both the surface and deep box. In the third set of

sensitivity analysis, we used the mixed later depth (MLD) at each grid point as the bottom of the surface box and kept the bottom of the deep box at 200 m ("0-MLD-200"). Areas with MLD deeper than 200 m due to convection and/or deep water mixing were ignored. The definition of MLD follows a fixed temperature difference criterion of $\Delta T = 0.8°C$ from 10 m (Kara et al. 2003).

Figures D.2 and D.3 show the regional averages of the true and the estimated N:P export ratios across 6 different model realizations. Agreement between with the true export ratios are generally good with percentage errors less than 20%. Vertical gradient underestimates the true $N : P_{exp}$ in North Atlantic, Equatorial Atlantic, and North Indian for roughly half of the 6 model configurations. However, these discrepancies are specific to the model configuration and therefore does not seem to be systematic. In general, shallower choice of the surface and deep boxes ("0-100-200" or "0-MLD-200") performs better than the large box configuration ("0-200-400").

Figures D.4 and D.5 show the regional averages of the true and the estimated remineralization O_2:P ratio. Overall, the large box "0-200-400" configuration performs best out of the three depth choices except in the South Atlantic Ocean where other two depth choices perform significantly better. Shallow boxes ("0-100-200" or "0-MLD-200") perform significantly worse in estimating O_2:P than N:P. The agreement between true and estimated ratios worsens in the subpolar and the polar regions. A likely explanation is the violation of the inherent assumption that the lateral tracer transport is much smaller than the vertical tracer transported for dissolved O_2. In addition, O_2 disequilibrium caused by seasonal ice, deep winter convection and heat loss can decouple AOU from the true remineralization signal (Ito et al. 2004).

Figures D.6 and D.7 show the regional averages of the true and the estimated remineralization O_2:C ratio calculated using equation (D.5) with $f = 0.11$ (consistent with the analyses in the main text). With the exception of Southern Ocean, fractional errors are less than 15% across all the model configurations. Calculated $O_2 : C_{rem}$ slightly underestimates the true $O_2 : C_{rem}$ because $O_2 : P_{rem}$ derived from the vertical gradient method generally overestimates the true value (Figure D.5). Nevertheless, mean $O_2 : C_{rem}$ estimated from vertical gradient method is able to reproduce true values within two standard deviations in large parts of the tropics and subtropics.

Based on the validation analyses, we made a judgement to eliminate subarctic ocean

north of 45°N and Southern Ocean south of 45°S from the analysis presented in the main text. Further, we have decided to take an ensemble mean of the three sets of analyses utilizing different depth choices in estimating vertical gradients from the gridded nutrient data. The shallower depth choices ("0-100-200" and "0-MLD-200") perform better at estimating $N : P_{exp}$ but the larger depth choice ("0-200-400") outperforms the other two at estimating $O_2 : P_{rem}$. Although the selection of depth range is arbitrary in nature, we argue that taking the ensemble mean would minimize the overall uncertainty in estimating $O_2 : C_{rem}$. We could not test the effects of seasonal variability in the model validation as there is currently no published model dataset available. However, we are accounting for the seasonality in the main text by using winter and summer averaged as well as annual mean concentrations. Overall, our validation test indicates that the vertical gradient method can estimate large scale $N : P_{exp}$ and $O_2 : P_{rem}$ satisfactorily within the geographic regions of 45°S - 45°N.

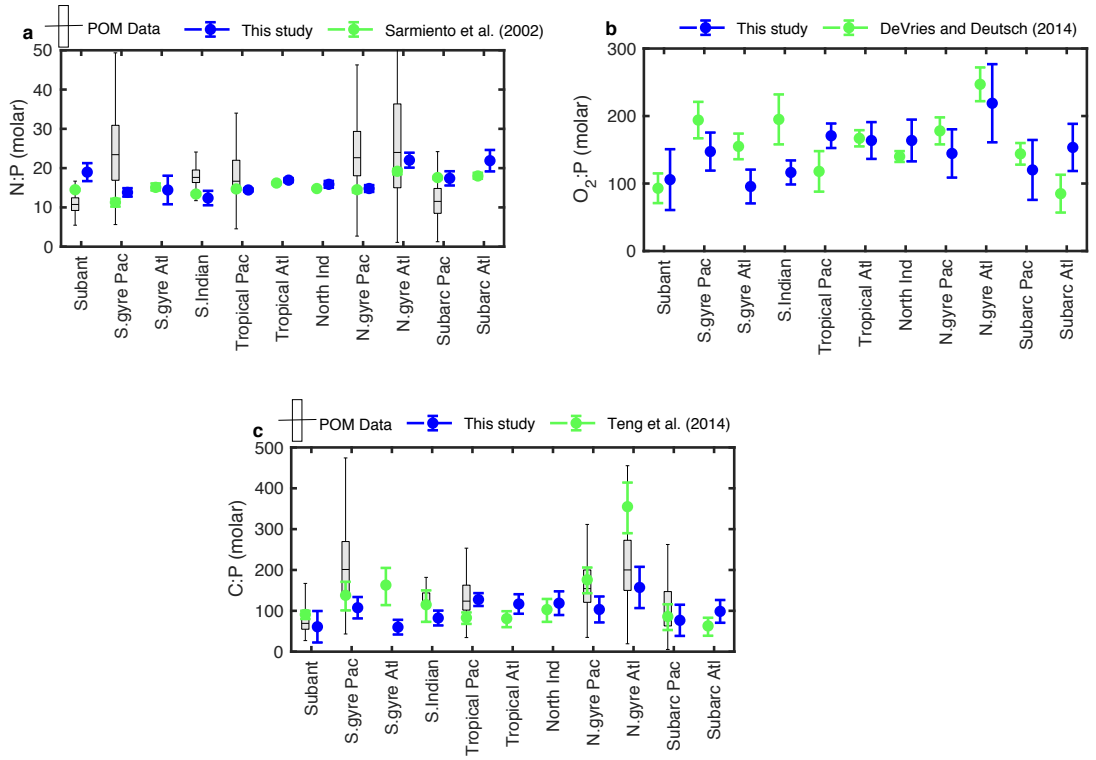

Figure D.1: Comparison of N:P, $O_2 : P_{rem}$, and C:P obtained from the vertical gradient method with previous estimates. a. Blue: N:P ($\pm 1\sigma$) of the ensemble median from this study. Grey box: N:P at top 300 m from POM data (Martiny et al. 2014). The box plots show 25, 50 and 75 percentiles. Green: N:P export ratio at 100 m from a previous study using the same method but different dataset (Sarmiento et al. 2002). Error bars correspond to 2.5% or 97.5% tails of the bootstrap distribution. b. Blue: $O_2 : P_{rem}$ ($\pm 1\sigma$) of the ensemble median from this study. Green: $O_2 : P_{rem}$ from data-constrained ocean circulation model (DeVries & Deutsch 2014). Error bars correspond to $\pm 1\sigma$ of the ensemble median $O_2 : P_{rem}$ at 200 m. c. Blue: C:P ($\pm 1\sigma$) of the ensemble median from this study. Grey box: C:P in the upper 300 m from POM data (Martiny et al. 2014). The box plots show 25, 50 and 75 percentiles. Green: C:P export ratio from geochemical inverse model (Teng et al. 2014). Error bars correspond to $\pm 1\sigma$ of the posterior pdf.

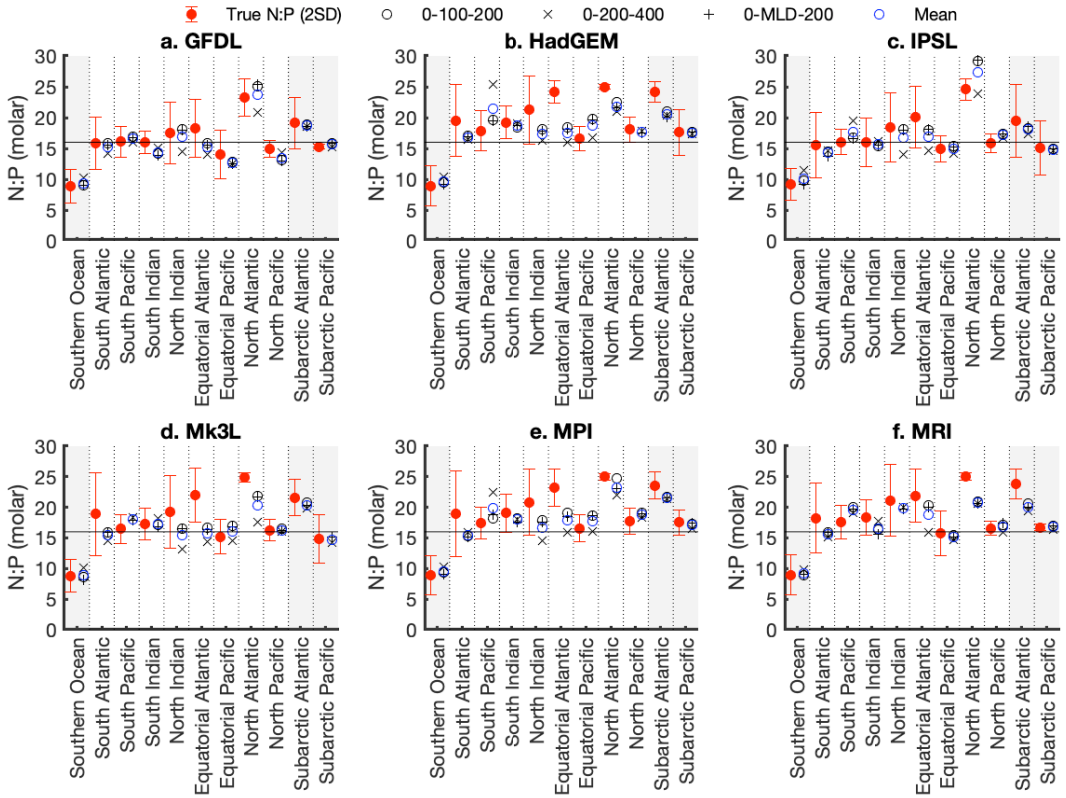

Figure D.2: Comparison of true vs. vertical gradient based estimate of N : P_{exp} across six model configurations and 3 depth choices. Mean is the simple mean of 3 depth estimates. Shaded areas are South of 45°S ("Southern Ocean") or North of 45°N ("Subarctic Atlantic" and "Subarctic Pacific") excluded in the main text. Black horizontal line shows the Redfield ratio of N:P = 16.

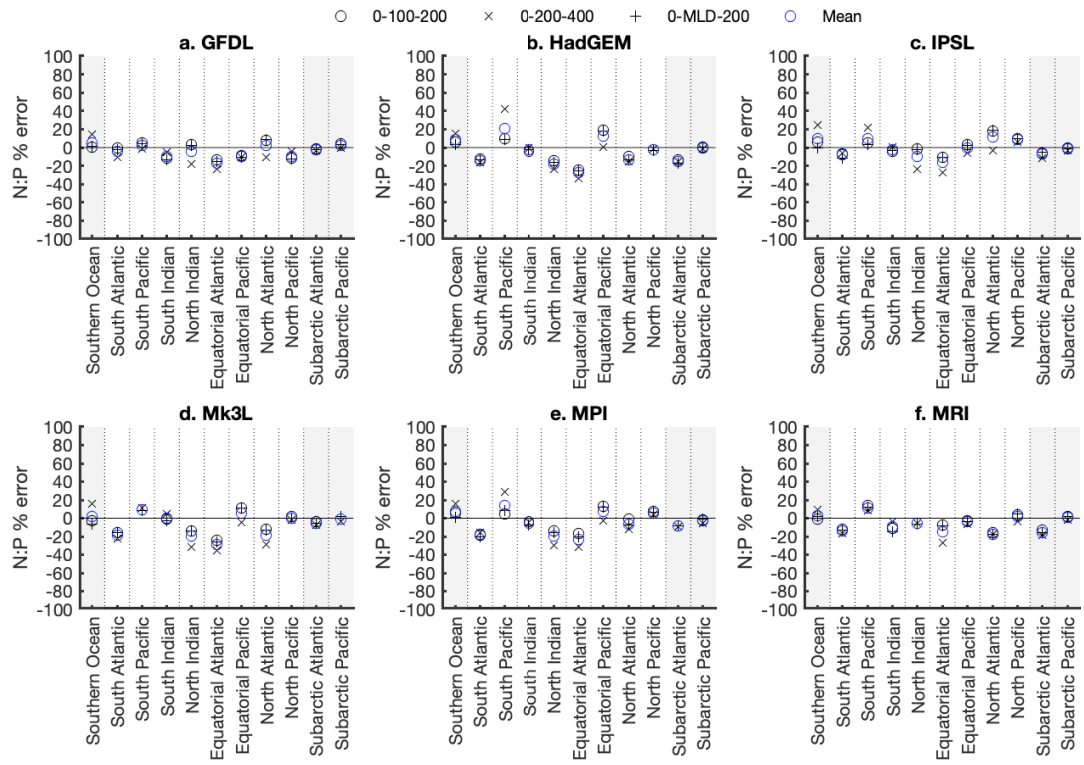

Figure D.3: Comparison of true vs. vertical gradient based estimate of $N : P_{exp}$ (% error). The % error is based on the difference from the true N:P in Figure D.2.

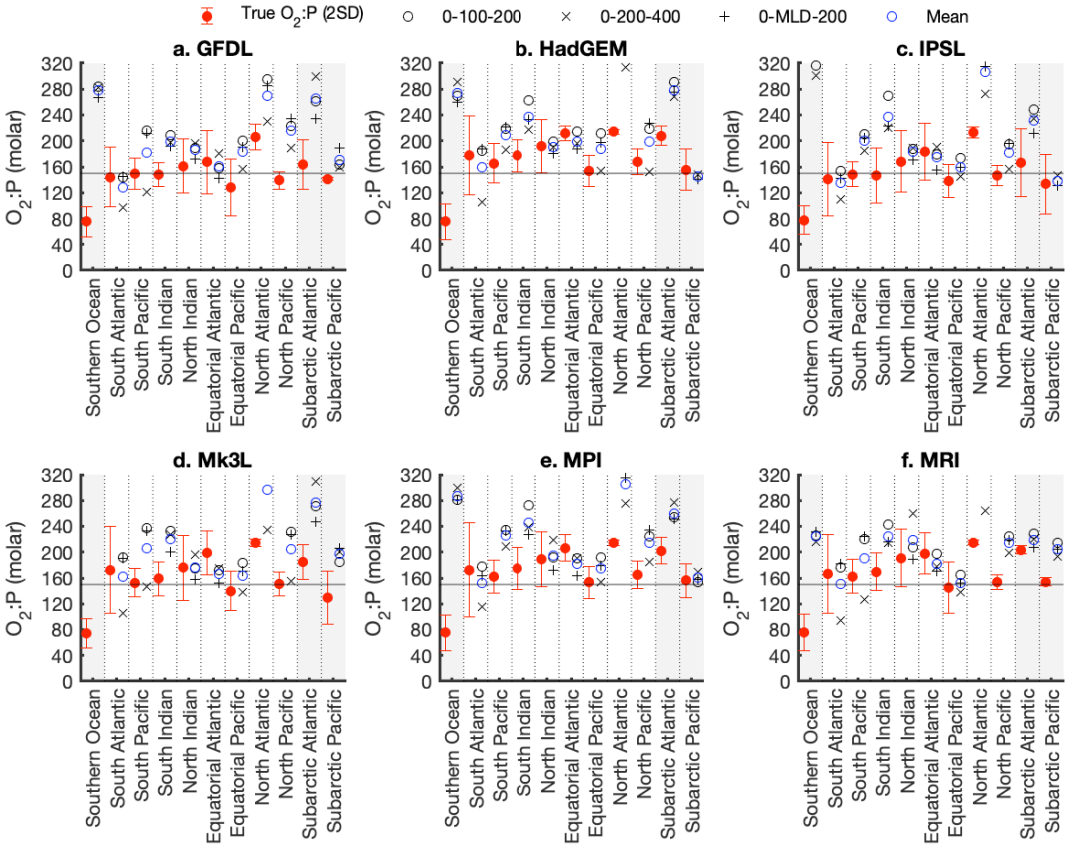

Figure D.4: Comparison of true vs. vertical gradient based estimate of $O_2 : P_{rem}$. Shaded areas are South of 45°S ("Southern Ocean") or North of 45°N ("Subarctic Atlantic" and "Subarctic Pacific") excluded in the main text. Black horizontal line shows the global mean $O_2 : P_{rem}$ of 150 obtained from previous studies (L. A. Anderson 1995; DeVries & Deutsch 2014).

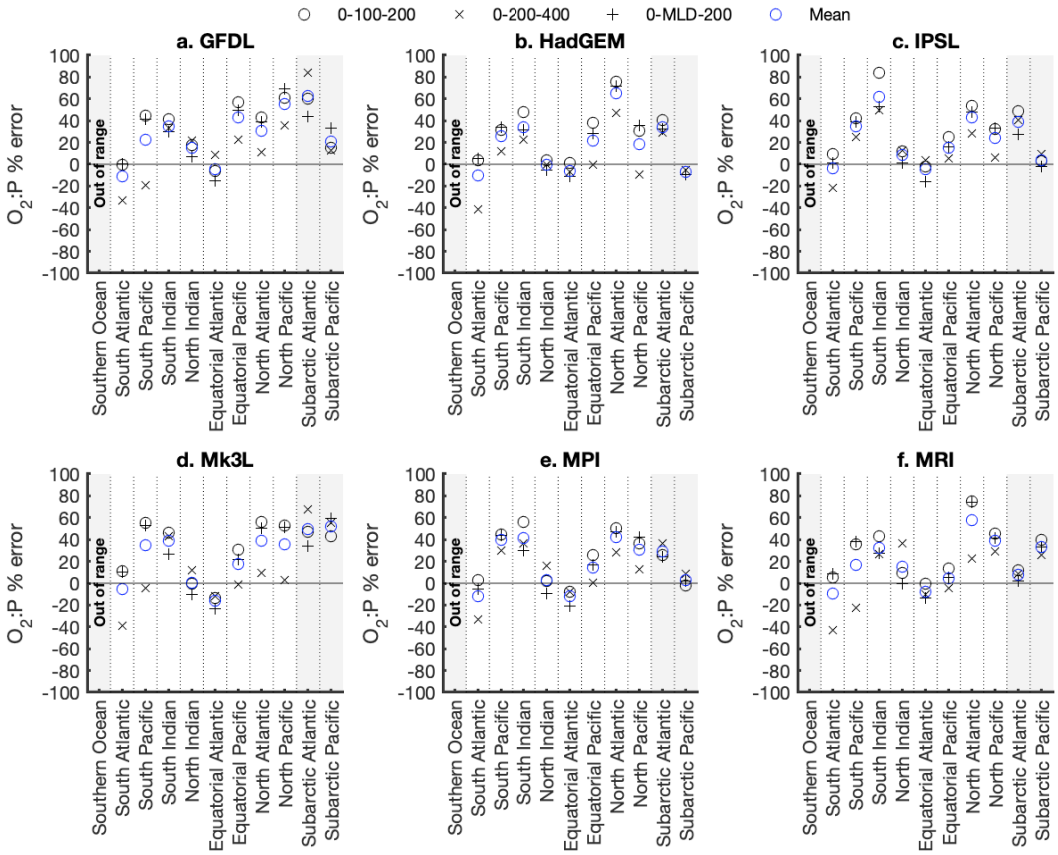

Figure D.5: Comparison of true vs. vertical gradient based estimate of $O_2 : P_{rem}$ (% error). The % error is based on the difference from the true $O_2 : P_{rem}$ in Figure D.4. The % error in the Southern Ocean exceeded 100% (out of range) in all 6 model runs.

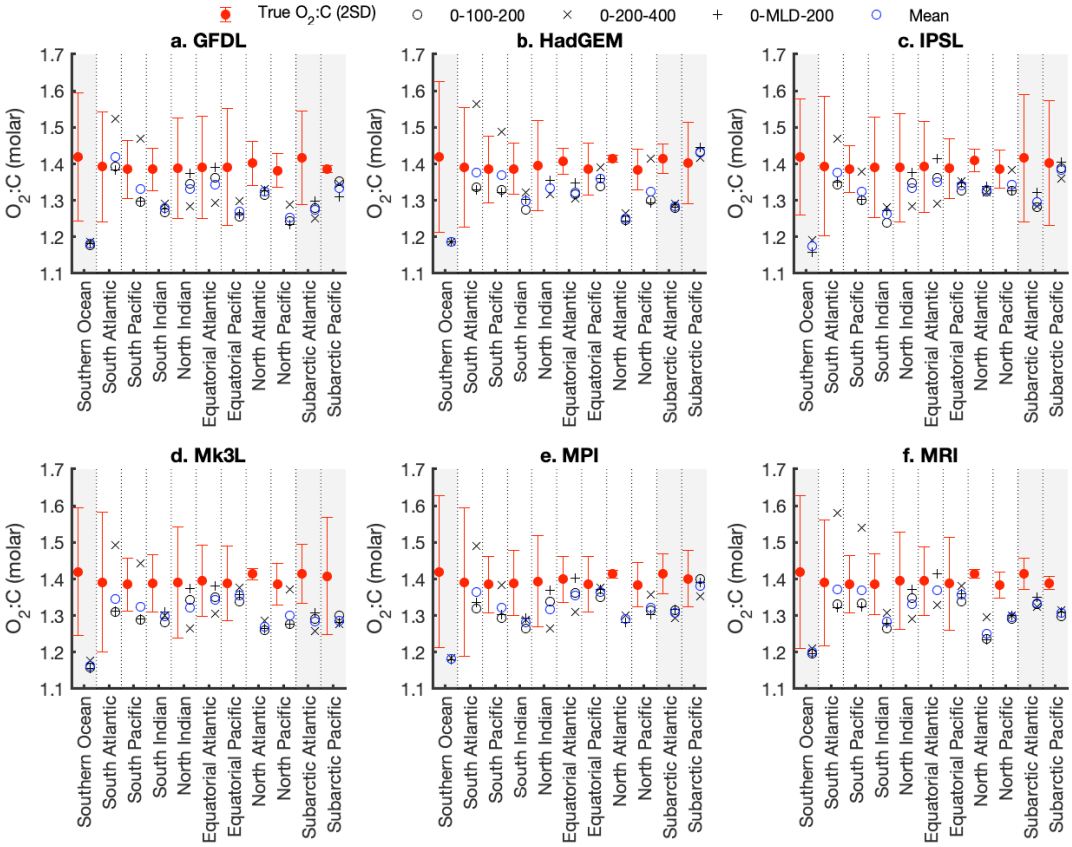

Figure D.6: Comparison of true vs. vertical gradient based estimate of $O_2 : C_{rem}$. $O_2 : C_{rem}$ is calculated from $O_2 : P_{rem}$ and $N : P_{exp}$ using equation (D.5). Standard deviations associated with true $O_2 : C_{rem}$ are derived by propagating standard deviations for $O_2 : P_{rem}$ and $N : P_{exp}$. Shaded areas are South of 45°S ("Southern Ocean") or North of 45°N ("Subarctic Atlantic" and "Subarctic Pacific").

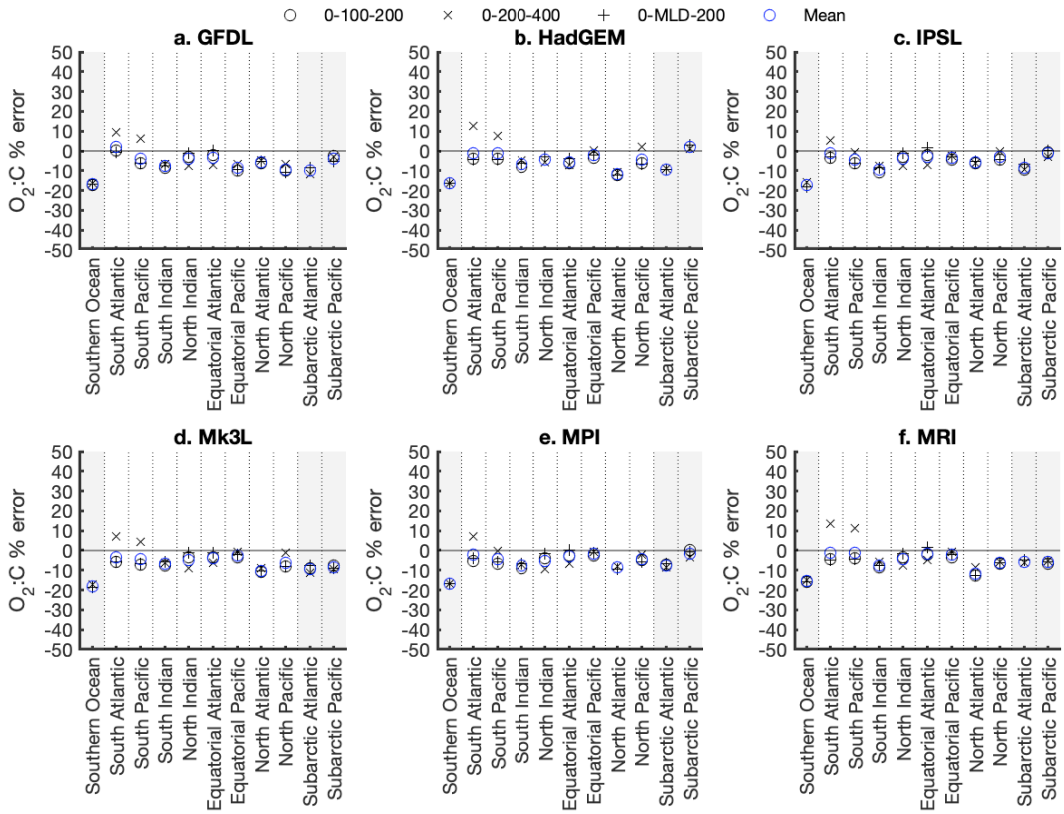

Figure D.7: Comparison of true vs. vertical gradient based estimate of $O_2 : C_{rem}$ (% error). The % error is based on the difference from the true $O_2 : C_{rem}$ in Figure D.6.

Table D.1: Assumed elemental composition of main phytoplankton macromolecules obtained from literatures.

Macromolecule	**Composition**	**Reference**
Protein	$C_{3.83}H_{6.05}O_{1.25}N$	L. A. Anderson (1995)
Lipid	$C_{40}H_{74}O_5$	L. A. Anderson (1995)
Phospholipid	$C_{37.9}H_{72.5}O_{9.4}N_{0.43}P$	Geider and La Roche (2002)
Carbohydrate	$C_6H_{10}O_5$	L. A. Anderson (1995)
Chlorophyll-a	$C_{55}H_{72}O_5N_4Mg$	Geider and La Roche (2002)
RNA	$C_{9.5}H_{13.75}O_8N_{3.75}P$	Geider and La Roche (2002)
DNA	$C_{9.75}H_{14.25}O_8N_{3.75}P$	Geider and La Roche (2002)
Nucleic Acid	$C_{9.625}H_{12}O_{6.5}N_{3.75}P$	L. A. Anderson (1995)

Table D.2: Uncertainties in satellite-derived estimate of macromolecules. These values correspond to algorithm uncertainties in the study by Roy (2018). Regions: 2 = Subpolar N. Pacific, 3 = Subpolar N. Atlantic, 4 = Subtropical N. Pacific, 5 = Subtropical N. Atlantic, 6 = Tropical Pacific, 7 = Tropical Atlantic, 8 = North Indian Ocean, 9 = South Indian Ocean, 10 = Subtropical S. Pacific, 11 = Subtropical S. Atlantic, 12 = Subantarctic Ocean.

Macromolecule	**Uncertainties (%)**			
	Regions 2, 3	**Regions 4,5,9,10,11**	**Regions 6,7,8**	**Region 12**
Carbohydrate	45	15	45	45
Protein	40	15	40	64
Lipid	50	25	50	80
Carbohydrate:Chl	45	15	45	45

Table D.3: Effects of changing percent fraction of nucleic acid in estimating $O_2 : C_{rem}$ from the satellite-derived estimate of phytoplankton macromolecules. Values in bold are used in Figure 5.1 of the main text.

Region	Longhurst	$O_2 : C_{rem}$ for a given % of nucleic acid in the total mass			
		0%	5%	10%	15%
Subpolar N. Pacific	PSAW	**1.42±0.16**	1.43±0.15	1.43±0.15	1.44±0.14
	PSAE	**1.42±0.16**	1.43±0.15	1.43±0.15	1.44±0.14
	KURO	**1.42±0.16**	1.42±0.15	1.43±0.15	1.44±0.14
	NPPF	**1.42±0.16**	1.43±0.15	1.44±0.15	1.44±0.14
Subpolar N. Atlantic	NADR	**1.42±0.16**	1.43±0.15	1.44±0.15	1.44±0.14
	GFST	**1.42±0.16**	1.43±0.15	1.43±0.15	1.44±0.14
Subtropical N. Pacific	NPSW	**1.44±0.07**	1.45±0.07	1.45±0.06	1.46±0.06
	NPTG	**1.44±0.07**	1.45±0.06	1.45±0.06	1.46±0.06
Subtropical N. Atlantic	NASW	**1.44±0.07**	1.44±0.06	1.45±0.06	1.45±0.06
	NASE	**1.43±0.07**	1.44±0.06	1.44±0.06	1.45±0.06
	NATR	**1.44±0.07**	1.44±0.06	1.45±0.06	1.45±0.06
Tropical Pacific	WARM	**1.44±0.16**	1.45±0.16	1.45±0.15	1.46±0.15
	PNEC	**1.44±0.16**	1.45±0.16	1.45±0.15	1.46±0.15
	PEQD	**1.44±0.16**	1.45±0.16	1.45±0.15	1.46±0.15
Tropical Atlantic	WTRA	**1.44±0.16**	1.44±0.16	1.45±0.15	1.45±0.15
	ETRA	**1.43±0.16**	1.43±0.16	1.44±0.15	1.45±0.15
North Indian	MONS	**1.44±0.16**	1.44±0.16	1.45±0.15	1.45±0.15
South Indian	ISSG	**1.44±0.07**	1.45±0.06	1.45±0.06	1.46±0.06
Subtropical S. Pacific	SPSG	**1.44±0.07**	1.45±0.06	1.45±0.06	1.46±0.06
Subtropical S. Atlantic	SATL	**1.44±0.07**	1.44±0.06	1.45±0.06	1.45±0.06
Subantarctic	SANT	**1.44±0.26**	1.44±0.25	1.45±0.24	1.45±0.23

Table D.4: Summary of macromolecular data from Roy (2018) used for Figure 5.1 in the main text. Uncertainties in carbohydrate, protein, lipid, Carb:Chl are based on the regional algorithm uncertainties (Table D.2). % Nucleic acid is estimated from $C : P_{exp}$. Numbers in bold are reported in the main text. (Notes: *Export C:P ratio from Teng et al. (2014). The values correspond to the location of the maximum of the posterior probability density function (pdf). The error bars correspond to ±1 standard deviation of the posterior pdf. **In Subtropical N. Atlantic, C:P export ratio of 355 exceeds C:P of macromolecules for any given % nucleic acid.)

Region	Longhurst	Carb (mg m^{-3})	Protein (mg m^{-3})	Lipid (mg m^{-3})	Carb:Chl	Chl (mg m^{-3})	Total (mg m^{-3})	$O_2 : C_{rem}$	$C : P_{exp}$*	% Nucleic acid
Subpolar N. Pacific	PSAW	2.75±1.24	8.08±3.23	4.88±2.44	5.96±2.68	0.46±0.29	16.17±5.01	1.42±0.16	86(+23,-20)	**13.0(+4.9,-3.6)**
	PSAE	2.28±1.03	6.85±2.74	4.17±2.09	6.02±2.71	0.38±0.24	13.68±4.50	1.42±0.16		
	KURO	2.06±0.93	5.86±2.34	3.53±1.77	6.49±2.92	0.32±0.20	11.77±4.24	1.42±0.16		
	NPPF	1.63±0.73	5.20±2.08	3.22±1.61	6.37±2.87	0.26±0.16	10.31±3.96	1.42±0.16		
	Mean	**2.18±0.98**	**6.50±2.60**	**3.95±1.98**	**6.21±2.79**	**0.35±0.22**	**12.98±4.41**	**1.42±0.16**		
Subpolar N. Atlantic	NADR	2.73±1.23	8.82±3.53	5.49±2.75	6.15±2.77	0.44±0.28	17.48±5.40	1.42±0.16	63(+24,-20)	**18.8(+9.7,-6.1)**
	GFST	1.85±0.83	5.53±2.21	3.36±1.68	6.21±2.79	0.30±0.19	11.04±4.03	1.42±0.16		
	Mean	**2.29±1.03**	**7.18±2.87**	**4.43±2.21**	**6.18±2.78**	**0.37±0.24**	**14.26±4.68**	**1.42±0.16**		
Subtropical N. Pacific	NPSW	0.42±0.06	2.11±0.32	1.38±0.35	8.95±1.34	0.05±0.01	3.96±1.42	1.44±0.07	176(+33,-30)	**3.8(+1.8,-1.4)**
	NPTG	0.54±0.08	2.49±0.37	1.62±0.41	8.22±1.23	0.07±0.01	4.72±1.35	1.44±0.07		
	Mean	**0.48±0.07**	**2.30±0.35**	**1.50±0.38**	**8.59±1.29**	**0.06±0.01**	**4.34±1.39**	**1.44±0.07**		
Subtropical N. Atlantic	NASW	0.72±0.11	2.97±0.45	1.92±0.48	7.35±1.10	0.10±0.02	5.71±1.29	1.44±0.07	355(+65, -59)	**0**(+0.3)**
	NASE	1.05±0.16	3.85±0.58	2.47±0.62	6.87±1.03	0.15±0.03	7.52±1.34	1.43±0.07		
	NATR	0.60±0.09	2.70±0.41	1.75±0.44	7.83±1.17	0.08±0.02	5.13±1.32	1.44±0.07		
	Mean	**0.79±0.12**	**3.17±0.48**	**2.05±0.51**	**7.35±1.10**	**0.11±0.02**	**6.12±1.31**	**1.44±0.07**		
Tropical Pacific	WARM	0.64±0.29	3.18±1.27	2.08±1.04	8.82±3.97	0.07±0.05	5.97±4.31	1.44±0.16	83(+15,-13)	**13.3(+3.2,-2.7)**
	PNEC	1.30±0.59	6.26±2.50	4.08±2.04	8.47±3.81	0.15±0.10	11.79±5.03	1.44±0.16		
	PEQD	1.43±0.64	6.83±2.73	4.45±2.23	8.23±3.70	0.17±0.11	12.88±5.15	1.44±0.16		
	Mean	**1.12±0.51**	**5.42±2.17**	**3.54±1.77**	**8.51±3.83**	**0.13±0.08**	**10.22±4.77**	**1.44±0.16**		
Tropical Atlantic	WTRA	1.18±0.53	4.95±1.98	3.19±1.60	7.59±3.42	0.16±0.10	9.48±4.29	1.44±0.16	81(+21,-18)	**13.8(+5.0,-3.6)**
	ETRA	1.55±0.70	5.51±2.20	3.48±1.74	7.06±3.18	0.22±0.14	10.76±4.30	1.43±0.16		
	Mean	**1.37±0.61**	**5.23±2.09**	**3.34±1.67**	**7.33±3.30**	**0.19±0.12**	**10.12±4.29**	**1.43±0.16**		
North Indian	**MONS**	**1.03±0.46**	**4.63±1.85**	**3.01±1.51**	**7.85±3.53**	**0.13±0.08**	**8.80±4.29**	**1.44±0.16**	103(+30,-26)	**9.9(+4.3,-3.3)**
South Indian	**ISSG**	**0.65±0.10**	**2.97±0.45**	**1.93±0.48**	**8.11±1.22**	**0.08±0.02**	**5.63±1.39**	**1.44±0.07**	115(+42,-35)	**8.4(+5.6,-3.5)**
Subtropical S. Pacific	**SPSG**	**0.56±0.08**	**2.68±0.40**	**1.75±0.44**	**8.67±1.30**	**0.06±0.01**	**5.05±1.43**	**1.44±0.07**	138(+37,-33)	**6.2(+3.4,-2.3)**
Subtropical S. Atlantic	**SATL**	**0.68±0.10**	**3.06±0.46**	**1.99±0.50**	**7.89±1.18**	**0.09±0.02**	**5.82±1.37**	**1.44±0.07**	163(+49,-42)	**4.5(+3.3,-2.2)**
Subantarctic	**SANT**	**1.49±0.67**	**6.46±4.13**	**4.19±3.35**	**7.37±3.32**	**0.20±0.13**	**12.34±6.31**	**1.44±0.26**	91(+11,-9)	**11.8(+1.8,-1.7)**

Table D.5: $O_2 : C_{rem}$ from 9 sensitivity analyses accounting for seasonal variability and depth choice. Uncertainty for each sensitivity run is calculated by propagating uncertainties in $O_2 : P_{rem}$ and $N : P_{exp}$ estimates. Ensemble mean (bold, reported in the main text) is calculated from ensemble mean of $O_2 : P_{rem}$ and $N : P_{exp}$ from 9 sensitivity experiments (errors being propagated).

Region	Annual 0-100-200	Annual 0-200-400	Annual 0-MLD-200	Summer 0-100-200	Summer 0-200-400	Summer 0-MLD-200	Winter 0-100-200	Winter 0-200-400	Winter 0-MLD-200	**Ensemble Mean**
North Pacific Subtropical Gyre	1.34±0.04	1.57±0.02	1.37±0.04	1.33±0.05	1.55±0.03	1.43±0.08	1.34±0.05	1.57±0.03	1.34±0.05	**1.40±0.56**
North Atlantic Subtropical Gyre	1.31±0.07	1.47±0.05	1.37±0.09	1.38±0.10	1.46±0.07	1.63±0.20	1.33±0.08	1.49±0.05	1.33±0.08	**1.39±0.59**
Tropical Pacific	1.32±0.02	1.32±0.03	1.37±0.02	1.33±0.02	1.32±0.03	1.38±0.02	1.33±0.02	1.32±0.03	1.37±0.02	**1.34±0.22**
Tropical Atlantic	1.39±0.04	1.36±0.03	1.50±0.03	1.40±0.04	1.37±0.04	1.51±0.04	1.37±0.05	1.35±0.03	1.48±0.05	**1.40±0.38**
North Indian	1.40±0.02	1.31±0.01	1.48±0.02	1.39±0.03	1.30±0.02	1.48±0.02	1.42±0.03	1.31±0.01	1.48±0.03	**1.38±0.42**
South Indian	1.35±0.05	1.60±0.05	1.37±0.06	1.34±0.07	1.62±0.06	1.41±0.11	1.34±0.07	1.55±0.06	1.34±0.07	**1.41±0.35**
South Pacific Subtropical Gyre	1.31±0.06	1.50±0.03	1.35±0.06	1.33±0.08	1.50±0.04	1.37±0.10	1.32±0.06	1.51±0.03	1.31±0.06	**1.37±0.42**
South Atlantic Subtropical Gyre	1.45±0.06	1.68±0.03	1.54±0.07	1.47±0.05	1.70±0.03	2.09±0.25	1.55±0.18	1.70±0.08	1.56±0.18	**1.59±0.75**